1-1-2006

# Selective metallization of well aligned block copolymers in thin films and confined geometries.

James D. Sievert
*University of Massachusetts Amherst*

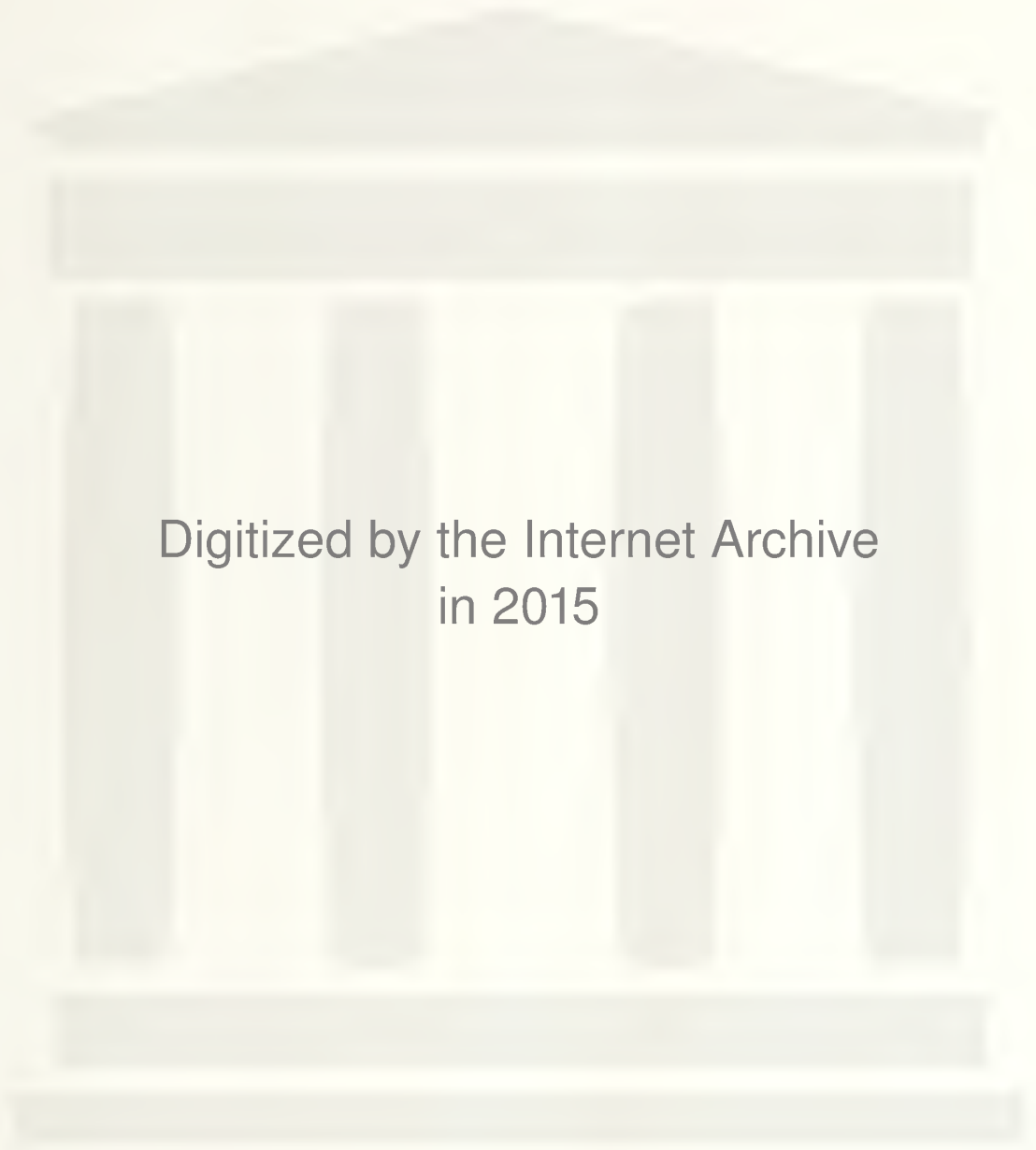

# SELECTIVE METALLIZATION OF WELL ALIGNED BLOCK COPOLYMERS IN THIN FILMS AND CONFINED GEOMETRIES

A Dissertation Presented

By

JAMES D. SIEVERT

Submitted to the Graduate School of the
University of Massachusetts, Amherst in partial fulfillment
of the requirements for the degree of

DOCTOR OF PHILOSOPHY

September 2006

Polymer Science and Engineering

# SELECTIVE METALLIZATION OF WELL ALIGNED BLOCK COPOLYMERS IN THIN FILMS AND CONFINED GEOMETRIES

A Dissertation Presented

By

JAMES D. SIEVERT

Approved to style and content by:

_____
Thomas P. Russell, Co-Chair

_____
James J. Watkins, Co-Chair

_____
E. Bryan Coughlin, Member

_____
Anthony D. Dinsmore, Member

_____
Shaw Ling Hsu, Department Head
Department of Polymer Science and Engineering

**SELECTIVE METALLIZATION OF WELL ALIGNED BLOCK COPOLYMERS IN THIN FILMS AND CONFINED GEOMETRIES**

A Dissertation Presented

By

JAMES D. SIEVERT

Approved to style and content by:

Thomas P. Russell, Co-Chair

James J. Watkins, Co-Chair

E. Bryan Coughlin, Member

Anthony D. Dinsmore, Member

Shaw Ling Hsu, Department Head
Department of Polymer Science and Engineering

## DEDICATION

In loving memory of my grandmother, Laverne C. Kennedy

## ACKNOWLEDGEMENTS

I must gratefully acknowledge the assistance of the many people who have contributed to and supported my educational career.

First, I wish to thank my advisors, Dr. Thomas P. Russell and Dr. James J. Watkins for their valuable suggestions, oversight, and support throughout the completion of this project. Both have inspired me professionally, and granted me an immense amount of freedom to pursue my research interests.

In addition, I wish to thank my committee member, Dr. E. Bryan Coughlin, for his steadfast encouragement and thoughtful feedback on my work. He has also been an invaluable resource in navigating the requirements of the Graduate School, as Graduate Program Director. Likewise, I am indebted to Dr. Anthony D. Dinsmore for his helpful comments and kindly agreeing to join my committee at the final stages of this project.

Next, I must express my gratitude to past and current members of the Russell and Watkins research groups for their friendship and assistance over the last five years. In particular, I wish to thank Xiaocuan, DuYeol, Matt, Kris, Siva, Suresh, Jaiyu and Ting.

Many other staff members have assisted me throughout my stay, and I would be remiss not to acknowledge their important contributions. It has truly been an honor and privilege to work among the distinguished faculty, staff, and students in the renowned Polymer Science and Engineering Department at the University of Massachusetts.

A brief internship at Seagate Technology also afforded me the opportunity to extend my work into an industrial setting. I am grateful to my mentor, Dr. Dorothea Buechel, for her guidance.

Finally, I wish to thank my family for the continual encouragement they have given me. Foremost, I thank my loving wife, Laurin Sievert, who has patiently supported and encouraged me throughout my career.

## ABSTRACT

SELECTIVE METALLIZATION OF WELL ALIGNED BLOCK COPOLYMERS IN THIN FILMS AND CONFINED GEOMETRIES

SEPTEMBER 2006

JAMES D. SIEVERT

B.S. UNIVERSITY OF WISCONSIN - STEVENS POINT

M.S. UNIVERSITY OF MASSACHUSETTS AMHERST

Ph.D. UNIVERSITY OF MASSACHUSETTS AMHERST

Directed by: Professor Thomas P. Russell
Professor James J. Watkins

Block copolymers are ideal templates for the fabrication of polymer-metal nanocomposites since they self-assemble into ordered, well-defined arrays of nanometer size domains. In this research, well aligned, microphase-separated structures of styrene-2-vinylpyridine block copolymers were used to prepare polymer-metal nanocomposites. Under optimal conditions, templates were prepared as thin films, confined in aluminum oxide membranes or sheared and metallized without disturbing the ordered structure. Using these methods, we developed a procedure that deposits metal within the polymer using supercritical carbon dioxide-soluble metal precursors. Supercritical carbon dioxide was used to allow for selective metallization of the polymer without disruption to its morphology. In addition, similar procedures have been investigated using metal salts and acids. Using these techniques, metals and metal-sulfides including silver, gold, platinum, iron and zinc sulfide were each selectively deposited.

## TABLE OF CONTENTS

## LIST OF TABLES

## LIST OF FIGURES

# CHAPTER 1

# INTRODUCTION

## 1.1 Project Overview

Block copolymers are ideal templates for the fabrication of macromolecule metal nanocomposites since they self-assemble into ordered, well-defined arrays of nanometer size domains where the size and shape of the domain may be tuned by varying the molecular weight and composition of the copolymer.[1] This dissertation describes the preparation of macromolecule metal complexes using a two-step method that embodies an ability to independently prepare template films with precisely controlled morphologies followed by efficient functionalization/metallization of the template without disruption to morphology or order. Specifically, the selective metallization of well aligned poly(styrene)-*block*-poly(2-vinylpyridine) copolymers in thin films, confined geometries and shear oriented samples are described within.

Chapter 1 treats the phase behavior of PS-*b*-P2VP copolymers in bulk, thin films and confined geometries, followed by the properties of supercritical carbon dioxide and why it was used in this project. Finally, an overview of macromolecule-metal complex preparation and categorization is discussed.

Chapter 2 describes the experimental methods used to prepare homopolymers and block copolymers by anionic polymerization, their metallization and the analytical techniques used to characterize these samples. Techniques used include: small and wide angle x-ray scattering (SAXS and WAXS), specular x-ray reflectivity, x-ray

photoemission spectroscopy (XPS), infrared spectroscopy and ultra violet-visible spectroscopy (UV-VIS).

In the third chapter, the preparation of poly(2-vinylpyridine) composites with silver, platinum, and zinc sulfide is described. The interaction of the metal precursors with the polymer, reduction methods and their effects on film thickness is presented.

Chapters 4, 5 and 6 describe the selective metallization of PS-b-P2VP copolymers in thin films, confined geometries and shear oriented samples respectively. Each chapter details sample preparation and metallization methods followed by a synopsis of all characterization results. Chapter 7 provides a discussion of conclusions derived from the described work and suggestions for future work.

**1.2 Introduction to Block Copolymers**

Block copolymers consist of two dissimilar blocks that can self-assemble into several ordered morphologies with nanoscale spacing through a process of microphase separation.[1-3] Microphase separation results from the enthalpy of demixing, while macrophase separation is prevented by covalent bonding of two blocks at one end. In this section, the basis for microphase separation morphologies and the phase diagram for polystyrene – poly (2-vinylpyridine) diblock copolymers are discussed.

Microphase separation in a block copolymer depends on four distinct factors: 1) the number of statistical segments, N; 2) the degree of immiscibility between the two monomers, $\chi_{AB}$ (the Flory-Huggins interaction parameter); 3) the volume fraction of the components, f; and 4) the conformational asymmetry parameter, $\epsilon$.[3] The product of $\chi N$ may be used to determine segregation limits, which are classified according to three

segregation regimes: weak, intermediate, and strong segregation limits. The $\chi N$ limits of each are 12, 100 and >100, respectively.

In 1996, Bates et al. reported the phase separation behavior of polystyrene-b-poly(2-vinylpyridine) copolymers. According to their research, the phase behavior of a series of diblocks may be characterized using several methods including: dynamic mechanical spectroscopy, transmission electron microscopy (TEM), small angle neutron scattering (SANS) and small angle X-ray scattering (SAXS). From these characterization methods, they were able to map out the phase diagram for a polymer system in the intermediate segregation limit.

Figure 1.1 below describes the phase diagram for PS-*b*-P2VP. In this case, values of $\chi N$ were estimated using Equation 1.1.

$$\chi_{PS\text{-}P2VP} = \frac{91.6}{T} - 0.095 \qquad \textbf{(1.1)}$$

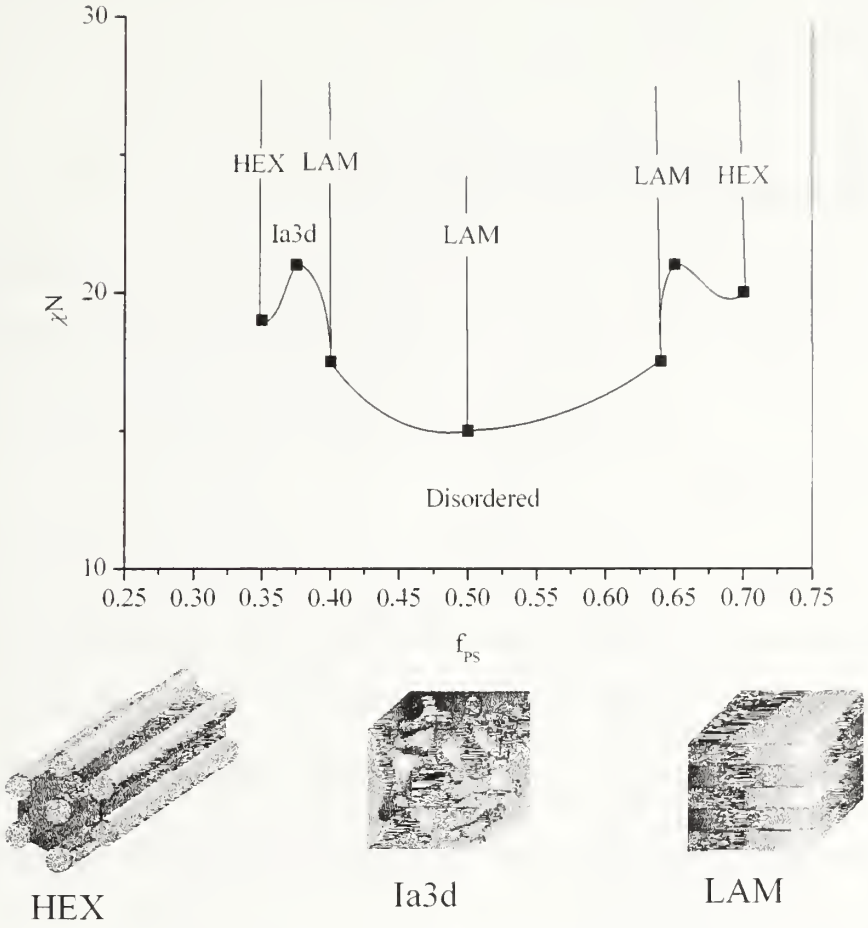


**Figure 1.1: Phase diagram of PS-*b*-P2VP diblock copolymers**

The diagram in Figure 1.1 illustrates the complex phase behavior of PS-*b*-P2VP diblock copolymers from hexagonally-packed cylinders to lamellar phases. The y-axis is the product $\chi N$, and the x-axis is the volume fraction of the polystyrene in the copolymer. By simply changing the volume fraction of one component of the copolymer it is possible to move across the phase diagram changing the microphase separated structure.

The resulting morphologies have been used for a wide range of applications including high surface area catalysts[4], materials with enhanced thermal, mechanical, and

separation properties[5], magnetic storage devices[6], and optoelectronic, photonic and electronic materials.[7-9]

### 1.3 Block Copolymers in Confined Geometries

Diblock copolymers confined within parallel walls[10] or more recently in nanoporous membranes[11-14] are of interest due to the wide range of structures that can be produced. These structures may differ from that in the bulk behavior due to confinement and forced curvature.

Simulations of the confinement of symmetric diblock copolymers in cylindrical pores have been performed by He et al. and Fraaije et al. The results of their theoretical calculations yield two different results for a symmetric polymer depending on the strength of the surface interactions. In both studies, strong surface interactions caused the polymers to align in concentric cylinders, while weak interactions produced orientations perpendicular to their walls[15, 16].

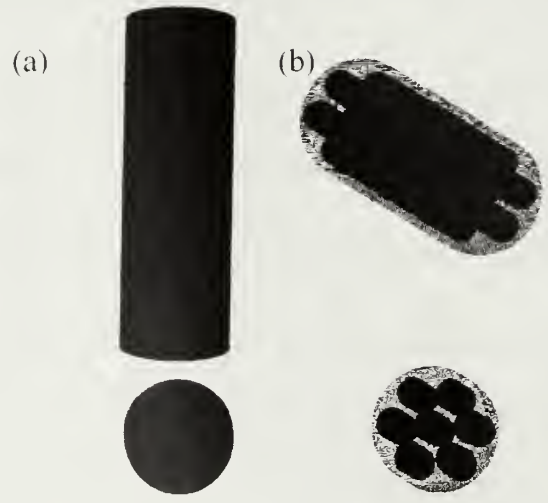


**Figure 1.2: schematic representations of block copolymers in confined geometries (a) symmetric (b) asymmetric copolymers**

Recent studies by Xiang et al. confirmed these predictions using styrene – butadiene block copolymers. In this study, both symmetric and asymmetric diblock copolymers were confined in anodized aluminum membranes with pore diameters of approximately 200 nm to form microphase-separated nanorods as drawn in Figure 1.2. Nanorods were produced by placing the membrane on a thick film of the polymer and annealing under vacuum for 24 hours above the glass transition. In this process, polymer was drawn into the pores by capillary forces.[11]

Capillary forces result from a reduction of free energy by replacing the air – wall interface with a copolymer – wall interface. The maximum height to which a copolymer may move into a pore is estimated to be:[17]

$$h_{max} = \frac{2\gamma_{copolymer/air}\cos\theta}{\rho g r} \qquad \textbf{(1.2)}$$

In this equation, $h_{max}$ describes the maximum height, $\theta$ the contact angle, g the gravitational constant, r the pore radius and $\gamma_{copolymer/air}$ the surface tension of the copolymer. As a result of its confinement, the polymer's symmetry and period varied greatly from that in the bulk.

### 1.4 Macromolecule-Metal Complexes

Macromolecule-metal complexes (MMCs) have been studied in great detail since they are prevalent in both natural and laboratory conditions. Examples of MMCs in nature occur in hemoglobin and in biological processes such as photosynthesis. They have also been prepared for diverse applications such as photonic band gap materials and self-healing materials.[18] This section includes an overview of the different types of macromolecular-metal complexes which have been prepared and how they are classified.

Macromolecular metal complexes are classified according to four different categories or types based on their bonds. Type I complexes describe bonding of metals to a polymer chain, while Type II complexes describe bonding of a ligand of a metal within a polymer chain. Similarly, Type III complexes describe a metal that is a part of the polymer and Type IV complexes describe metal particles that are physically incorporated into the polymer. This system of classification was first described by Wöhrle et al.[19] in 1996. Each category is discussed in further detail below.

Type I complexes typically form covalent, coordinative, complex, ionic and π-bonds with the macromolecule. Representative diagrams of each type are shown in Figure 1.3 below.

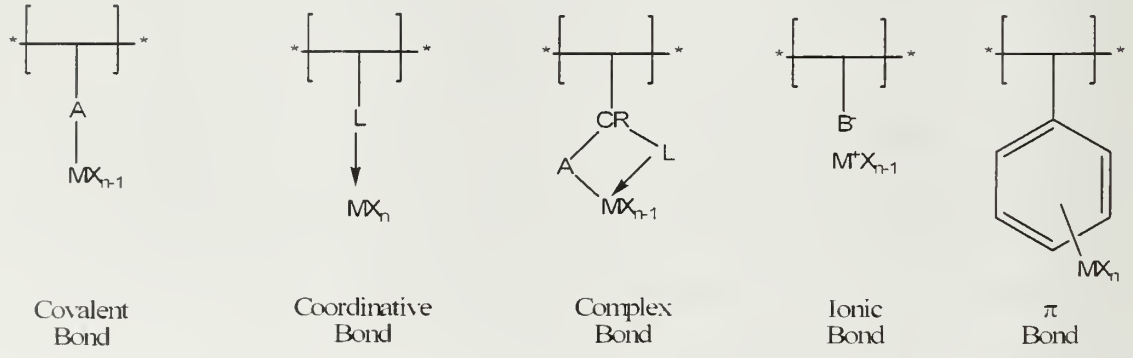


**Figure 1.3: Type I MMCs: Metals bound to macromolecules**

Several examples of Type I complexes can be found in current literature. For example, ionic bonding was used by Sohn et al.[7] and Möller[8] to produce polymer nanocomposites using PS-*b*-P4VP and PS-*b*-P2VP block copolymers, respectively. Sohn et al.'s method involved preparing a thin film of the block copolymer, annealing the sample to generate a lamellar structure parallel to the surface and then exposing it to $HAuCl_4$ and a reducing agent. In contrast, Möller prepared his films by casting them from a polymer/metal salt

solution followed by treatment with hydrogen sulfide gas. In both cases the metal particles were only formed in the vinylpyridine domain of the polymer.

An example of a Type II complex where the ligand of a metal or metal complex is incorporated within the polymer is shown in Figure 1.4. In this example the metal is associated with oxygen and nitrogen within the polymer. This type of complex is prepared by adding the metal to the monomer prior to its polymerization or by directly adding the metal to the polymer.[20]

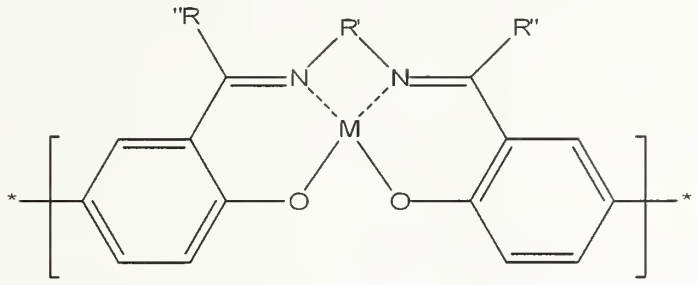


**Figure 1.4: Type II MMCs: noncyclic organic ligands chelate the metal to the polymer**

Type III complexes where the metal is part of the polymer chain can take many forms. For example homochain polymers with covalent metal-metal bonds and metallocenes as part of a polymer chain. Examples of these can be seen in Figure 1.5.

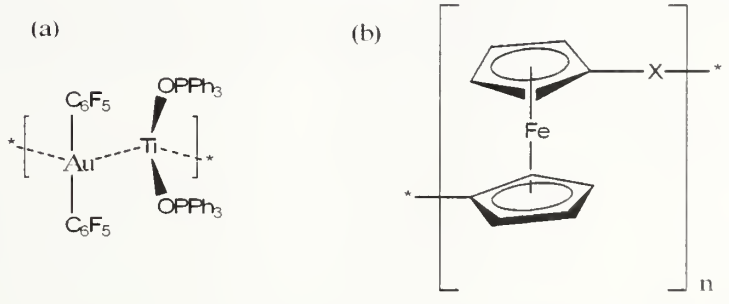


**Figure 1.5: Type III MMCs: (a) Gold and Titanium Polymer by Metal-Metal**

**Interaction[21] (b) Ferrocene Polymer[22]**

The final type of complex, Type IV features the physical incorporation of metal nanoparticles or complexes in polymers. A recent example of this type of complex from Lin et al. where they added cadmium selenide nanoparticles to a polystyrene-b-poly(2-vinylpyridne) solution and spun cast films.[23] The incorporation of the nanoparticles changed the surface interaction of the film resulting in domains perpendicular to the surface.

In this research Type I complexes were prepared and the metal complex was reduced to form a Type IV complex. These complexes were then characterized using the various techniques described in Chapter 2.

## 1.5 Supercritical Carbon Dioxide

The state of a pure substance under known conditions is often expressed graphically through a phase diagram. Phase diagrams illustrate how substances change their physical states when sufficient pressure or temperature is increased or decreased. This relationship is visible in the example phase diagram for carbon dioxide, as shown in Figure 1.5. As temperature and pressure increase along the liquid-gas line, the distinction between these two states eventually diminishes and the phases become virtually identical. This is said to occur at a substance's *critical point*. For carbon dioxide, this threshold occurs at 73.82 bar and 31.03°C. Beyond these conditions, carbon dioxide is said to be in its supercritical state.

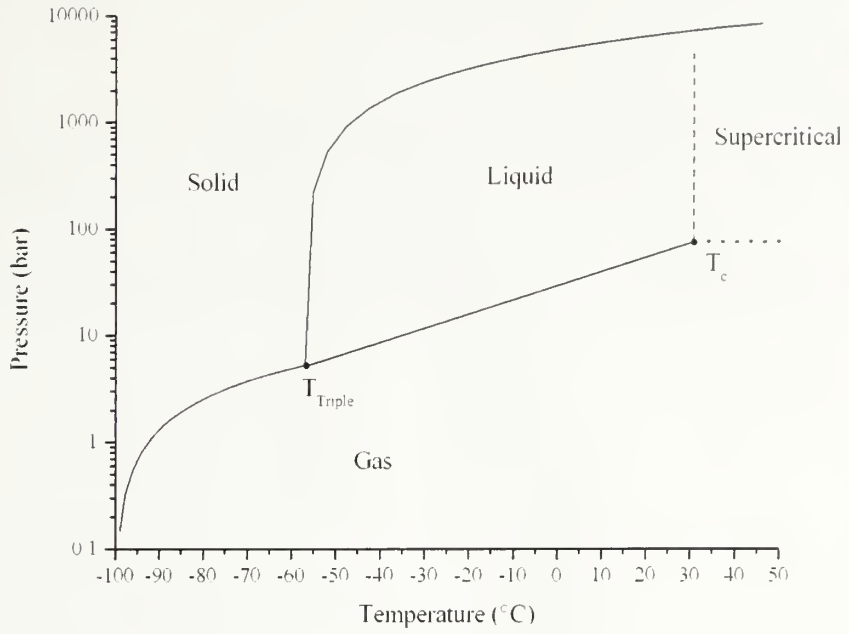


**Figure 1.6: Phase diagram for carbon dioxide**

The use of supercritical fluids in the laboratory provides many advantages including tunable densities, a lack of surface tension, higher diffusion rates and lower viscosity than conventional liquid systems. Densities ranging from 0.1 -1.0 g/mL are easily achieved by varying pressure or temperature.

Supercritical carbon dioxide does not dissolve most polymers; however, most polymers swell once exposed. It is therefore important to understand how this affects the free volume and glass transition, $t_g$. Research from Wissinger et al. examines these effects and documents a dramatic decrease in glass transition temperatures at relatively low pressures of carbon dioxide. [24] For instance, at 60 bars of pressure the glass transition of poly(styrene) was suppressed by 60°C.

Supercritical carbon dioxide is also an excellent solvent for most small molecules which makes it useful for practical applications including coffee decaffeination[25] and

substrate cleansing[26], as well as for research applications including various polymerizations[27, 28], and the formation of nanocomposites.[9] Here, supercritical carbon dioxide was used due to its high diffusion rates into polymers and solubility and rapid delivery of the organometallic precursors into the films. These properties make it possible to selectively metallize polymer films without the need to crosslink the film.

## 1.6 References


1. Bates. F. S.: Fredrickson. G. H.. Block Copolymers - Designer Soft Materials. *Physics Today* 1999, **52**. (2). 32-38.

2. Bates. F. S.. Block Copolymers near the Microphase Separation Transition 2. Linear Dynamic Mechanical Properties. *Macromolecules* 1984, **17**. 2607-2613.

3. Schultz. M. F.: Khandpur. A. K.: Bates. F. S.. Phase Behavior of Polystyrene-Poly(2-vinylpyridine) Diblock Copolymers. *Macromolecules* 1996, **29**. 2857-2867.

4. Seregina. M. V.: Bronstein. L. M.: Platonova. O. A.: Chernyshov. D. M.: Valetsky. P. M.. Preparation of Noble metal Colloids in Block Copolymer Micelles and Their Catalytic Properties in Hydrogenation. *Chem. Mater.* 1997, **9**. 923-931.

5. Kuo. S. W.: Wu. C. H.: Chang. F. C.. Thermal Properties. Interaction. Morphologies. and Conductivity Behavior in Blends of Poly(vinylpyridine)s and Zinc Perchlorate. *Macromolecules* 2004, **37**. (1). 192-200.

6. Kim. S. H.: Misner. M. J.: Russell. T. P.. Solvent-Induced Ordering in Thin Film Diblock Copolymer/Homopolymer Mixtures. *Adv. Mater.* 2004, **16**. 2119.

7. Sohn. B. H.: Seo. B. H.. Fabrication of the Multilayer Nanostructure of Alternating Polymers and Gold Nanoparticles with Thin Films of Self-Assembling Diblock Copolymers. *Chem. Mater.* 2001, **13**. 1752-1757.

8. Möller. M.. Inorganic Nanoclusters in Organic Glasses - Novel Materials for Electro-Optical Applications. *Synthetic Metals* 1991. 1159-1162.

9. Brown. G. D.: Watkins. J. J.. Carbon Dioxide - Dialated Block Copolymer Templates for Nanostructured Materials. *Mat. Res. Soc. Symp. Proc.* 2000, **585**. 169-174.

10. Walton. D. G.: Kellogg. G. J.: Mayes. A. M.: Lambooy. P.: Russell. T. P.. A Free Energy Model for Confined Diblock Copolymers. *Macromolecules* 1994, **27**. 6225-6228.

11. Xiang. H.: Shin. K.: Kim. T.: Moon. S. I.: McCarthy. T. J.: Russell. T. P.. Block Copolymers under Cylindrical Confinement. *Macromolecules* 2004, **37**. 5660-5664.

12. Xiang, H.; Shin, K.; Kim, T.; Moon, S.; McCarthy, T. J.; Russell, T. P., The influence of confinement and curvature on the morphology of block copolymers. *Journal of Polymer Science, Part B: Polymer Physics* 2005, **43**, (23), 3377-3383.

13. Xiang, H.; Shin, K.; Kim, T.; Moon, S.; McCarthy, T. J.; Russell, T. P., From Cylinders to Helices upon Confinement. *Macromolecules* 2005, **38**, (4), 1055-1056.

14. Shin, K.; Xiang, H.; Moon, S.; Kim, T.; McCarthy, T. J.; Russell, T. P., Curving and Frustrating Flatland. *Science* 2004, **306**, (5693), 76.

15. Sevink, G. J. A.; Zvenlindovsky, A. V.; Fraaije, J. G. E. M., Morphology of symmetric block copolymer in a cylindrical pore. *J. Chem. Phys.* 2001, **115**, (17), 8226-8230.

16. He, X.; Song, M.; Liang, H.; Pan, C., Self-assembly of the symmetric diblock copolymer in a confined state: Monte Carlo simulation. *J. Chem. Phys.* 2001, **114**, (23), 10510-10513.

17. Suh, K. Y.; Kim, Y. S.; Lee, H. H., Capillary Force Lithography. *Adv. Mater.* 2001, **13**, (18), 1386.

18. Lin, Y.; Zhang, Q.; Gupta, S.; Wang, Q.; Balazs, A.; Emrick, T.; Russell, T. P. In *Nanoparticles at interfaces: From membranes to crack healing*, Abstracts of Papers, 230th ACS National Meeting, Washington, DC, 2005; Washington, DC, 2005.

19. Ciardelli, F.; Tsuchida, E.; Wöhrle, D., *Macromolecule-Metal Complexes*. Springer: Berlin, 1996.

20. Wöhrle, D., Polymer square planar metal chelates for science and industry. Synthesis, properties and applications. *Adv. Polym. Sci.* 1983, **50**, 45-134.

21. Kodaira, T.; Wantabe, A.; Ito, O.; Mochida, K., Third-order nonlinear optical properties of thin films of organogermane homopolymers and organogermane-organosilane copolymers. *Adv. MAter.* 1995, **7**, (11), 917-919.

22. Manners, I., Ring-opening polymerization of metallocenophanes. *Adv. MAter.* 1994, **6**, (1), 68-71.

23. Lin, Y.; Boeker, A.; He, J.; Sill, K.; Xiang, H.; Abetz, C.; Li, X.; Wang, J.; Emrick, T.; Long, S.; Wang, Q.; Balazs, A.; Russell, T. P., Self-directed self-assembly of nanoparticle/copolymer mixtures. *Nature* 2005, **434**, (7029), 55-59.

24. Wissinger, R. G.; Paulaitis, M. E., Swelling and Sorption in Polymer-$CO_2$ Mixtures at Elevated Pressures. *Journal of Polymer Science Part B* 1987, **25**, (12), 2497-2510.

25. Udayasankar, K.; Manohar, B.; Chokkalingam, A., A Note on Supercritical Carbon Dioxide Decaffeination of Coffee. *Journal of Food Science and Technology* 1986, **23**, (6), 326.

26. Spall, W. D.; Laintz, K. E., A Survey on the use of Supercritical Carbon Dioxide as a Cleaning Solvent. *Supercritical Fluid Cleaning* 1998, **162**, (194), 162-194.

27. DeSimone, J. M.; Guan, Z.; Elsbernd, C. S., Synthesis of fluoropolymers in supercritical carbon dioxide. *Science* 1992, **257**, (5072), 945-947.

28. Guan, Z.; Combes, J. R.; Menceloglu, Y. Z.; DeSimone, J. M., Homogeneous free radical polymerizations in supercritical carbon dioxide: 2. Thermal decomposition of 2,2'-azobis(isobutyronitrile). *Macromolecules* 1993, **26**, (11), 2663-2669.

# CHAPTER 2

# EXPERIMENTAL METHODS

## 2.1 Introduction

This research project required a variety of techniques and instrumentation to study the selective metallization of block copolymer thin film and bulk samples. Techniques and instrumentation utilized include: anionic polymerization, small (SAXS) and wide (WAXS) angle x-ray scattering (SAXS); x-ray reflectivity; x-ray photoemission spectroscopy (XPS); transmission electron microscopy (TEM); infrared spectrometry (IR); and ultra violet-visible spectroscopy (UV-VIS). A brief overview of the theory behind each of these techniques is described within this chapter.

## 2.2 Anionic Polymerization

Living anionic polymerization is a powerful technique that allows for the synthesis of well defined, low polydispersity polymers.[1, 2] The important features of living polymerizations are the absence of termination reactions, rapid initiation of all polymer chains, and a linear growth throughout the reaction. To achieve living conditions the monomers, solvents and glassware must be completely free of reactive gases such as carbon dioxide and oxygen, and water. The purification of starting materials and the polymerization reaction will be described in this section.

Anionic polymerization for the preparation of homopolymers and block copolymers of styrene and 2-vinylpyridine were carried out in tetrahydrofuran (THF) at

-78 °C under ultrahigh purity argon with secondary-butyl lithium as the initiator. All glassware was cleaned and flame dried before use.

THF was purified by passing it through two aluminum oxide columns and collecting it into a 2 L flask containing 5 g of sodium in paraffin wax and 10 g of benzophenone. The solvent was then stirred until a deep purple color develops, indicating it is dry and oxygen free. Styrene and 2-vinylpyridine monomers were degassed and stirred over calcium hydride for 24 hours. Next, styrene and 2-vinylpyridine were distilled directly onto dried dibutylmagnesium and trioctylaluminum, respectively, and stirred for at least 4 hours. After purifying, the desired amounts of solvent and monomer is distilled into specially designed flasks and burettes and attached to the polymerization reactor. THF is then added to the reactor and cooled to -78 C using a dry ice/isopropyl alcohol bath (~30 min). Next, the required amount of sec-butyl lithium is added via syringe to the cool THF. Styrene monomer is then added drop-wise to the reaction, allowed to stir for 30 min and an aliquot is taken to determine the block molecular weight. 2-vinylpyridne is then added and allowed to react for 45 minutes followed by a small amount of anhydrous isopropyl alcohol to terminate the reaction. The final product is precipitated in hexanes and dried in a vacuum oven.

The total molecular weight and polydispersity were determined by gel permeation chromatography. Finally, the mole fractions of the polymer were determined by proton NMR.

### 2.3 Organometallic Reduction Using Hydrogen Sulfide Gas

Hydrogen sulfide gas was used in this research for the reduction of organometallics to prepare zinc sulfide within block copolymers. In this section the procedure developed and the safe use of hydrogen sulfide gas will be described.

A metallized polymer sample on a silicon wafer was placed into a 6 mL high-pressure vessel and sealed. The threads of the end caps were wrapped in fresh Teflon tape prior to sealing. Stainless steel plugs of different sizes were used to reduce the volume of the vessel. After the vessel was sealed it was pressurized with nitrogen to ensure that there were no leaks. If no leaks were detected, the vessel was heated to 80°C by using a band heater. An Omega temperature controller and thermocouple were used to monitor the temperature. Once the desired temperature was reached, each connection was covered with moistened lead acetate paper and the vessel was pressured to 5 bar of $H_2S$. If there was a leak, the lead acetate paper turned black from continuous exposure to the gas and the vessel was resealed.

After the reaction the vessel and the line were vented through a series of lead nitrate solutions. The hydrogen sulfide gas reacted with the lead in solution to form a black precipitate of lead sulfide. To ensure that the system was clear of any hydrogen sulfide gas, it was pressurized with nitrogen and vented through fresh lead nitrate solutions. This was repeated until lead sulfate precipitate stopped forming.

### 2.4 Small and Wide Angle X-ray Scattering

Small angle x-ray scattering (SAXS) is a technique used extensively for studying the structural features and orientation of polymers[3]. In the case of polymers, and more

specifically block copolymers, an electron density difference is required to determine the spacing or morphological characteristics of a polymer. In a typical SAXS experiment, an incident x-ray beam is sent through a polymer sample, where scattered x-rays are detected as a function of the scattering wave vector, q, as described by Equation 2.1 below.

$$q = \frac{4\pi}{\lambda}\sin\theta \qquad \textbf{(2.1)}$$

In this equation, $\lambda$ represents the wavelength of the x-rays and $2\theta$ is the scattering angle. In addition, the spacing of a polymer, d, is determined by Equation 2.2 below.

$$d = \frac{2\pi}{q^*} \qquad \textbf{(2.2)}$$

where represents the value of q of the first order reflection.

Small angle x-ray scattering may be used to determine block copolymer morphologies by comparing the relative positions of the maxima in an intensity versus q plot. For example, copolymers with lamellar, cylindrical, and spherical morphologies will have peaks that have a ratio in q of 1:2:3:4, 1:$\sqrt{3}$:$\sqrt{7}$:$\sqrt{9}$, and 1:$\sqrt{2}$:$\sqrt{3}$:$\sqrt{4}$:$\sqrt{5}$ respectively[4]. In lamellar systems where the polymer is perfectly symmetric, even order peaks may not be apparent.

Wide angle x-ray scattering (WAXS) experiments are conducted in the same geometry as SAXS; but at larger angles and hence, probe features on a smaller distance scale. Consequently, it is possible to determine the crystalline structures of metals and the intermolecular spacing in polymer chains.

In this project, the block copolymer spacing, d, and morphologies were determined by the use of SAXS. WAXS was used to verify the state of the metal in the

polymer and determine the intermolecular spacings of the polymer chains and any changes the metals might have caused.

### 2.5 Transmission Electron Microscopy

In transmission electron microscopy (TEM), electrons are transmitted through thin samples and focused so an image or diffraction pattern can be viewed. The scattering that is observed in the diffraction pattern obeys Bragg's Law, Equation 2.3:

$$\lambda = 2d\sin\theta \qquad \textbf{(2.3)}$$

where $\lambda$ is the wavelength, d the plane spacing, and $\theta$ is the angle of diffraction. The diffraction pattern of a sample provides structural information in Fourier space. Use of lenses further allows one to observe a real space image of the sample.

TEM may be used in several different modes including mass-thickness contrast, bright field diffraction contrast, and dark field diffraction contrast. In mass-thickness contrast, distinctions arise from thickness and electron density differences. In bright field mode, electrons are diffracted from crystalline regions within the sample and appear dark. Conversely, in dark field mode electrons which are not scattered appear dark.

TEM was used extensively throughout this project to visually investigate locations where nanoparticles formed, to verify selective metallization occurred, and to determine the crystalline structure of the nanoparticles by electron diffraction.

### 2.6 X-ray Reflectivity

X-ray reflectivity is a technique that is commonly used to study the surface behavior and structure of polymer thin films. This technique detects variations in

electron density as a function of depth over distances of hundreds of nanometers with a spatial resolution of ~1 nm.[5] In a typical reflectivity experiment x-rays reflected from a surface is measured as a function of the wavevector $k_z$ (Equation 2.4) as represented in Figure 2.1.

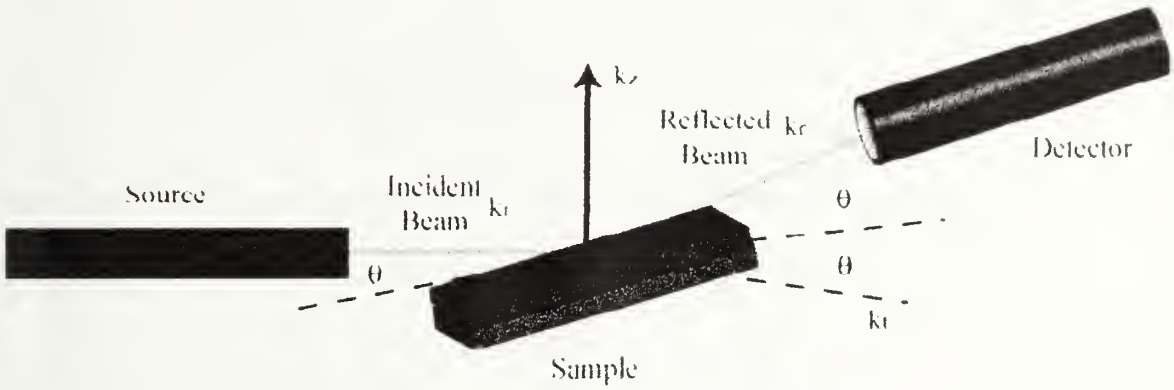


**Figure 2.1 Diagram of reflectivity from a surface**

In the diagram, θ is the grazing angle of the incidence, and $k_i$, $k_r$ and $k_t$ are the incident, reflected and transmitted wavevectors, respectively, where

$$k_z = \frac{2\pi}{\lambda}\sin\theta \qquad \textbf{(2.4)}$$

It is important to note that the refractive index of materials for x-rays is only slightly less than one. The refractive index of a given material is approximated using the formula in Equation 2.5.

$$n = 1 - \delta + i\beta \qquad \textbf{(2.5)}$$

In this case, ρ is the electron density of the material while $r_0$ represents the classical electron radius where:

$$\delta = \frac{\lambda^2 \rho r_0}{2\pi} \qquad \textbf{(2.6)}$$

The absorbance of the material, β, is given by:

$$\beta = \frac{\lambda \mu}{4\pi} \qquad \textbf{(2.7)}$$

where, μ is the absorption coefficient of the material.

The reflection coefficient at the interface between layers i and i+1 is calculated using Fresnel's equation (Equation 2.8).

$$r_{i,i+1} = \frac{(k_{zi} - k_{z(i+1)})}{(k_{zi} + k_{z(i+1)})} \qquad \textbf{(2.8)}$$

The reflectivity Figure 2.1 depicts, shows a sample has two important interfaces: air/polymer and polymer/substrate. Both of these interfaces has its own reflectivity coefficient, $r_{0,1}$ and $r_{1,2}$ respectively, which may be used to determine reflectivity, as calculated by Equation 2.9 below.

$$r = \frac{r_{0,1} + r_{1,2} e^{(2ik_{z1}d)}}{1 + r_{0,1} r_{1,2} e^{(2ik_{z1}d)}} \qquad \textbf{(2.9)}$$

In this research, x-ray reflectivity was used to investigate both homopolymer and diblock copolymer thin films before and after metallization. From this data, sample thicknesses and scattering length density profiles were each calculated.

## 2.7 UV-VIS Spectroscopy

Absorption of light in the visible (7000-4000 Angstroms) and ultraviolet (UV) (3900-10 Angstroms) range is dependent on the electronic structure of a molecule or metal nanoparticle. In organic molecules the absorbed energy causes an excitation of electrons from their ground states to higher orbitals. For metal nanoparticles the absorption bands are from the excitation of plasmon resonances.[6] Therefore,

characteristic groups and the presence and size of nanoparticles can be determined using UV-VIS spectroscopy.

In this project, UV-VIS spectroscopy was used to determine the infusion and reduction of the metal precursors and the formation of metal nanoparticles. In some cases, the precursor or metal particle did not absorb light in the accessible light range. In these cases, x-ray scattering and electron diffraction were used to determine if any reaction occurred.

**2.8 IR Spectroscopy**

Infrared radiation (IR) with wavelengths between 10,000-100 $cm^{-1}$ are absorbed and converted by organic and polymeric molecules into molecular vibration. Stretching and bending are two kinds of the several molecular vibrations which are possible. Stretching vibrations occur along a bond axis, while bending vibrations result in a change in the bond angle. The frequency of theses vibrations depends on three factors: 1) the relative masses of the atoms, 2) the force constants of the bonds, and 3) the geometry of the molecule. Consequently, IR- spectroscopy was used in this research to determine functional groups, bond types, and changes to specific bonds within a molecular structure[7].

Specifically, IR spectroscopy was used in this project to investigate how metal precursors and metal nanoparticles interacted within the polymer system. A similar method was investigated by Kou et al.[8] using FT-IR to determine various bending and stretching modes in poly(2-vinylpyridine) and poly(4-vinylpyridine) and their interactions with zinc perchlorate. Their results revealed an increase in wavenumber of

the stretching mode vibrations, which they attributed to π-bonding coordination of the cation with the polymer. These results demonstrate it is possible to determine whether a metal precursor is binding to a polymer and if metal particles continue to interact with the polymer after reduction.

### 2.9 X-ray Photoelectron Spectroscopy

X-ray photoelectron spectroscopy (XPS) techniques employ a monochromatic X-ray beam that is directed at a sample tilted at an angle between 0 and 90 degrees. This particular geometry allows photoelectrons from the top 10-100 Angstroms of the surface to escape. XPS utilizes these emitted photoelectrons to determine the structural composition of a sample's surface. In addition, because the energy of the emitted photoelectrons are characteristic to each element within a sample, it is possible to determine its elemental composition, distribution throughout the sample and chemical bonding characteristics near the surface.[9]

X-ray photoemission spectroscopy was used throughout this investigation to probe the macromolecule-metal nanocomposites produced in the project. Specifically, the physical state and atomic percent of the metals produced were investigated.[8]

## 2.10 References


1. Hadjichistidis, N.; Iatrou, H.; Pispas, S.; Pitsikalis, M., Anionic Polymerization: High Vacuum Techniques. *J. Polym. Sci. Part A Polym. Chem.* 2000, **38**, 3211-3234.

2. Hadjichristidis, N.; Pispas, S.; Floudas, G. A., ***Block Copolymers Synthetic Strategies, Physical Properties, and Applications***. John Wiley and Sons: Hoboken, New Jersey, 2003.

3. Glatter, O.; Kratky, O., *Small Angle X-ray Scattering*. Academic Press: New York, 1982.

4. Hameley, I. W., *The Physics of Block Copolymers*. Oxford University Press: New York, 1998.

5. Russell, T. P., X-ray and Neutron Reflectivity for the investigation of polymers. *Materials Science Reports* 1990, 173-271.

6. Creighton, J. A.; Eadon, D. G., Ultraviolet-Visible Absorption Spectra of the Colloidal Metallic Elements. *J. Chem. Soc. Faraday Trans.* 1991, **87**, (24), 3881-3891.

7. Silverstein, R. M.; Bassler, G. C.; Morrill, T. C., *Spectrometric Identification of Organic Compounds*. Fifth ed.; John Wiley and Sons: New York, 1991.

8. Kuo, S. W.; Wu, C. H.; Chang, F. C., Thermal Properties, Interaction, Morphologies, and Conductivity Behavior in Blends of Poly(vinylpyridine)s and Zinc Perchlorate. *Macromolecules* 2004, **37**, (1), 192-200.

9. Gauglitz, G.; Vo-Dinh, *Handbook of Spectroscopy*. Wiley-VCH: 2003; Vol. 1.

# CHAPTER 3

# PREPARATION OF POLY(2-VINYLPYRIDINE) NANOCOMPOSITE THIN FILMS

## 3.1 Introduction

Nanocomposites have been prepared using a variety of techniques including solution casting films of polymer with metal salts or organometalics[1-3], exposing thin films to metal acid and salt solutions[4-6], and infusing metal or metal oxide precursors using supercritical carbon dioxide[7, 8]. These types of metallizations have been extensively studied in macromolecules containing pyridine or bipyridyl functionality due to their excellent complexing abilities.[9-11] Previous studies have included the quaternization of both 2- and 4-vinylpyridine to complex with metal ions and form coordinative bonds through ligand exchange reactions.[1, 2, 4, 5, 7, 12, 13]

In this chapter the preparation and characterization of metal complexes of poly(2-vinylpyridine) with silver, platinum and zinc used in this project are discussed. Both thin and thick films were investigated to probe the interactions and reductions of the bound metal precursors.

## 3.2 Experimental

Metal-polymer composites of poly(2-vinylpyridine) with silver, platinum and zinc sulfide were prepared using supercritical carbon dioxide soluble metal precursors. These composites were then characterized using FT-IR and UV-VIS spectroscopies, wide angle x-ray scattering (WAXS), x-ray reflectivity and x-ray photoluminescent spectroscopy (XPS).

### 3.2.1 Materials

All materials in this project were used as received from their manufacturers unless otherwise stated. Homopolymer poly(2-vinylpyridine) (P2VP) samples of molecular weight 47 k and PDI 1.03 and 50 k and PDI 1.04 were each prepared by living anionic polymerization, as previously described in Chapter 2 or used directly as purchased from Polymer Source, Inc. Hydrogen sulfide gas and metal precursors including (1,5-Cyclooctadiene) (hexafluoroacetylacetanato)silver(I), (1,5-Cyclooctadiene) dimethylplatinum(II), and Zinc hexafluoroacetylacetonate dihydrate were purchased from Aldrich Chemical Company and Strem Inc. Coleman grade carbon dioxide and ultra-high purity hydrogen were purchased from Merriam-Graves Company, and quartz slides and doped and undoped silicon wafers were each purchased from Chemglass, Inc. and International Wafer Services, respectively. All wafers were cleaned using a NoChromix™ – sulfuric acid bath and thoroughly rinsed with deionized water prior to their use.

### 3.2.2 Preparation and Characterization of Poly(2-vinylpyridine)-Silver Nanocomposites

Thin films of P2VP were spun cast onto high resistance silicon wafers and quartz slides from solutions of the polymer in n-propanol (~3 wt%). The polymer films, ranging from 40-100 nm in thickness, were then annealed for 24 hours at 170 °C to remove any excess solvent. Thick films (~100 μm) for wide angle x-ray scattering were prepared by melt pressing the dry polymer powder at 5000 psi and 170 °C. Next, each film was cut into a 2.5 cm x 1.5 cm section and placed into a 25 mL stainless steel high pressure vessel purchased from Thar Technologies, Inc. with a known quantity of Ag(COD)hfac (5 mg)

and sealed under nitrogen. Carbon dioxide was introduced to the vessel at 40 °C using a computer controlled syringe pump from Teledyne ISCO at 100 bar and the reaction was allowed to proceed for one hour. Following reaction, the vessel was slowly depressurized to prevent any foaming of the polymer film. Remaining, unbound metal precursor was subsequently extracted from the films using $CO_2$ at 40°C and 100 bar. Finally, reduction of the metal precursor was performed under high pressure hydrogen at 70 bar and 60 °C or by exposing the film to a solution of $NaBH_4$ (5 mg/mL) in a water/ethanol mixture. Reduction times ranged from 30 seconds to 24 hours.

Following reduction, the UV-VIS absorption spectra of P2VP homopolymer and composites were obtained using an Agilent 8453 UV-Visible spectrophotometer, by scanning between 200 and 600 nm. A clean quartz slide was run as a blank and subtracted from each spectrum to adjust for background absorbance. Similarly, metallized homopolymer P2VP on undoped silicon wafers were analyzed using a Bio-Rad FTS 3000 FT-IR spectrometer in transmission mode and scanned from 400 to 4000 $cm^{-1}$. Background scans were collected and subtracted from each spectrum. Finally, x-ray reflectivity and wide angle x-ray scattering (WAXS) were used to analyze each sample.

Figures 3.1 and 3.2 show the UV-VIS absorbance spectra for two P2VP thin films (40 nm) metallized with Ag(COD)hfac: (a) was reduced with hydrogen gas at 70 bar and 60°C, and (b) was reduced using $NaBH_4$ in solution. Absorption of the films were measured at regular intervals to monitor the reduction of the precursor, as depicted in Figure 3.1. The P2VP, diketone ligand of the metal precursor, and silver nanoparticles

formed following reduction show three absorbencies at 260, 316 and 426 nm, respectively.

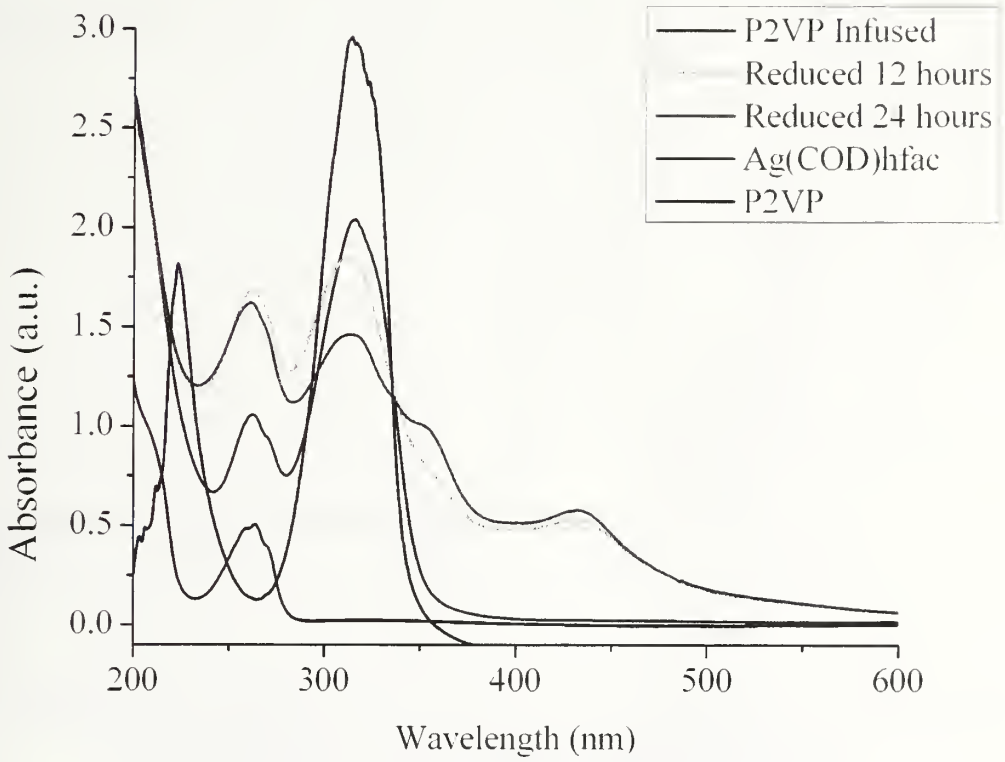


**Figure 3.1: UV-VIS spectroscopy of Poly(2-vinylpyridine) infused with Ag(COD)hfac and reduced with hydrogen gas**

Figure 3.2 shows three similar peaks; however, in this case, the reduction of the precursor occurred more rapidly, reaching complete reduction after 30 seconds of exposure to the $NaBH_4$ solution. The absorbance of the silver nanoparticles in the dielectric medium is consistent with previously reported measurements.[14-19]

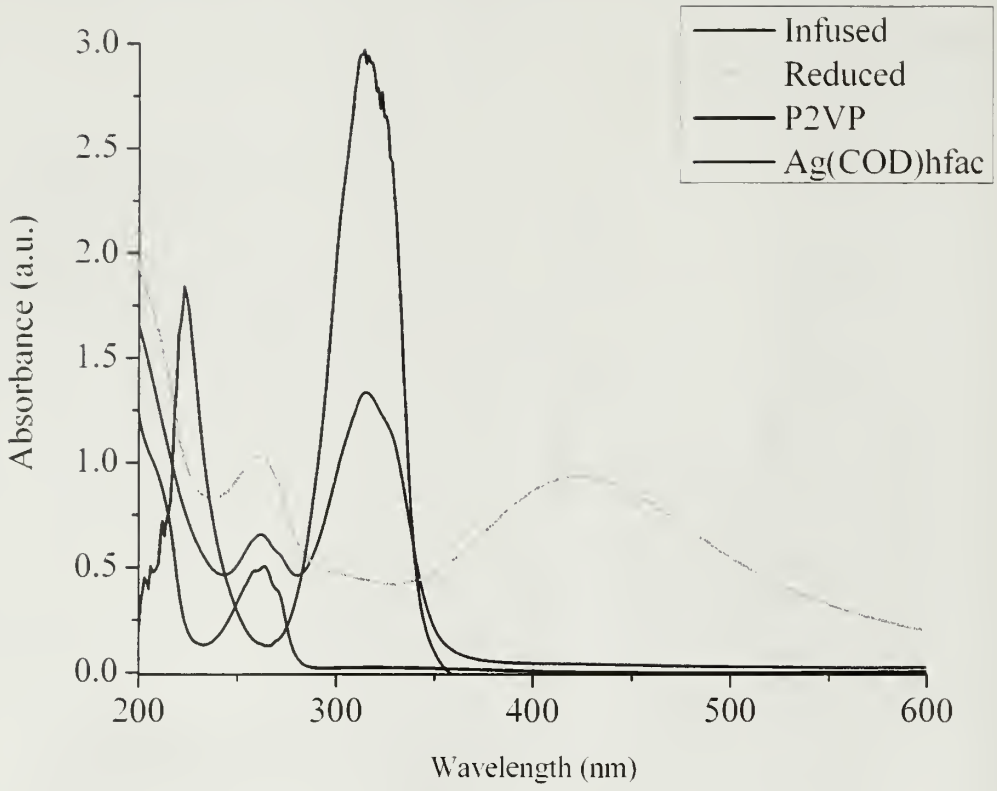


**Figure 3.2: UV-VIS spectroscopy of Poly(2-vinylpyridine) infused with Ag(COD)hfac and reduced with sodium borohydride**

Infrared spectroscopy of homopolymer P2VP shows characteristic peaks for select pyridine ring stretching (1590, 1568, 1473, 1433, 993 and 625 $cm^{-1}$) and for the carbon–hydrogen bending (733 $cm^{-1}$) modes.[20, 21] Figure 3.3 focuses on the carbon–nitrogen stretch at 1590 $cm^{-1}$ before and after infusion of Ag(COD)hfac and following reduction with $NaBH_4$.[22] The carbon–nitrogen stretch increased to 1603 $cm^{-1}$ revealing a strong interaction between the metal precursor and the pyridine ring of the polymer. Kuo et al. describe similar behavior in blends of zinc perchlorate and P2VP and P4VP homopolymers.[21] Finally, following reduction, the carbon-nitrogen stretch returns to its original position suggesting that the polymer no longer interacts strongly with the silver nanoparticles formed.

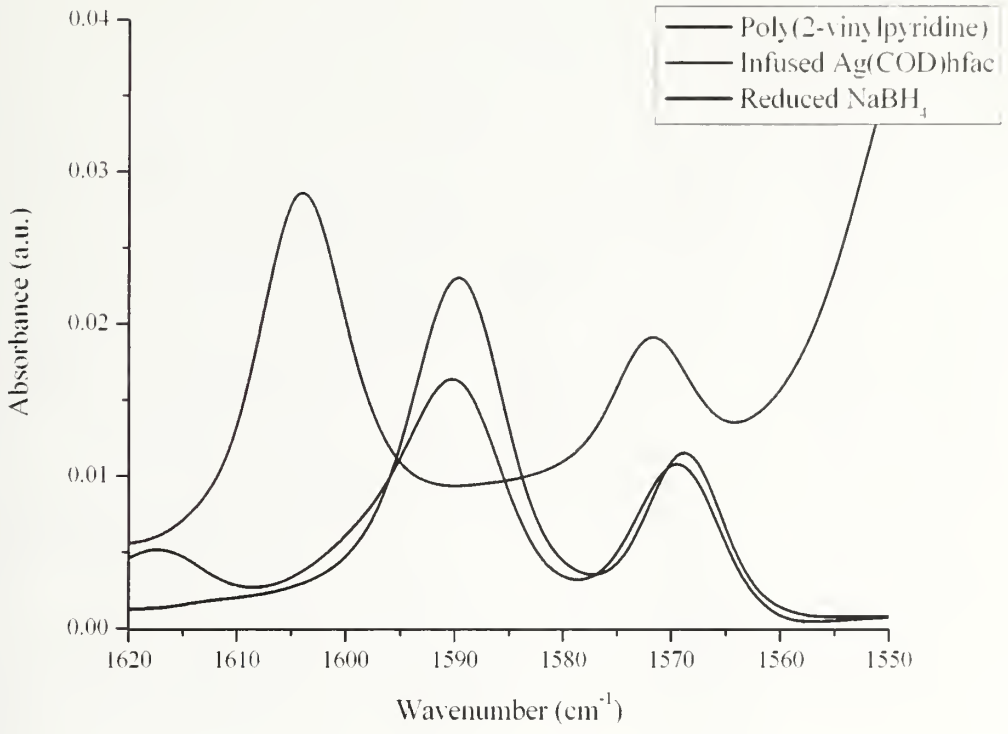


**Figure 3.3: FT-IR of Poly(2-vinylpyridine) infused with Ag(COD)hfac and reduced with $NaBH_4$**

Specular x-ray reflectivity of the homopolymer and composite films are shown in Figure 3.4. By use of Equation 3.1[23] and the average separation of the Kiessig fringe, the film thicknesses of the P2VP and P2VP/silver composites were determined to be 51.0 and 96.8 nm, respectively. The increase in overall film thickness was ~45.8 nm or 89%.

$$d = \frac{\pi}{\Delta k_{z0}} \qquad \textbf{(3.1)}$$

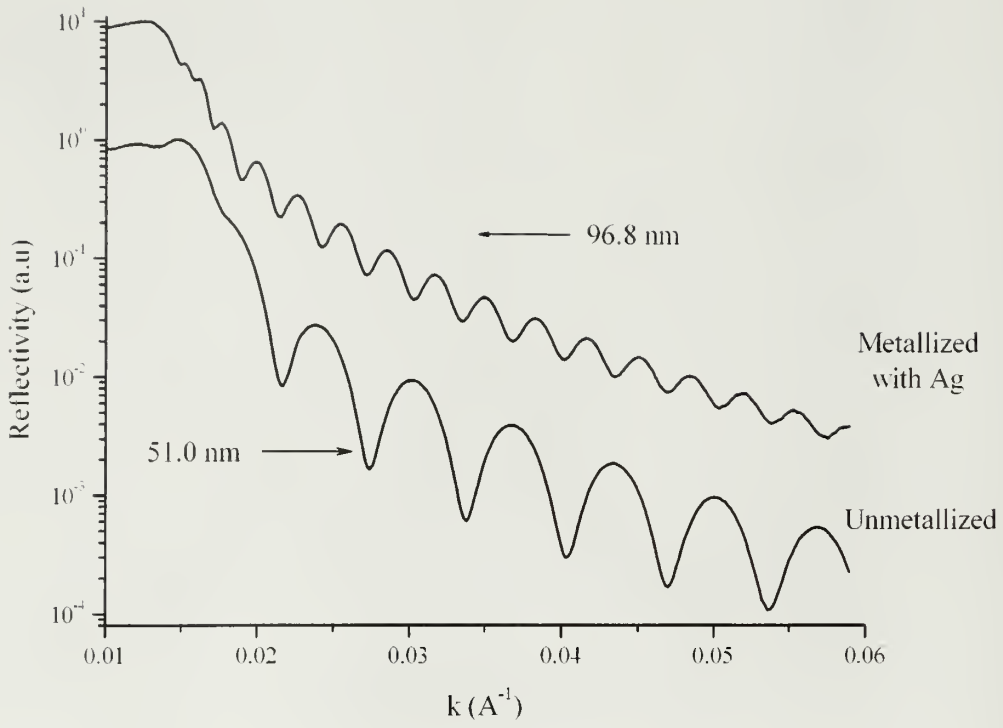


**Figure 3.4: Specular x-ray reflectivity of P2VP and P2VP/Silver films**

Wide angle x-ray scattering (WAXS) was performed on thick P2VP and P2VP/silver films to determine how the polymers interchain and pendent group spacings were each affected during metallization. Figure 3.4 illustrates the scattering profiles for both the unmetallized and metallized samples. While literature values for the interchain and pendent group spacings were 7.8 and 4.4 Å, respectively[21]; the measured values before and after metallization were 8.0 and 4.6 Å and 14.9 and 4.5 Å, respectively. Thus, an increase in the interchain spacing by 7.1 Å or 89 % was recorded over the initial measurement.

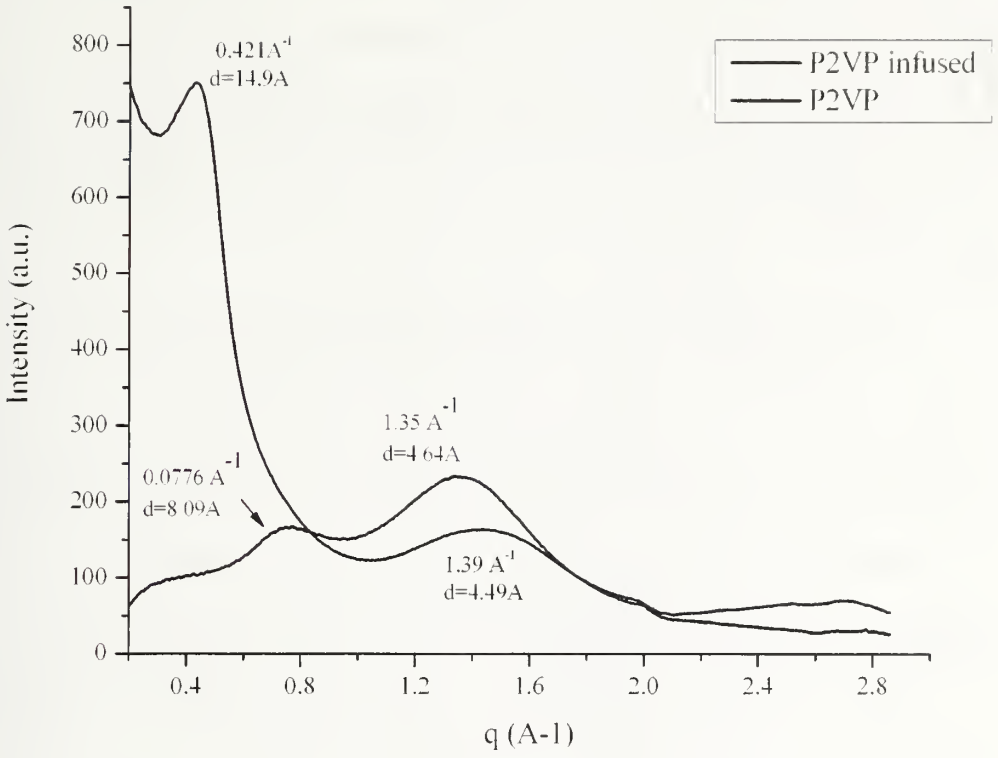


**Figure 3.5: Wide angle x-ray scattering of P2VP and P2VP/silver composite films**

### 3.2.3 Preparation and Characterization of Poly(2-vinylpyridine)-Platinum Nanocomposites

Thin films of P2VP were spin coated onto high resistance silicon wafers and quartz slides using solutions of the polymer in n-propanol (~3 wt%). The polymer films, ranging from 40-150 nm in thickness, were then annealed for 24 hours at 170 °C to remove any excess solvent. Next, each film was cut into a 2.5 cm x 1.5 cm section and placed into a 25 mL stainless steel high pressure vessel from Thar Technologies, Inc. with a known quantity of $Pt(COD)Me_2$ (5 mg) and sealed under nitrogen. Carbon dioxide was then introduced to the vessel at 60 °C using a computer controlled syringe pump purchased from Teledyne ISCO at 200 bar and the reaction was allowed to proceed

for 1 hour. Following reaction, the vessel was slowly depressurized to prevent any foaming of the polymer film. Unbound metal precursor was extracted from the films using $CO_2$ at 60°C and 200 bar. Finally, reduction of the metal precursor was performed under high pressure hydrogen at 70 bar and 60 °C. Reduction times varied between 1-24 hours.

Following reduction, the metallized homopolymer P2VP deposited on undoped silicon wafers were analyzed using a Bio-Rad FTS 3000 FT-IR spectrometer in transmission mode. Samples were scanned from 400 to 4000 $cm^{-1}$ and background scans were collected and subtracted from each spectrum. Lastly, specular x-ray reflectivity was performed on a Panalytical XPERT instrument to further analyze each sample.

Figure 3.6 focuses on the carbon–nitrogen stretch at 1590 $cm^{-1}$ before and after infusion of $Pt(COD)Me_2$.[22] This data reveals that the carbon–nitrogen stretch does not change suggesting there is no interaction between the metal precursor and the pyridine ring of the polymer. This lack of interaction may result from the thermal reduction of the platinum precursor at 60 °C.

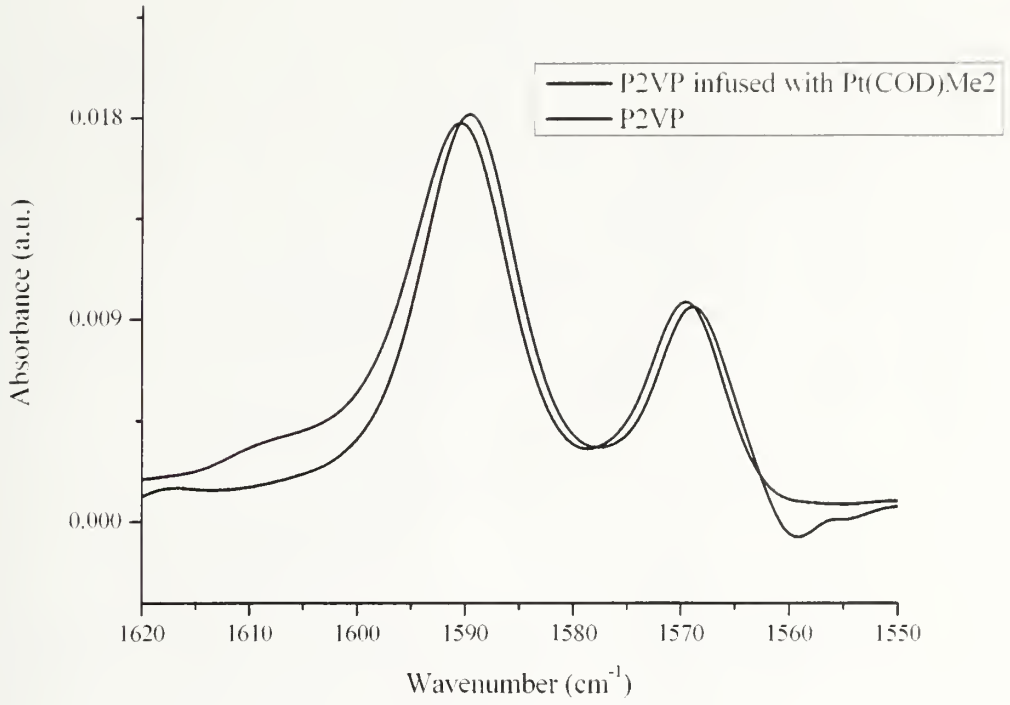


**Figure 3.6: FT-IR of Poly(2-vinylpyridine) before and after infusion with $Pt(COD)Me_2$**

Specular x-ray reflectivities of the homopolymer and composite films are shown in Figure 3.7. Again, equation 3.1[23] was used to determine the films thickness by calculating the average separation of the Kiessig fringes. These were determined to be 123.2 and 136.1 nm, respectively; while the increase in overall film thickness was ~12.9 nm or 10.5%.

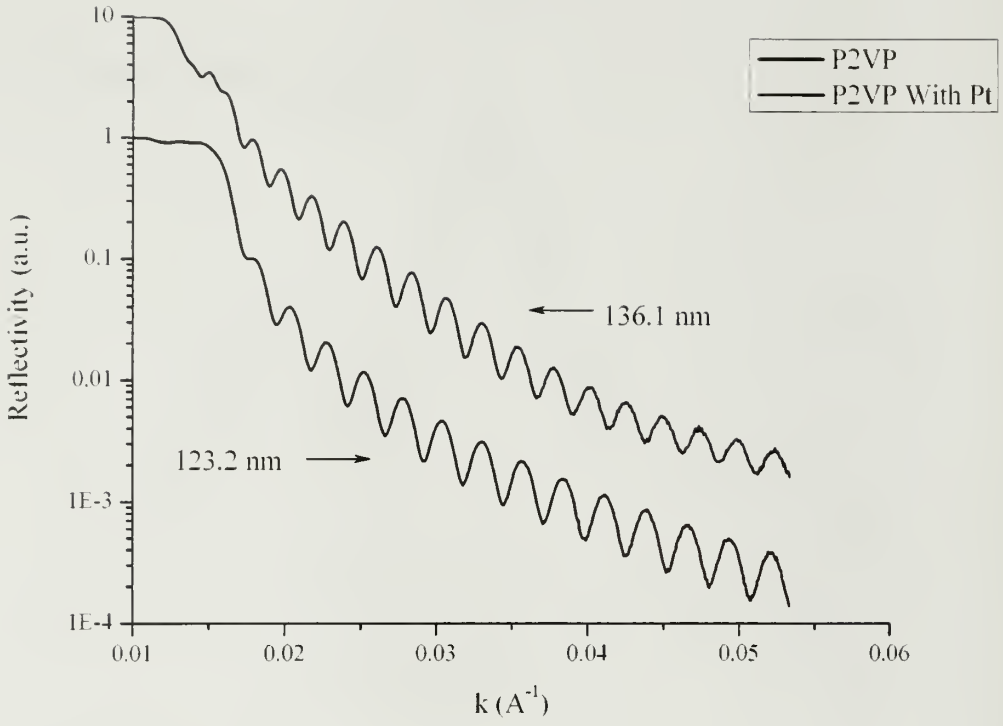


**Figure 3.7: Specular x-ray reflectivity of P2VP and P2VP/platinum films**

### 3.2.4 Preparation and Characterization of Poly(2-vinylpyridine)-Zinc Sulfide Nanocomposites

Thin films of P2VP were spun cast onto high resistance silicon wafers and quartz slides from solutions of the polymer in n-propanol (~3 wt%). The polymer films, ranging from 40-125 nm in thickness, were annealed for 24 hours at 170 °C to remove any excess solvent. Thick films (~100 μm) were prepared by melt pressing the dry polymer powder at 5000 psi and 170 °C. Each film was then cut into a 2.5 cm x 1.5 cm section and placed into a 25 mL stainless steel high pressure vessel from Thar Technologies, Inc. with a known quantity of $Zn(hfac)_2$ dihydrate and sealed under nitrogen. Carbon dioxide was introduced to the vessel at 60 °C using an automated syringe pump purchased from Teledyne ISCO at 150 bar and reacted for one hour. The vessel was subsequently

depressurized slowly to prevent disruption of the polymer film and unbound metal precursor was extracted from the films using $CO_2$ at 60°C and 150 bar. Finally, reduction of the metal precursor was performed under high pressure hydrogen sulfide gas at 5 bar and 80 °C for one hour. Remaining hydrogen sulfide gas was decomposed by bubbling it through solutions of lead nitrate as described in Chapter 2.

To trace the metallization of P2VP with the zinc precursor, both thin and thick films were photographed and XPS was performed on each sample before and after each step of the procedure.

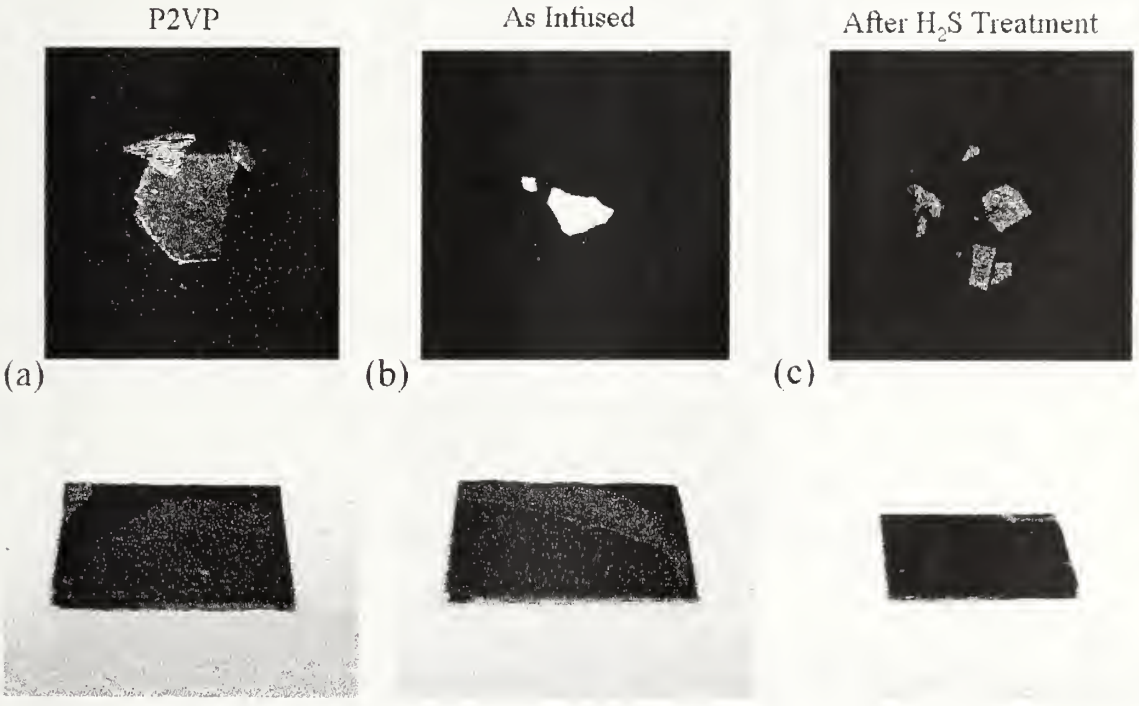


**Figure 3.8: P2VP (a) cast and melt pressed (b) infused with $Zn(hfac)_2$ dihydrate (c) reduced with hydrogen sulfide gas**

In Figure 3.8 (a) shows the cast and melt pressed P2VP films. (b) shows the P2VP films infused with the zinc precursor, and (c) the films following hydrogen sulfide gas treatment. The thin films' thicknesses were determined by profilometry and were 42 nm, 117 nm, and 82 nm, respectively. Any decrease in film thickness can be attributed to a

loss of $Zn(hfac)_2$ dihydrate from the film during reduction. This is visible in the XPS spectra in Figures 3.9 and 3.10.

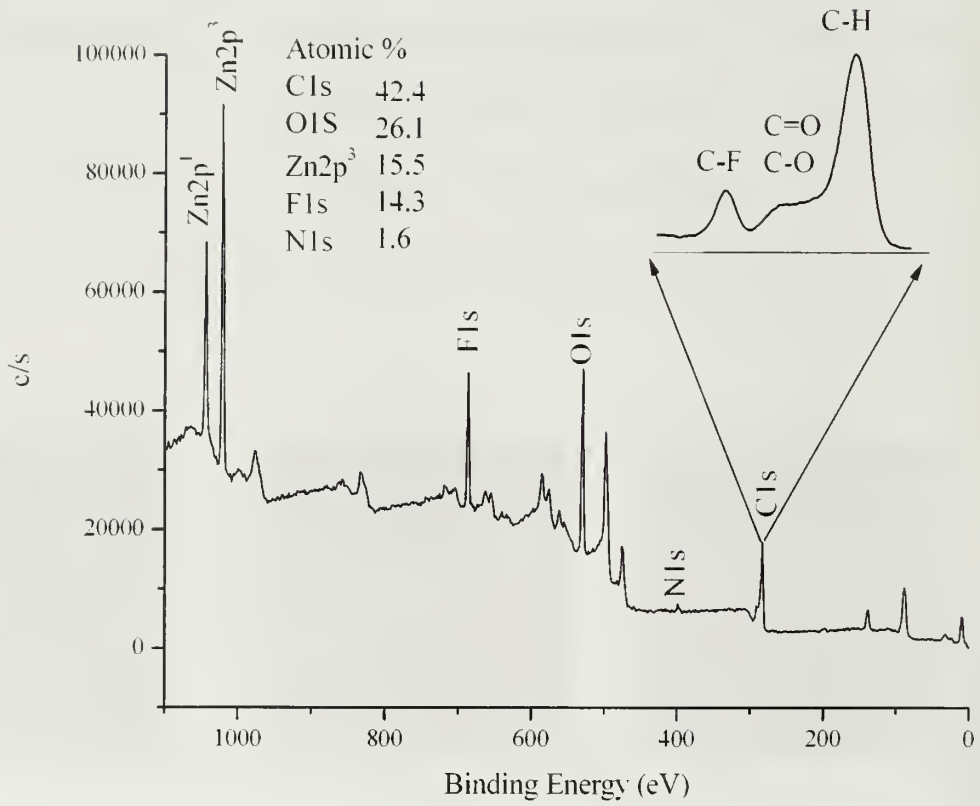


**Figure 3.9: XPS of P2VP infused with $Zn(hfac)_2$ inset of three distinct carbon peaks**

Figure 3.9 above shows the XPS spectrum collected at a 75% take off angle for a P2VP thin film infused with $Zn(hfac)_2$: the inset of the $C_{1s}$ peak records three different types of carbon present. These three peaks correspond to carbon-fluorine, carbon-oxygen and carbon hydrogen at binding energies of 291, 287 and 285 eV, respectively. Figure 3.10 depicts the XPS survey spectrum for the same film following its reduction with hydrogen sulfide gas.

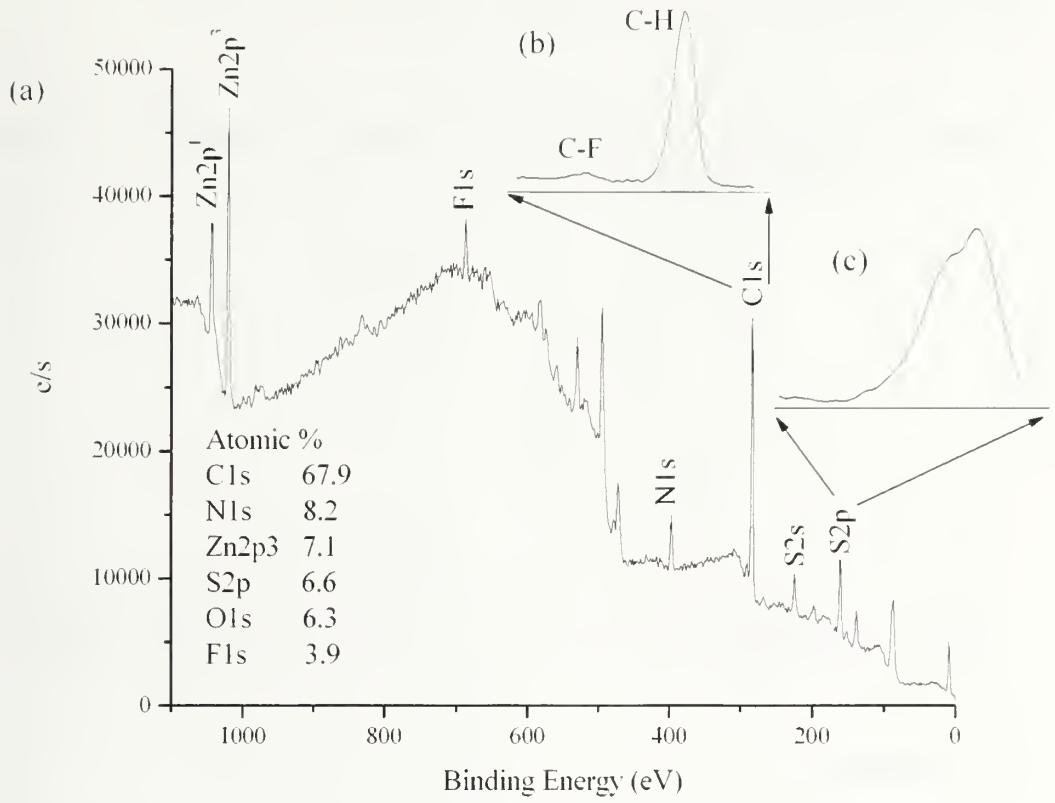


**Figure 3.10: XPS of (a) P2VP infused with $Zn(hfac)_2$ and reduced with hydrogen sulfide gas (b) $C_{1s}$ carbon peaks (c) $S_{p2}$ sulfide peak**

Inset graphs b and c above show the $C_{1s}$ and $S_{2p}$ peaks within the spectrum, respectively. A comparison of the $C_{1s}$ peaks from Figures 3.9 and 3.10 clearly demonstrate a reduction in the amount of fluorine and oxygen bound to carbon, indicating that the hfac ligand has been reduced and removed from the film. Likewise, the sulfide peak at 160 eV confirms the presence of zinc sulfide.

Another important area of the XPS spectrum is the nitrogen $1_s$ peak shown in detail in Figure 3.11. The first plot is from an infused poly(2-vinylpyridine) sample and the second is from a reduced sample. The majority of $N_{1s}$ peak shifts from a value of 399

to 397 eV, the measured value for pure P2VP, with a small shoulder remaining at 399 eV. This data indicates nitrogen is no longer interacting with the metal.

**Figure 3.11: XPS of $N_{1s}$ areas of (a) P2VP infused with $Zn(hfac)_2$ (b) reduced with hydrogen sulfide gas**

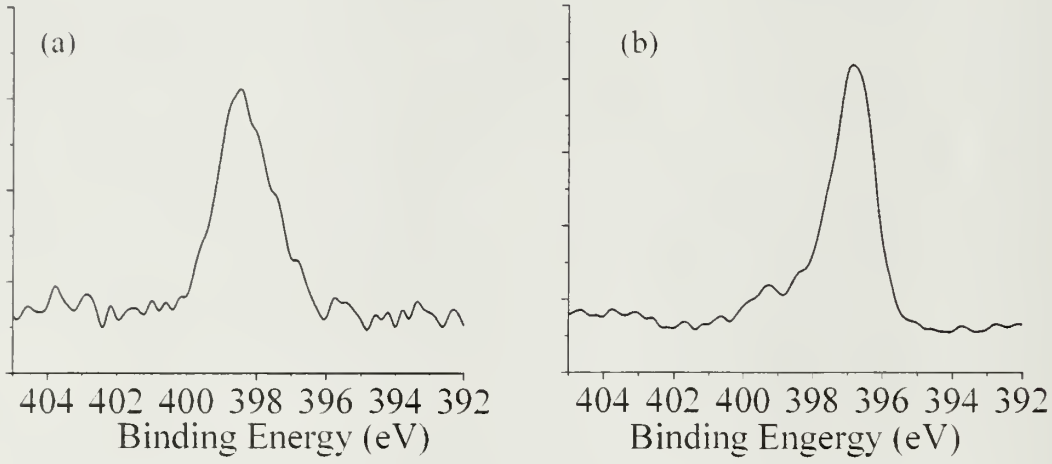


### 3.3 Conclusions

The interaction and reduction of silver, platinum and zinc metal precursors within poly(2-vinylpyridine) was thoroughly studied in this project by a variety of analytical techniques. Through the use of infrared and x-ray photoemission spectroscopies, it was found that silver and zinc precursors strongly interact with the poly(2-vinylpyridine) before reduction; however, subsequent to reduction these strong interactions ceased.

Reductions of Ag(COD)hfac with hydrogen gas and sodium borohydride were also examined. It was determined that hydrogen reduction was extremely slow and was incomplete even after 24 hours. Conversely, sodium borohydride was reduced after 30 seconds.

### 3.4 References


1. Möller, M., Inorganic Nanoclusters in Organic Glasses - Novel Materials for Electro-Optical Applications. *Synthetic Metals* 1991, 1159-1162.

2. Chan, Y. N. C.; Schock, R. R.; Cohen, R. E., Synthesis of Silver and Gold Nanoclusters within Microphase-Separated Diblock Copolymers. *Chem. Mater.* 1992, **4**, (1), 24-27.

3. Cummings, C. C.; Schrock, R. R.; Cohen, R. E., Synthesis of ZnS and CdS within ROMP Block Copolymer Microdomains. *Chem. Mater.* 1992, **4**, (1), 27-30.

4. Saito, R.; Okamura, S.; Ishizu, K., Introduction of Colloidal Silver into Poly(2-vinylpyridine) Microdomain of Microphase Separated Poly(Styrene-b-2-vinylpyridine) Film. *Polymer* 1992, **33**, (5), 1099-1101.

5. Sohn, B. H.; Seo, B. H., Fabrication of the Multilayer Nanostructure of Alternating Polymers and Gold Nanoparticles with Thin Films of Self-Assembling Diblock Copolymers. *Chem. Mater.* 2001, **13**, 1752-1757.

6. Bennett, R. D.; Xiong, G. Y.; Ren, Z. F.; Cohen, R. E., Using Block Copolymer Micellar Thin Films as Templates for the Production of Catalysts for Carbon Nanotube Growth. *Chem. Mater.* 2004, **16**, (26), 5589-5595.

7. Brown, G. D.; Watkins, J. J., Carbon Dioxide - Dilated Block Copolymer Templates for Nanostructured Materials. *Mat. Res. Soc. Symp. Proc.* 2000, **585**, 169-174.

8. Pai, R. A.; Humayun, R.; Schulberg, M. T.; Sengupta, A.; Sun, J.; Watkins, J. J., Mesoporous Silica Prepared Using Preorganized Templates in Supercritical Fluids. *Science* 2004, **303**, 507-510.

9. Wöhrle, D.; Pomogailo, A. D., *Metal Complexes and Metals in Macromolecules: Synthesis, Structure and Properties*. Wiley-VCH: 2003.

10. Wexler, R. M.; Tsai, M. C.; Friend, C. M.; Muetterties, E. L., Pyridine Coordination Chemistry of Nickel and Platinum. *J. Am. Chem. Soc.* 1982, **104**, (7), 2034-2036.

11. Wu, D. Y.; Hayashi, M.; Chang, C. H.; Liang, K. K.; Lin, S. H., Bonding Interaction, Low-lying States and Excited Charge-Transfer States of Pyridine-Metal Clusters: Pyridine-Mn (Cu, Ag, Au; n=2-4). *Journal of Chemical Physics* 2003, **118**, (9), 4073-4085.

12. Tsutsumi, K.; Funaki, Y.; Hirokawa, Y.; Hashimoto, T., Selective Incorporation of Palladium Nanoparticles into Microphase Separated Domains of Poly(2-vinylpyridine)-block-polyisoprene. *Langmuir* 1999, **15**, 5200-5203.

13. Ishizu, K.; Yamada, Y.; Saito, R.; Kanbara, T.; Yamamoto, T., Anisotropic conductivity on diblock copolymers with lamellar microdomains. *Polymer* 1993, **34**, 2256-2258.

14. Creighton, J. A.; Eadon, D. G., Ultraviolet-Visible Absorption Spectra of the Colloidal Metallic Elements. *J. Chem. Soc. Faraday Trans.* 1991, **87**, (24), 3881-3891.

15. Gao, J.; Fu, J.; Lin, C.; Lin, J.; Han, Y.; Yu, X.; Pan, C., Formation and Photoluminescence of Silver Nanoparticles Stabilized by Two-Armed Polymer with a Crown Ether Core. *Langmuir* 2004, **20**, 9775-9779.

16. Henglein, A., Reduction of $Ag(CN)_2^-$ on Silver and Platinum Colloidal Nanoparticles. *Langmuir* 2001, **17**, 2329-2333.

17. Mafune, F.; Kohno, J.; Takeda, Y.; Kondow, T.; Swabe, H., Structure and Stability if Silver Nanoparticles in Aqueous Solution Produced by Laser Ablation. *J. Phys. Chem. B* 2000, **104**, (35), 8333-8337.

18. Malynych, S.; Chumanov, G., Light-Induced Coherent Interactions between Silver Nanoparticles in Two-Dimentional Array. *JACS* 2003, **125**, 2896-2898.

19. Petit, C.; Lixon, P.; Pileni, M., In Situ Synthesis of Silver Nanoclusters in AOT Reverse Micelles. *J. Phys. Chem.* 1993, **97**, 12974-12983.

20. *The Aldrich Library of Infrared Spectra* III ed.; Aldrich Chemical Company: 1981.

21. Kuo, S. W.; Wu, C. H.; Chang, F. C., Thermal Properties, Interaction, Morphologies, and Conductivity Behavior in Blends of Poly(vinylpyridine)s and Zinc Perchlorate. *Macromolecules* 2004, **37**, (1), 192-200.

22. Silverstein, R. M.; Bassler, G. C.; Morrill, T. C., *Spectrometric Identification of Organic Compounds*. Fifth ed.; John Wiley and Sons: New York, 1991.

23. Russell, T. P., X-ray and neutron reflectivity for the investigation of polymers. *Material Science Reports* 1990, **5**, (4), 171-271.

# CHAPTER 4

## PREPARATION OF POLY(STYRENE)-*BLOCK*-POLY(2-VINYLPYRIDINE) NANOCOMPOSITE THIN FILMS

### 4.1 Introduction

The preparation of block copolymer nanocomposites has been studied extensively for over twenty years.[1-10] Many methods have been utilized to form these composites including solution casting films of the polymer with metal salts or organometalics[5, 8, 11], exposure of thin films to metal acid and salt solutions[2, 9, 10], and infusion of metal or metal oxide precursors using supercritical carbon dioxide[4, 12]. These techniques are characterized as either cooperative self-assemblies or serial processes. In cooperative self-assembly, the polymer and metal precursor form a metallized microstructure together upon evaporation of the solvent. In serial processes, metallization occurs after the formation of the microphase separated structure. In both cases, the metal precursor must preferentially segregate to only one domain for selective metallization to occur.

It has recently been reported that carbon dioxide dilated block copolymers are useful templates for composite materials prepared by reagent infusion and subsequent reaction.[12, 13] In this project selective metallization of PS-*b*-P2VP diblock copolymers and poly(2-vinylpyridine) (P2VP) homopolymers using supercritical carbon dioxide soluble metal precursors was accomplished. The use of symmetric PS-*b*-P2VP enables the fabrication of thin films with well-aligned, alternating layers of metallized P2VP and metal-free PS domains. Two advantages of this approach include: 1) an ability to manipulate the template morphology and alignment prior to infusion and 2) the use of supercritical carbon dioxide. Since supercritical carbon dioxide only causes minimal

swelling, polymer microphase separation[14, 15] and domain alignment is maintained without crosslinking. Meanwhile, sorption of small amounts of carbon dioxide significantly enhances the diffusion of reagents within the film[16] enabling infusion and binding of the metal precursors. Further, a two-step process allows for the independent preparation of template films with precisely controlled morphologies on silicon wafers by simple spin coating, followed by efficient functionalization/metallization of the template on the wafer without disruption of the template order, is well-suited for the production of device structures over large areas.

## 4.2 Experimental

Metal-polymer composites of polystyrene-*block*-poly(2-vinylpyridine) with silver, platinum, and zinc sulfide were prepared using supercritical carbon dioxide soluble metal precursors. These composites were then characterized using transmission electron microscopy (TEM) and x-ray photoluminescent spectroscopy (XPS).

### 4.2.1 Materials

All materials in this project were used as received unless otherwise stated. PS-*b*-P2VP (54k-*b*-50k) was purchased from Polymer Source, Inc. Hydrogen sulfide gas, iodine and metal precursors including (1,5-Cyclooctadiene) (hexafluoroacetylacetanato)silver(I), (1,5-Cyclooctadiene) dimethylplatinum(II), and Zinc hexafluoroacetylacetonate dihydrate were purchased from Aldrich Chemical Company and Strem Inc. Coleman grade carbon dioxide and ultra-high purity hydrogen were purchased from Merriam-Graves Company, and quartz slides and doped and

undoped silicon wafers were obtained from Chemglass, Inc. and International Wafer Services, respectively. All wafers were cleaned using a NoChromix™ – sulfuric acid bath and thoroughly rinsed with deionized water prior to their use.

### 4.2.2 Preparation and Characterization of Polystyrene-*b*-Poly(2-vinylpyridine)-Silver Nanocomposites

Thin films of PS-*b*-P2VP were spun cast onto high resistance silicon wafers and quartz slides from solutions of the polymer in toluene (~3 wt%). The polymer films, ranging from 50-500 nm in thickness, were then annealed for 24 hours at 170 °C to remove any excess solvent and to develop their microphase separated structures. Next, each film was cut into a 2.5 cm x 1.5 cm section and placed into a 25 mL stainless steel high pressure vessel by Thar Technologies, Inc. with 5 mg of Ag(COD)hfac and sealed under nitrogen. Subsequently, carbon dioxide was introduced to the vessel at 40°C using a computer controlled syringe pump (Teledyne ISCO) at 100 bar and reacted for one hour. The vessel was then gradually depressurized to prevent foaming of the polymer film, and unbound metal precursor was extracted using carbon dioxide at 40 °C and 100 bar. Finally, the metal precursors were reduced by high pressure hydrogen at 70 bar and 60 °C or through exposure of the film to a solution of $NaBH_4$ (5 mg/mL) in a water/ethanol mixture. Reduction times varied between 30 seconds and 24 hours.

Following the preparation of the microphase separated and composite films, the samples were imaged by transmission electron microscopy (TEM) using a JEOL 200EX electron microscope. A barrier layer of carbon (~10 nm thick) was evaporated onto the surface and a layer of epoxy was added and cured for 24 hours at 60 °C to prepare the samples for imaging. Samples were then removed from their silicon substrates by

immersion in liquid nitrogen and gradual warming to room temperature. Thin sections of the released epoxy-copolymer composite were attained using a Leica Ultracut UCT microtome and diamond knife. Microtomed sections less than 100 nm thick were collected onto a copper grid, and block copolymer films without metal had their P2VP domains stained with iodine prior to imaging.

Figures 4.1 (a) and (b) are both cross-sectional TEM images of PS-*b*-P2VP (54k-*b*-50k) before and after infusion with Ag(COD)hfac, respectively. In both images the air-polymer interface is identified by a light grey carbon layer which was evaporated onto the polymer surface prior to embedding in epoxy. Figure 4.1 (a) depicts the polystyrene domains as bright white layers, while the P2VP domains appear dark as a result of iodine staining. It is important to note the thickness of the P2VP domain prior to infusion is approximately 25nm, as measured by the micrograph. In Figure 4.1 (b) the P2VP domains of the infused sample contain large silver particles which were formed during the thermal reduction of the metal precursor. In this image it is clear the polymers layers remain intact and parallel to the substrate after infusion.

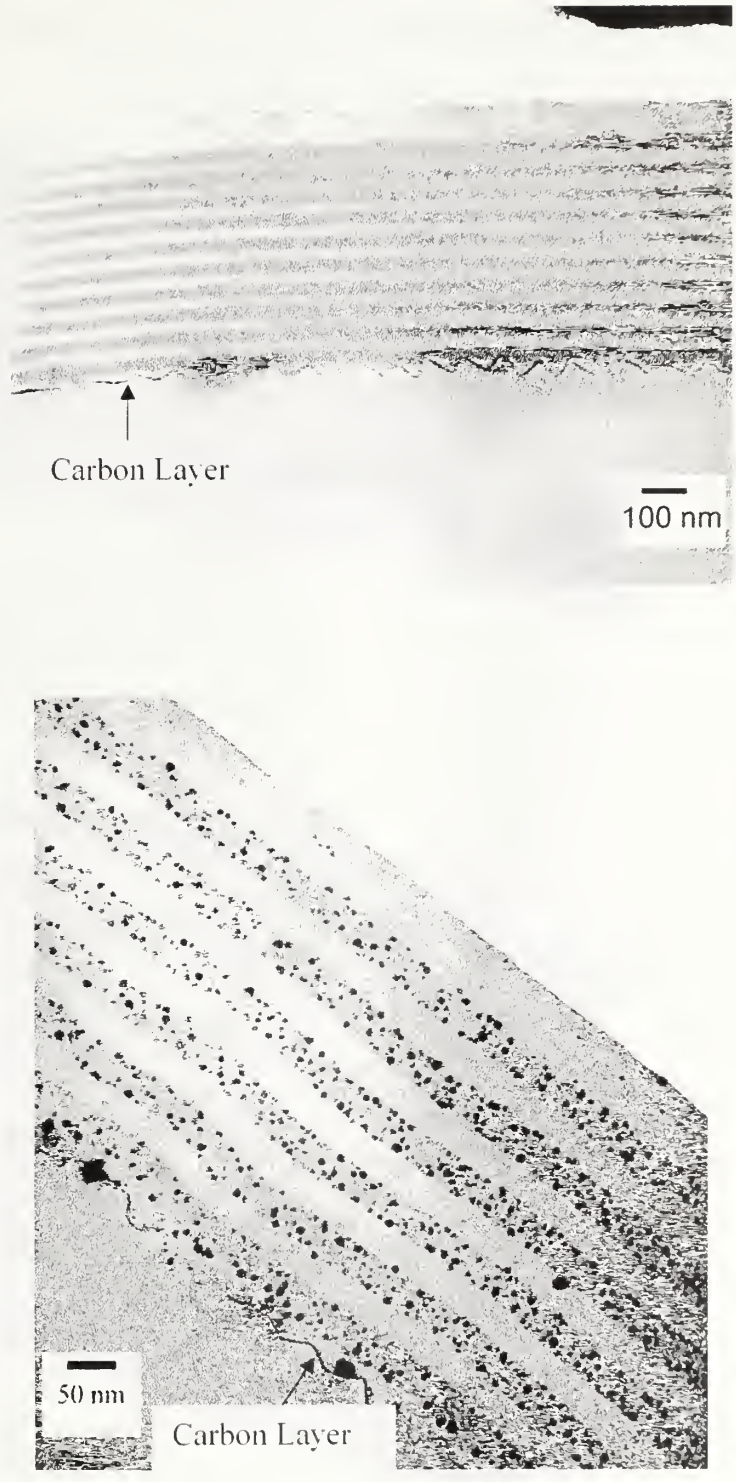


**Figure 4.1: (a) PS-*b*-P2VP (54k-*b*-50k) thin film P2VP phase stained with iodine (b) PS-*b*-P2VP (54k-*b*-50k) thin film infused with Ag(COD)hfac**

Figure 4.2 depicts similar samples reduced with hydrogen. These cross-sectional images at 20k and 200k magnification, each confirm the formation of silver nanoparticles ~ 2-5 nm in diameter.

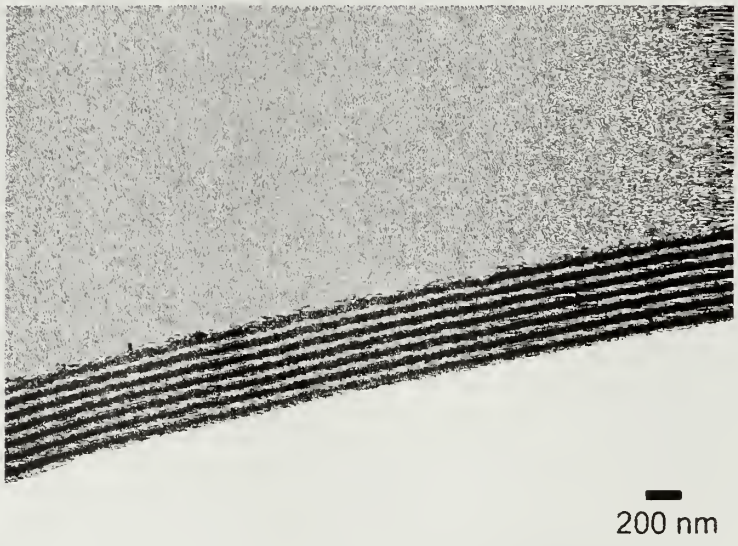


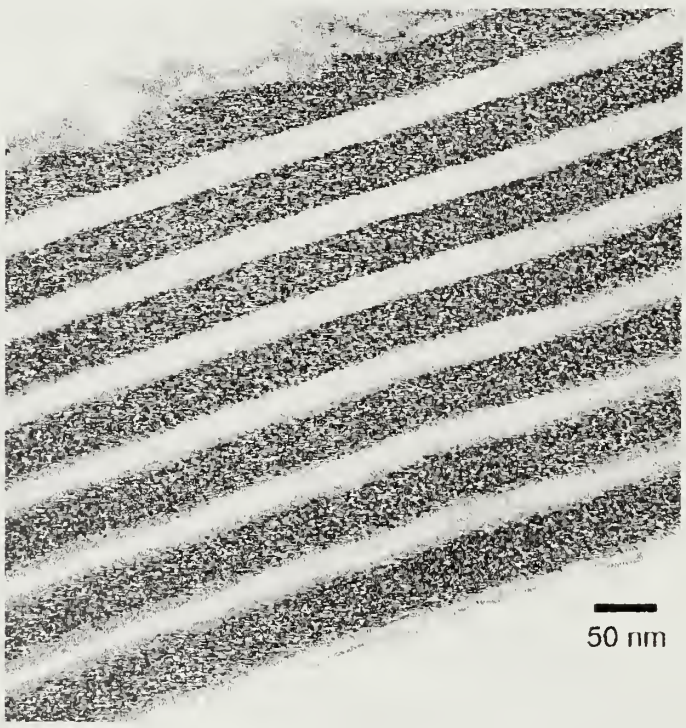


**Figure 4.2: PS-*b*-P2VP (54k-*b*-50k) after the infusion and reduction of Ag(COD)hfac with hydrogen gas for 24 hours**

As stated in Chapter 3, hydrogen did not allow complete reduction of the metal precursor, Ag(COD)hfac. Therefore, sodium borohydride was used for the reduction of the samples shown in Figures 4.3 (a) and (b) below.

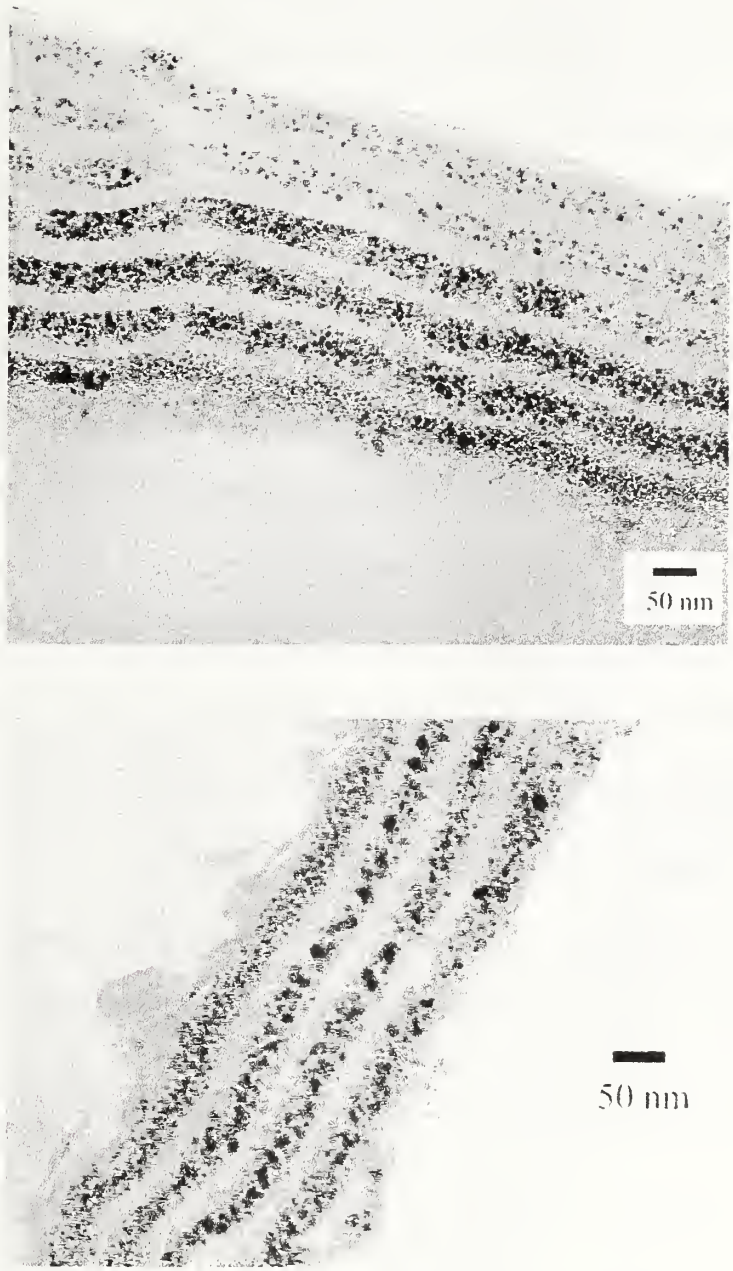


**Figure 4.3: PS-*b*-P2VP (54k-*b*-50k) after the infusion and reduction of Ag(COD)hfac with sodium borohydride for (a) 30 seconds (b) 12 hours**

In Figure 4.3 (a), a sample reduced with $NaBH_4$ for 30 seconds shows how the reduction of the metal precursor was limited by diffusion of the reducing solution through the PS layers. Figure 4.3 (b) shows another sample reduced with $NaBH_4$ for 12 hours to allow the reducing solution to penetrate the entire film. However, after this extended reduction step, the distribution of particles became less defined. Additionally, the particles in this sample were comparatively larger in size at ~10 nm. These differences are likely due to increased mobility of the polymer upon exposure to the liquid reducing solution. Further, the results suggest that the use of precursors which are readily reduced by vapor phase reducing agents are best suited for retaining the copolymer morphology.

Next, thermal stability of the nanoparticles produced was investigated by annealing the metallized block copolymer samples at 170 °C for 1.5 hrs. During this procedure, it was observed that the particles aggregated and moved to the air-polymer interface. This was unexpected considering the literature values for the surface energy of polystyrene and silver are 40.7 and 1240 mN/m, respectively.[17] According to these values, the particles were expected to remain in the polymer film upon annealing. It was initially thought that any remaining fluorinated hfac ligand would reduce the surface energy of the particles causing them move to the air-polymer interface. Therefore, to investigate the validity of this assumption, XPS was performed. This data indicated that no fluorine was present in the sample.

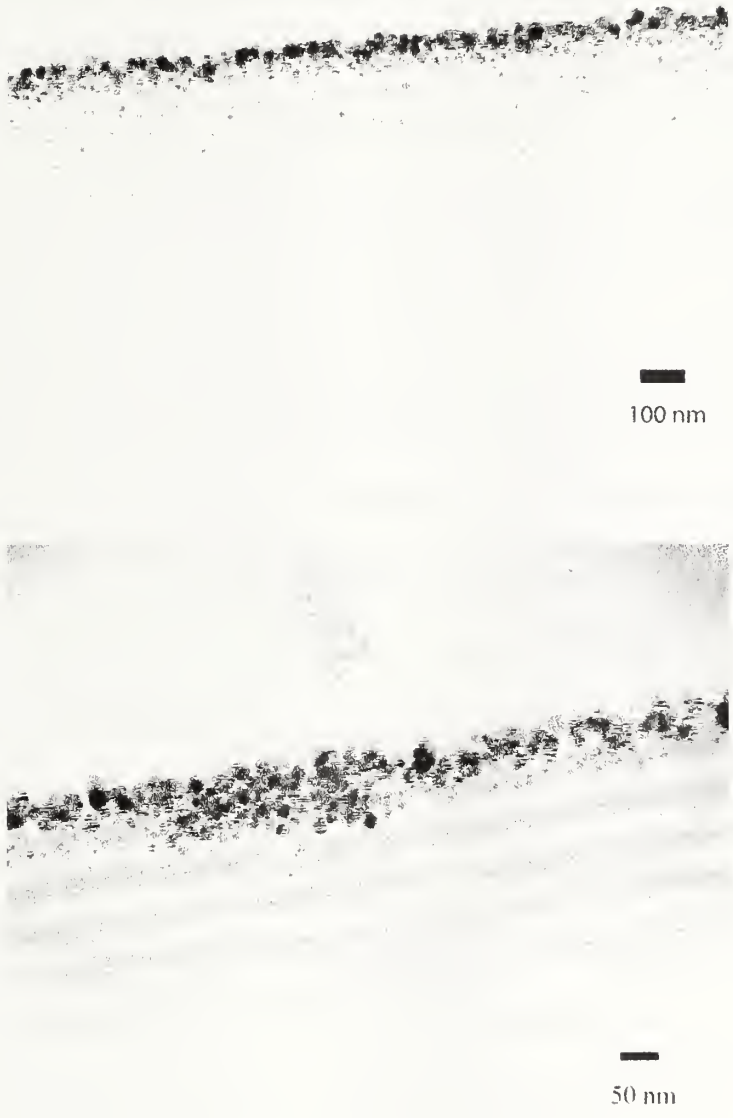


**Figure 4.4: PS-*b*-P2VP (54k-*b*-50k) after the infusion and reduction of Ag(COD)hfac with hydrogen gas for 24 hours and annealed for 1.5 hours at 170 °C**

### 4.2.3 Preparation and Characterization of Polystyrene-*b*-Poly(2-vinylpyridine)-Platinum Nanocomposites

Thin films of PS-*b*-P2VP were spun cast onto high resistance silicon wafers and quartz slides from solutions of the polymer in n-toluene (~3 wt%). The polymer films, ranging from 50-500 nm in thickness, were then annealed for 24 hours at 170 °C to remove any excess solvent and to develop their microphase separated morphologies. Next, each film was cut into a 2.5 cm x 1.5 cm section and placed into a 25 mL stainless steel high pressure vessel (Thar Technologies, Inc.) with 5 mg of $Pt(COD)Me_2$ and sealed under nitrogen. Carbon dioxide was then introduced to the vessel at 60 °C using a computer controlled syringe pump (Teledyne ISCO) at 200 bar and the reaction was allowed to proceed for one hour. The vessel was then slowly depressurized to prevent foaming of the polymer film. Unbound metal precursor was extracted from the films using carbon dioxide at 60 °C and 100 bar. Finally, the metal precursor was reduced under high pressure hydrogen at 70 bar and 60 °C over 1-24 hours.

Following the preparation of the microphase separated and composite films, the samples were imaged by transmission electron microscopy (TEM) using a JEOL 200EX electron microscope. To prepare the samples for imaging, a barrier layer of carbon ~10 nm in thickness was evaporated onto the surface in addition to a layer of epoxy and cured for 24 hours at 60 °C. Samples were then removed from their silicon substrates by immersion in liquid nitrogen and subsequent warming to room temperature. Thin sections of the released epoxy-copolymer composites were removed using a Leica Ultracut UCT microtome and diamond knife. Microtomed sections less than 100 nm in thickness were then collected on a copper grid.

Figure 4.5 shows the selective metallization of the P2VP domain with platinum. It is noteworthy that the lamellar morphology was not disturbed during metallization and that the particles are ~5-10 nm in diameter, as measured from the micrographs. However, the selectivity to this domain is not as pronounced as with the silver particles, reported in Chapter 3. This is likely a result of the autocatalytic reduction of the metal precursor during infusion. Finally, there is an overall increase in the P2VP domain of 3 nm or 12% from the original, unmetallized film by the addition of the platinum metal.

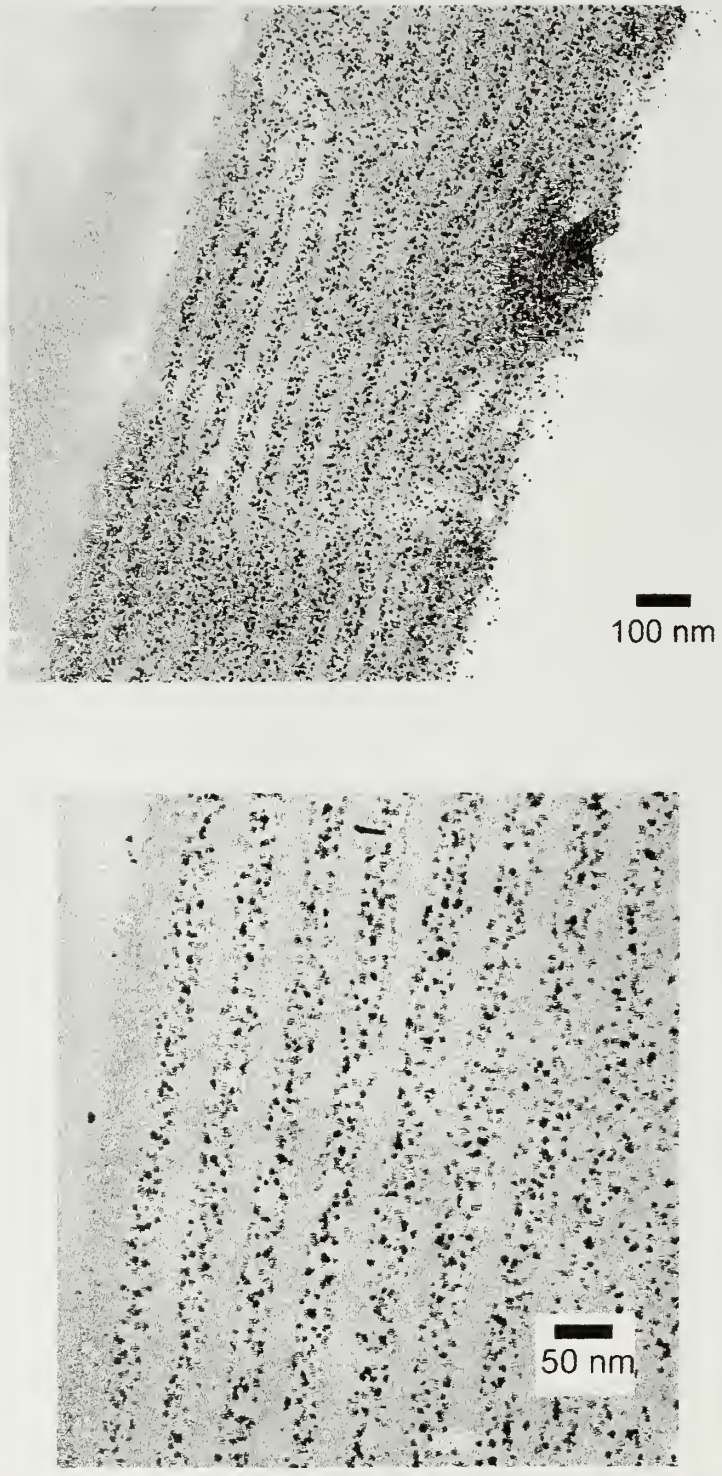


**Figure 4.5: PS-*b*-P2VP (54k-*b*-50k) after the infusion and reduction of $Pt(COD)Me_2$ with hydrogen gas for one hour**

### 4.2.4 Preparation and Characterization of Polystyrene-*b*-Poly(2-vinylpyridine)-Zinc Sulfide Nanocomposites

Thin films of PS-*b*-P2VP were spin coated onto high resistance silicon wafers and quartz slides from solutions of the polymer in n-toluene (~3 wt%). The polymer films, ranging from 50-500 nm in thickness, were then annealed for 24 hours at 170 °C to remove any excess solvent and to develop the microphase separated morphologies. Again, each film was prepared into a 2.5 cm x 1.5 cm section and placed into a 25 mL stainless steel high pressure vessel (Thar Technologies, Inc.) with 5 mg of $Zn(hfac)_2$ dihydrate and sealed under nitrogen. Carbon dioxide was then introduced to the vessel using a syringe pump (Teledyne ISCO) at 60 °C and 150 bar. This reaction was allowed to proceed for one hour. The vessel was then slowly depressurized to prevent foaming of the polymer film and residual unbound metal precursor was extracted using carbon dioxide at 60 °C and 100 bar. Finally, the metal precursor was reduced by exposure to hydrogen sulfide gas at 80 °C and 5 bar for one hour, as described in Chapter 2.

After the preparation of the microphase separated and composite films, the samples were imaged by transmission electron microscopy (TEM) using a JEOL 200EX electron microscope. To prepare the samples for imaging, a barrier layer of carbon ~10 nm in thickness was evaporated onto the surface and a layer of epoxy was added and cured for 24 hours at 60 °C. Samples were next removed from their silicon substrates by immersion in liquid nitrogen and subsequent warming to room temperature. Thin sections of the released epoxy-copolymer composite were cut less than 100 nm thick using a Leica Ultracut UCT microtome and diamond knife and collected on a copper grid.

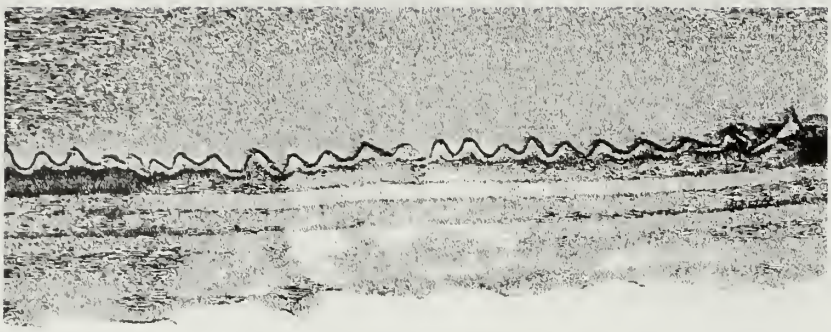


**Figure 4.6: PS-*b*-P2VP (54k-*b*-50k) after the infusion and reduction of $Zn(hfac)_2$ dihydrate with hydrogen sulfide gas for one hour**

In Figure 4.6 above, zinc sulfide is visible in the P2VP layers while the styrene domains remain unchanged. Dark domains indicate the P2VP with zinc sulfide, while light domains show the unchanged PS layers. Again, this data reveals the versatility of supercritical carbon dioxide for the metallization of PS-*b*-P2VP with a variety of metals without disruption to the microphase separated structure.

### 4.3 Conclusions

Multilayered nanocomposites of PS-*b*-P2VP with silver, platinum, and zinc sulfide were successfully fabricated through a serial process using supercritical carbon dioxide soluble metal precursors. This project demonstrates how metallization may be restricted to one microdomain of a block copolymer while preserving its microphase separation without the need for crosslinking the film. Finally, annealing results document

the expulsion of silver particles from the copolymer film, confirming that the particles are no longer interacting with the polymer subsequent to reduction.

## 4.4 References


1. Agnew, N. H., Transition metal complexes of poly(vinylpyridines). *Journal of Polymer Science: Polymer Chemistry Edition* **1976,** 14, (11), 2819-2830.

2. Bennett, R. D.; Xiong, G. Y.; Ren, Z. F.; Cohen, R. E., Using Block Copolymer Micellar Thin Films as Templates for the Production of Catalysts for Carbon Nanotube Growth. *Chem. Mater.* **2004,** 16, (26), 5589-5595.

3. Boontongkong, Y.; Cohen, R. E.; Rubner, M. F., Selective Electroless Copper Deposition within Block Copolymer Microdomains. *Chem. Mater.* **2000,** 12, 1628-1633.

4. Brown, G. D.; Watkins, J. J., Carbon Dioxide - Dialated Block Copolymer Templates for Nanostructured Materials. *Mat. Res. Soc. Symp. Proc.* **2000,** 585, 169-174.

5. Chan, Y. N. C.; Schock, R. R.; Cohen, R. E., Synthesis of Silver and Gold Nanoclusters within Microphase-Separated Diblock Copolymers. *Chem. Mater.* **1992,** 4, (1), 24-27.

6. Ciardelli, F.; Tsuchida, E.; Wöhrle, D., *Macromolecule-Metal Complexes.* Springer: Berlin, 1996.

7. Hashimoto, T.; Harada, M.; Sakamoto, N., Incorporation of Metal Nanoparticles into Block Copolymer Nanodomains via in-Situ Reduction of Metal Ions in Microdomain Space. *Macromolecules* **1999,** 32, 6867-6870.

8. Möller, M., Inorganic Nanoclusters in Organic Glasses - Novel Materials for Electro-Optical Applications. *Synthetic Metals* **1991,** 1159-1162.

9. Saito, R.; Okamura, S.; Ishizu, K., Introduction of Colloidal Silver into Poly(2-vinylpyridine) Microdomain of Microphase Separated Poly(Styrene-b-2-vinylpyridine) Film. *Polymer* **1992,** 33, (5), 1099-1101.

10. Sohn, B. H.; Seo, B. H., Fabrication of the Multilayer Nanostructure of Alternating Polymers and Gold Nanoparticles with Thin Films of Self-Assembling Diblock Copolymers. *Chem. Mater.* **2001,** 13, 1752-1757.

11. Cummings, C. C.; Schrock, R. R.; Cohen, R. E., Synthesis of ZnS and CdS within ROMP Block Copolymer Microdomains. *Chem. Mater.* **1992,** 4, (1), 27-30.

12. Pai, R. A.; Humayun, R.; Schulberg, M. T.; Sengupta, A.; Sun, J.; Watkins, J. J., Mesoporous Silicated Prepared Using Preorganized Templates in Supercritical Fluids. *Science* **2004,** 303, 507-510.

13. Watkins, J. J.; McCarthy, T. J., Polymerization in Supercritical Fluid-Swollen Polymers: A New Route to Polymer Blends. *Macromolecules* **1994,** 27, (17), 4845-4847.

14. Vogt, B. D.; Brown, G. D.; RamachandraRao, V. S.; Watkins, J. J., Phase Behavior of Nearly Symmetric Polystyrene-block-polyisoprene Copolymers in the Presence of CO2 and Ethane. *Macromolecules* **1999,** 32, (23), 7907-7912.

15. Vogt, B. D.; RamachandraRao, V. S.; Gupta, R. R.; Lavery, K. A.; Francis, T. J.; Russell, T. P.; Watkins, J. J., Phase Behavior of Polystyrene-block-poly(n-alkyl methacrylate)s Dilated with Carbon Dioxide. *Macromolecules* **2003,** 36, (22), 4029-4036.

16. Gupta, R. R.; RamachandraRao, V. S.; Watkins, J. J., Measurement of Probe Diffusion in CO2-Swollen Polystyrene Using in Situ Fluorescence Nonradiative Energy Transfer. *Macromolecules* **2003,** 36, (4), 1295-1303.

17. Vitosa, L.; Rubana, A. V.; Skrivera, H. L.; Kollárb, J., The surface energy of metals *Surface Science* **1998,** 411, (1-2), 186-202.

# CHAPTER 5

## PREPARATION OF SOLVENT ANNEALED AND SEAR ORIENTED POLY(STYRENE)-*BLOCK*-POLY(2-VINYLPYRIDINE) NANOCOMPOSITES

### 5.1 Introduction

Many of the potential applications of block copolymers will require control over both the alignment and orientation of their microdomains in order to produce a useful device or template.[1] Over the last decade there have been numerous studies seeking to control these properties in thin films and bulk samples. Methods developed for this purpose include: surface modification[2], E-field alignment[3], graphoepataxy[4], directed assembly by patterned surfaces[5, 6], shearing[7-14] and solvent annealing.[1, 15] This chapter discusses both shearing and solvent annealing methods used in this project and presents data on thin film and bulk PS-*b*-P2VP samples.

Shearing of block copolymers in bulk and, more recently, thin films[8] is a well established technique used to align and orient the domains of a polymer. For example, Gupta et al.[7] studied the shear alignment of symmetric styrene-isoprene diblock copolymers at different temperatures and shear amplitudes. They found that at high temperatures and low amplitudes the domains were oriented perpendicular to the surface; however at lower temperatures and high amplitudes the domains were parallel. In another study, Angelescu et al. used a poly(dimethylsiloxane) pad to shear cylinder forming styrene-ethylene-*alt*-propylene block copolymer thin films. They observed that when a single layer of the copolymer was sheared at a rate of at least 10 $s^{-1}$, the copolymer domains were aligned in the direction of the shear and showed no defects by AFM.

Solvent annealing and solvent evaporation can also be used to control the orientation and alignment block copolymers. In a recent example by Kim et al.[1], highly ordered arrays of styrene-ethylene oxide block copolymers were prepared by controlling the rate of solvent removal from thin films. Their results from transmission electron microscopy and grazing incidence x-ray spectroscopy demonstrated that ordering of the microdomains is induced at the surface and propagates to the substrate. Further, the enhanced orientation and order are a result of the increased mobility of the polymer in the presence of solvent and the gradient filed normal to the surface arising from solvent evaporation.

## 5.2 Experimental

In this chapter two methods of shearing (i.e. melt pressing and parallel plate rheometry) and two methods of solvent annealing (i.e. closed and controlled flow) were used to orient and order PS-*b*-P2VP samples. The samples were then characterized using scanning force microscopy and transmission electron microscopy. Results from each of the oriented and aligned samples are presented.

### 5.2.1 Materials

All materials in this project were used as received unless otherwise stated. PS-*b*-P2VP (54k-*b*-50k), (57k-b-57k), (55k-b-21k) and (81k-b-25k) were each prepared by living anionic polymerization or purchased from Polymer Source, Inc. Sodium borohydride and metal precursors including (1,5-Cyclooctadiene) (hexafluoroacetylacetanato)silver(I) and iron (II) Chloride were also purchased from

Aldrich Chemical Company. Coleman grade carbon dioxide and ultra-high purity hydrogen were purchased from Merriam-Graves Company, and silicon wafers were obtained from International Wafer Services. All wafers were cleansed using a NoChromix™ – sulfuric acid bath and thoroughly rinsed with deionized water prior to their use.

### 5.2.2 Shear Alignment and Metallization of PS-b-P2VP Block Copolymers

Shear alignment of PS-*b*-P2VP (54k-*b*-50k) was accomplished by first preparing one millimeter thick samples with diameters of 5 mm or 18 mm by melt pressing dry polymer powder into brass molds at 170 °C. Smaller samples were then sheared by melt pressing them at 170 °C at varying pressures of 5000, 10000 and 20000 psi for 30 seconds in a Carver laboratory press, while larger samples were pressed to a thickness of 200 μm and sheared in a parallel plate rheometer with shear rates of 5 $s^{-1}$, 10 $s^{-1}$, and 20 $s^{-1}$ for 120, 60 and 30 seconds, respectively. Samples were then viewed before and after metallization using small angle x-ray scattering (SAXS) and transmission electron microscopy (TEM).

Figure 5.1 below is the small angle x-ray scattering profile and 2D image for the copolymer sample melt pressed at 170 °C and 5000 psi.

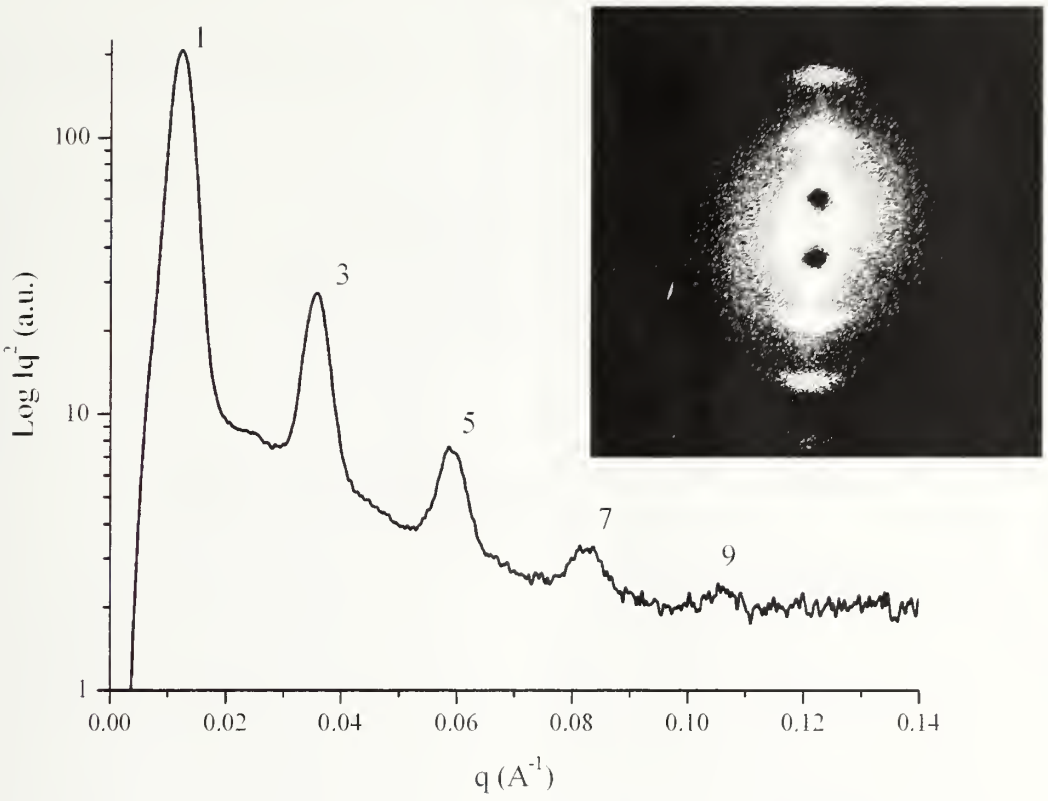


**Figure 5.1: Small Angle x-ray Scattering of PS-b-P2VP 54k-b-50k Melt Pressed at 5000 psi**

In the 2D image, the measurement of single spots rather than rings confirms the sample is highly oriented. The plot of $Iq^2$ vs. q shows a peak with the maximum intensity at 0.0123 $Å^{-1}$ and four higher order reflections at a ratio of 3:5:7:9 indicating that the polymer has a lamellar morphology. The absence of even numbered peaks is indicative of a nearly symmetric morphology where the thickness of the PS and P2VP layers are identical. Similar data was obtained for the melt pressed samples at 10000 and 20000 psi. Orientation was determined for each sample by calculating the Hermans orientation function, described by Equation 5.1.[16]

$$f = \frac{3 < \cos^2 \phi > -1}{2} \qquad \textbf{(5.1)}$$

Further, $<\cos^2\phi>$ was estimated using Equation 5.2 and a plot of the intensity versus azimuthal angle was prepared for each sample. An example of this plot for the 5000 psi sample is shown in Figure 5.2 below.

$$<\cos^2\phi>=\frac{\sum_{0}^{\frac{\pi}{2}} I(\phi)\cos^2\phi\sin^2\phi\Delta\phi}{\sum_{0}^{\frac{\pi}{2}} I(\phi)\sin\phi\Delta\phi} \quad \textbf{(5.2)}$$

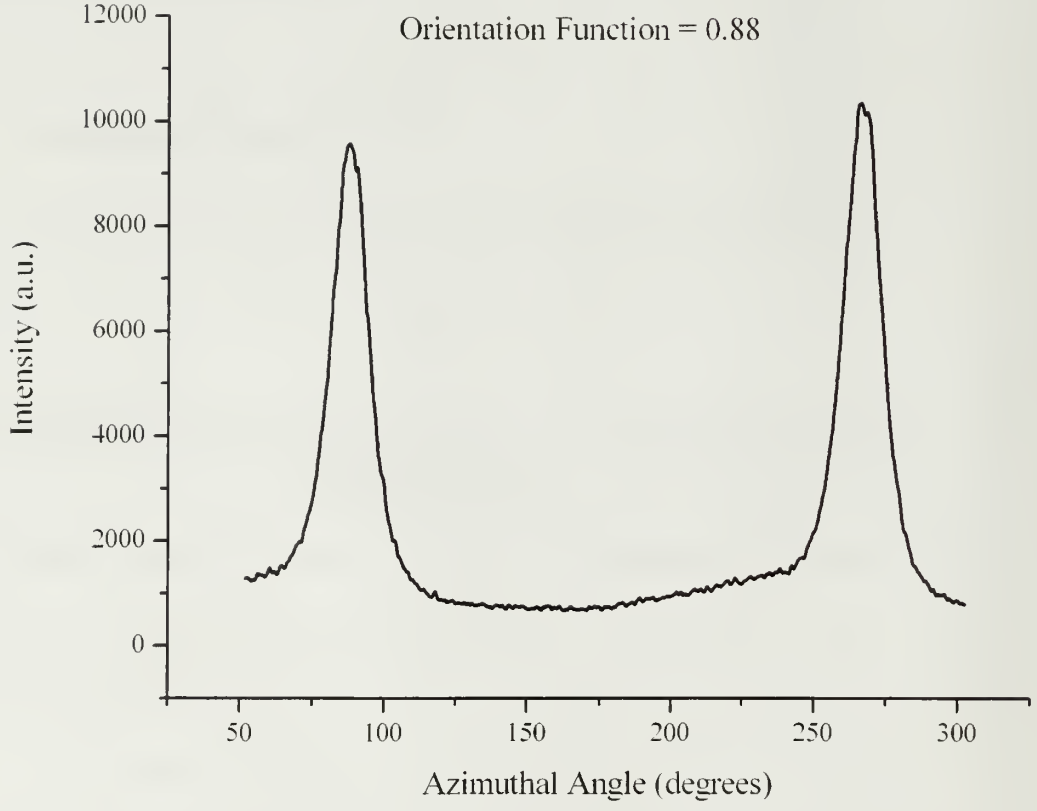


**Figure 5.2:I vs. Azmuthal Angle of PS-b-P2VP 54k-b-50k Melt Pressed at 5000 psi**

The values for this function can vary between -0.05 and 1. A value of -0.5 indicates crystalline planes are oriented perpendicular to the scattering direction, while a

value of 0 indicates random orientation, and a value of 1 indicates perfect orientation. Calculated orientations for the samples used in this project are listed in Table 5.1 below.

**Table 5.1: Calculated orientation for melt pressed PS-*b*-P2VP samples**

| Pressure (psi) | Orientation, *f* |
|---|---|
| 5000 | 0.88 |
| 10000 | 0.85 |
| 20000 | 0.81 |

By simply melt pressing the samples, the orientations of the copolymer were all calculated to be greater than 80%. Interestingly, as pressure increased, the orientation of the sample decreased. Figure 5.3 depicts a TEM image of the microtomed 5000 psi sample. The dark domains visible are the P2VP stained with iodine, while the light domains are the PS. In this image, a high degree of orientation, large grain size, and the presence of very few defects were observed in the sample.

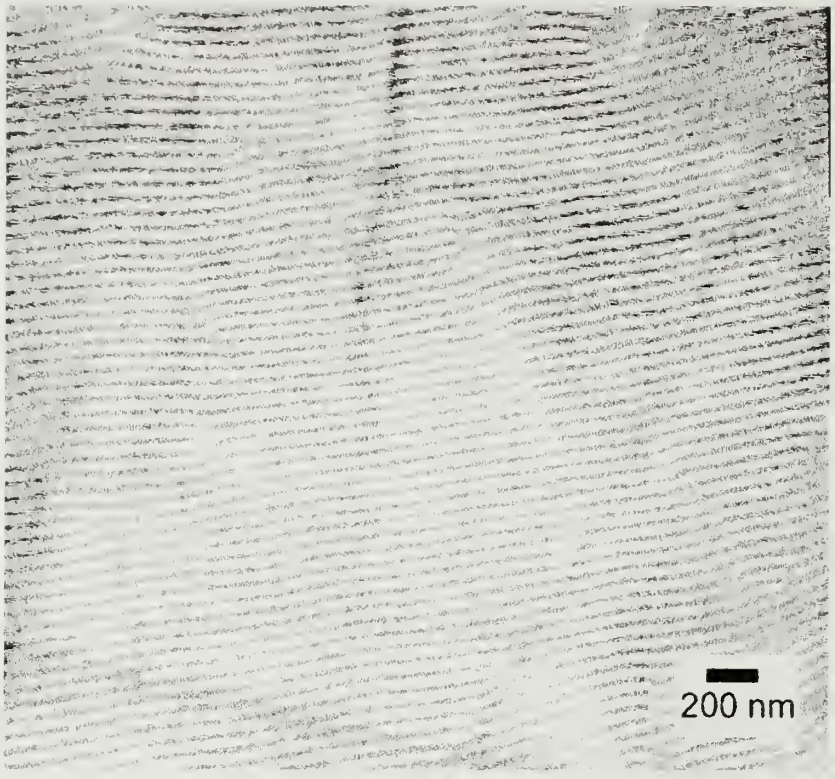


**Figure 5.3: TEM of PS-b-P2VP 54k-b-50k Melt Pressed at 5000 psi**

The samples sheared in parallel plate rheometer were characterized using the same methods. Calculated orientation functions for each of these samples are listed in Table 5.2 below.

**Table 5.2: Calculated orientation for parallel plate sheared PS-*b*-P2VP samples**

| Shear Rate ($s^{-1}$) | Time (s) | Orientation, *f* |
|---|---|---|
| 5 | 120 | 0.87 |
| 10 | 60 | 0.86 |
| 20 | 30 | 0.84 |

Again the orientation of the polymer samples under these conditions were greater than 80%; yet, Table 5.2 records a slight decrease in the orientation at shorter time intervals and higher shear rates. This indicates that either the extended shear time for the

first sample increased the orientation or the higher shear rate caused some disorder within the sample.

Next, a copolymer sample, sheared by melt pressing at 20000 psi was metallized with silver as described in Chapter 3. Figure 5.4 depicts a microtomed section of this sample below.

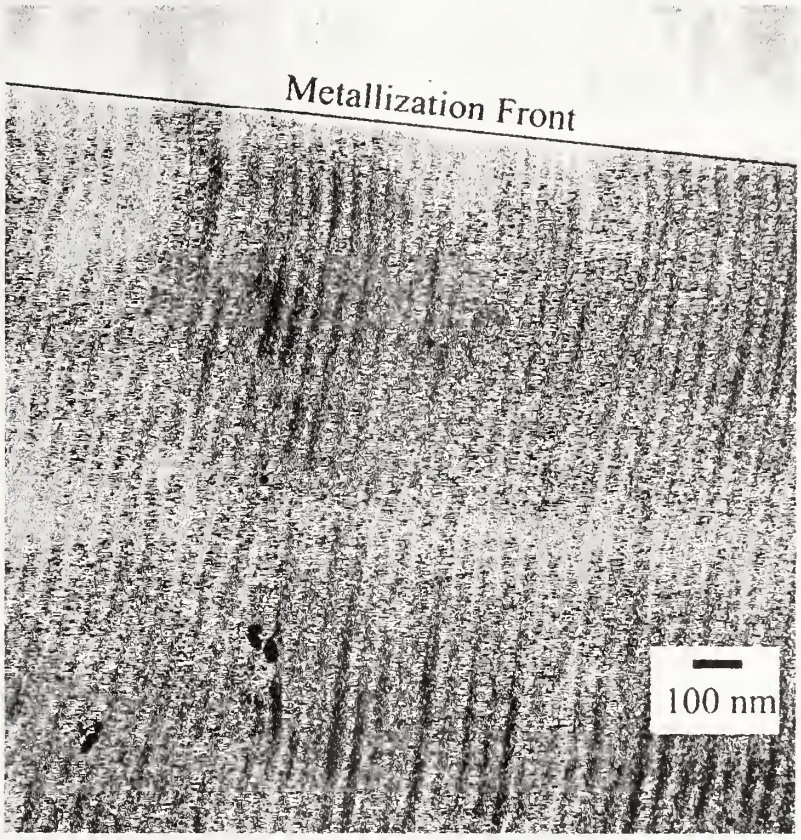


**Figure 5.4: PS-b-P2VP Sheared at 20000 psi and Metallized with Silver**

Using this image, it was observed that the metallization penetrates the film by several microns and there is a metallization front where the upper portion of the image meets the unmetallized polymer. The uniform metallization of the outer portion of the sample indicates that the metallization is diffusion controlled.

Small angle x-ray scattering (SAXS) performed on this sample showed an increase in the d-spacing from 50 nm to 80 nm, as depicted in Figure 5.5. The presence

of higher order reflections, at ratios of two and three, indicate that the symmetry of the copolymer also changed as a result of the metallization. The overall orientation calculated by the Hermans orientation function was determined to decrease to 66%.

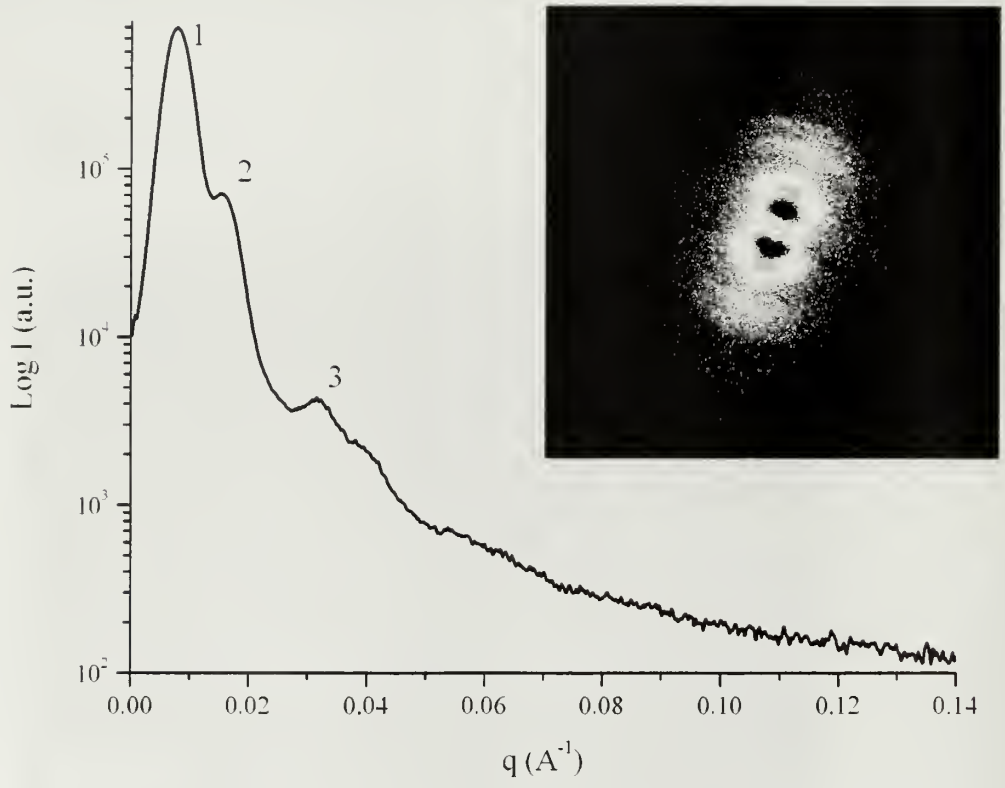


**Figure 5.5: Small Angle x-ray Scattering of PS-b-P2VP 54k-b-50k Melt Pressed at 20000 psi and Metallized with Silver**

### 5.2.3 Solvent Annealing and Metallization of PS-b-P2VP Block Copolymers

Block copolymer thin films of PS-*b*-P2VP with molecular weights of 54k-b-50k, 81k-b-21k, and 55k-b-25k were solvent annealed in both closed and controlled flow systems..

In the closed system, the polymer thin film and a small beaker of solvent were sealed in a glass jar for 1-24 hours. During this time, the film became saturated and the

polymer chains were mobilized. The beaker of solvent was then removed and the cover loosely replaced so that the remaining solvent could evaporate within a few hours. These samples were then examined by scanning force microscopy (SFM) using a Digital Instrument. Dimension TM 3100 atomic force microscope.

Figures 5.6 (a) and (b) are SFM phase images of two copolymer samples with molecular weights of 81k-*b*-21k and 57k-*b*-57k that were each annealed in chloroform vapor for 24 hours. Annealing produced enhanced order in the 81k-*b*-21k sample and an orientation of the lamella normal to the surface in the 57k-*b*-57k sample. The P2VP domains of the 81k-b-21k and 57-k-b-57k were measured to be 22 and 42 nm. respectively. These results suggest that chloroform is not selective to either block of the polymer. otherwise a preferential wetting of one polymer to the solvent-polymer interface would occur.

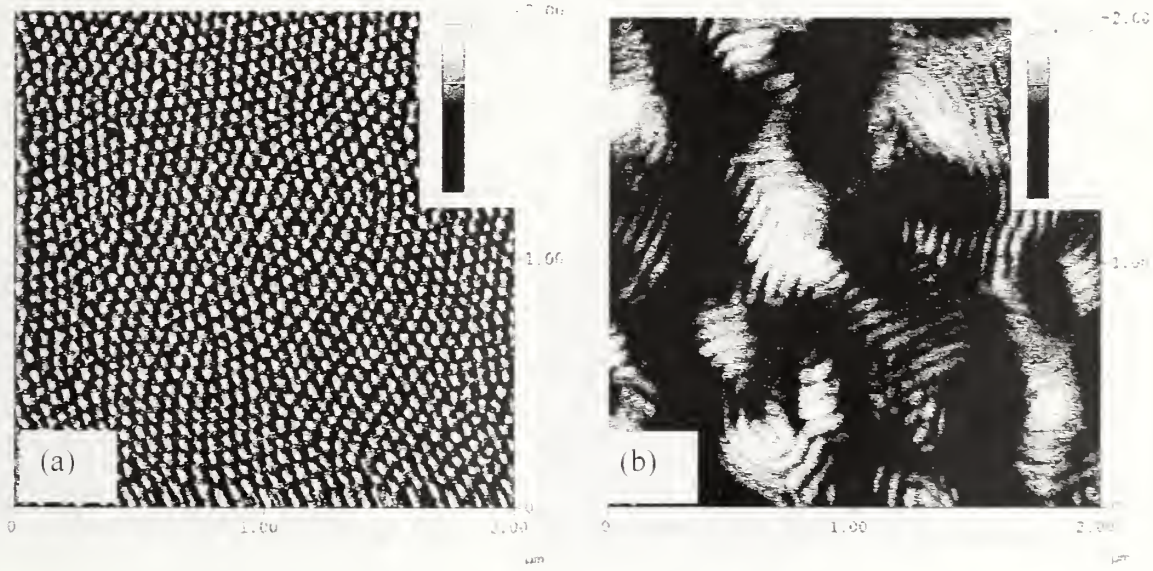


**Figure 5.6: SPM Phase images of (a) 81k-b-21k and (b) 57k-b-57k PS-b-P2VP Copolymers Solvent Annealed in Chloroform for 24 Hours**

These samples were then infused with silver using the procedure detailed in Chapter 3 and reduced with sodium borohydride. The infused and reduced samples were subsequently imaged using SPM and TEM. The SPM images obtained are shown in Figure 5.7 below.

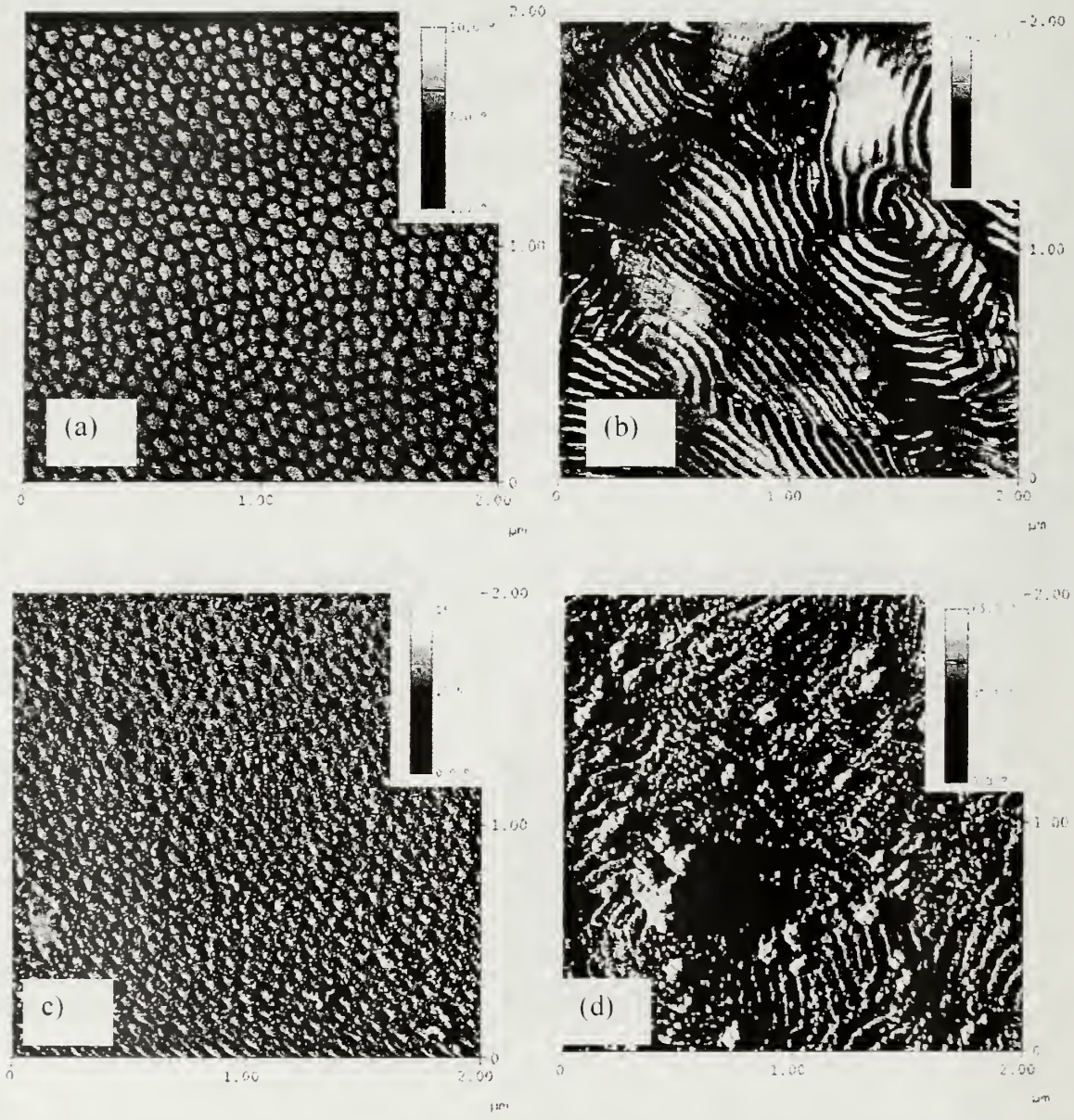


**Figure 5.7: SPM Before and After Metallization of Solvent Annealed (a & c) 81k-b-21k and (b &d ) 54k-b-50k**

Figures 5.7 (a) and (b) show the infused samples prior to reduction, where the P2VP domains increased to 45 and 55 nm, respectively. The images in Figures 5.7 (c) and (d) show the samples following their reduction. Both images show that the morphology was not disrupted and the formation of silver nanoparticles. In Figure 5.7 (d), large silver particles are visible at the surface of the P2VP domains, whereas the PS domains are flat. TEM images of these samples again confirmed the presence of the nanoparticles and their location within the film, as seen in Figures 5.8 (a) and (b) below.

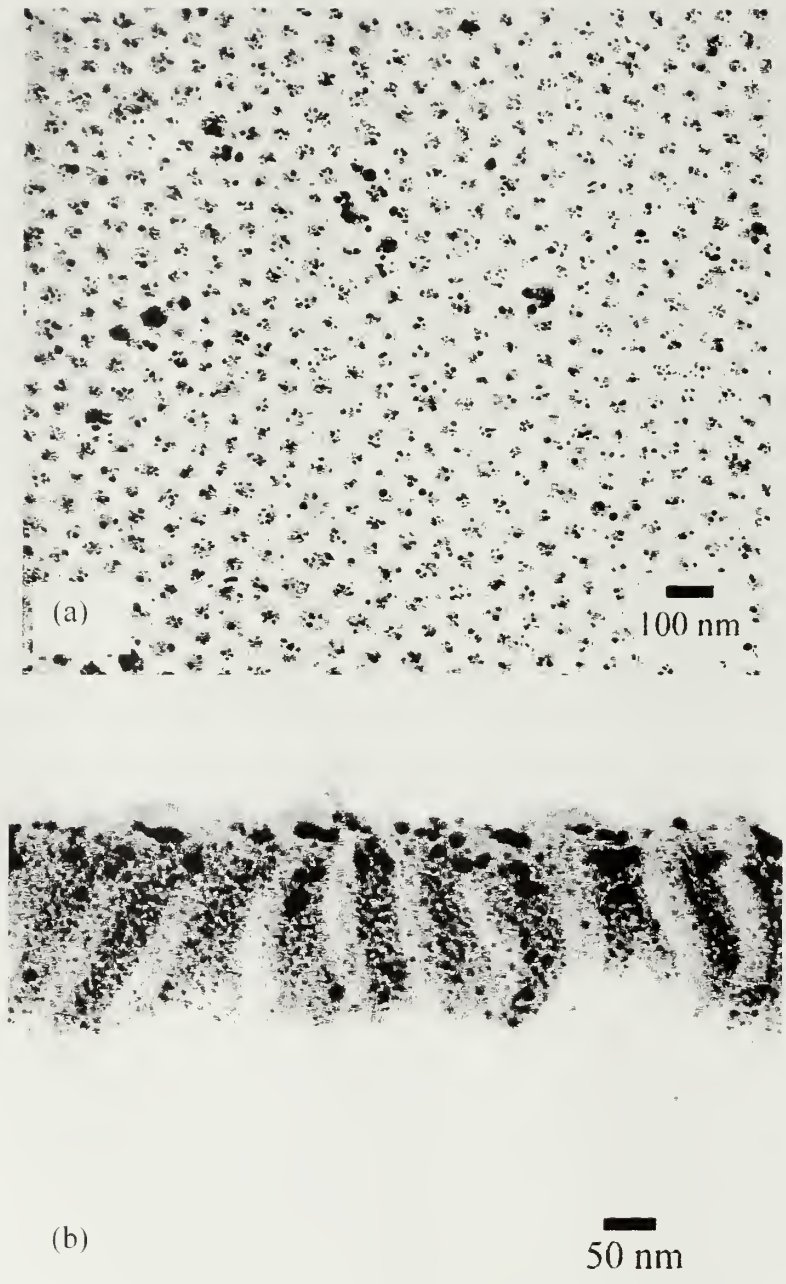


**Figure 5.8: TEM images of (a) 81k-b-21k and (b) 57k-b-57k PS-b-P2VP Copolymers After Reduction of Ag(COD)hfac**

The final sample studied was of PS-b-P2VP (55k-b-25k) with cylindrical morphology. This sample was first solvent annealed in a closed system with acetone and

methylene chloride and imaged using SFM. A pair of phase images from this study are shown in Figure 5.9 below.

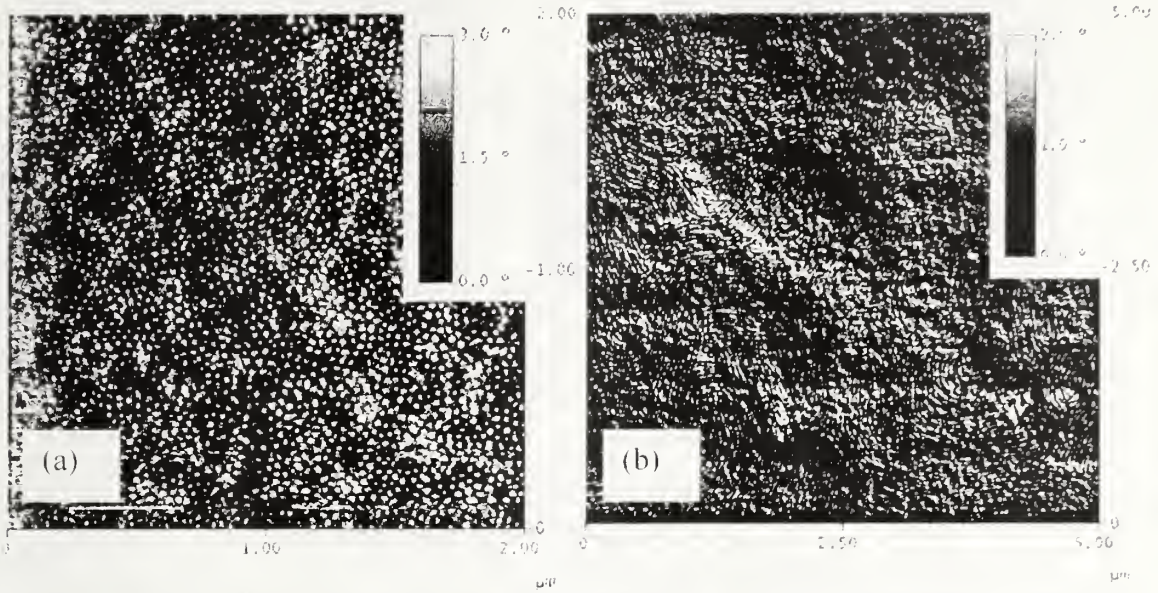


**Figure 5.9: SPM Phase images of PS-b-P2VP (55k-b-25k) Solvent Annealed in (a) Acetone (B) Methylene Chloride for 24 Hours**

Figure 5.9 (a) contains a phase image of the acetone annealed sample. This sample appears to have cylinders oriented nornmal to the surface. however did not exhibit any hexagonal packing. In Figure 5.9 (b). a sample annealed with methylene chloride reveals cylinders lying parallel to the surface with no directional order. These images also indicate that there is a preferential wetting of the polymer on the surface.

The PS-b-P2VP (55k-b-25k) sample was also annealed in a controlled flow system with toluene and a 50:50 mixture of toluene and hexane at a flow rate of 40 mL/min for 16 hours. In these experiments the polymer films are sealed in a glass vessel with inlet and outlet ports for the saturated gas. Dry argon gas, controlled by a flow meter, was then bubbled through the solvent and into the vessel. After 16 hours the vessel was purged with pure argon for 2 hours to remove the solvent. Results from these experiments are shown in Figures 5.10 and 5.11 respectively.

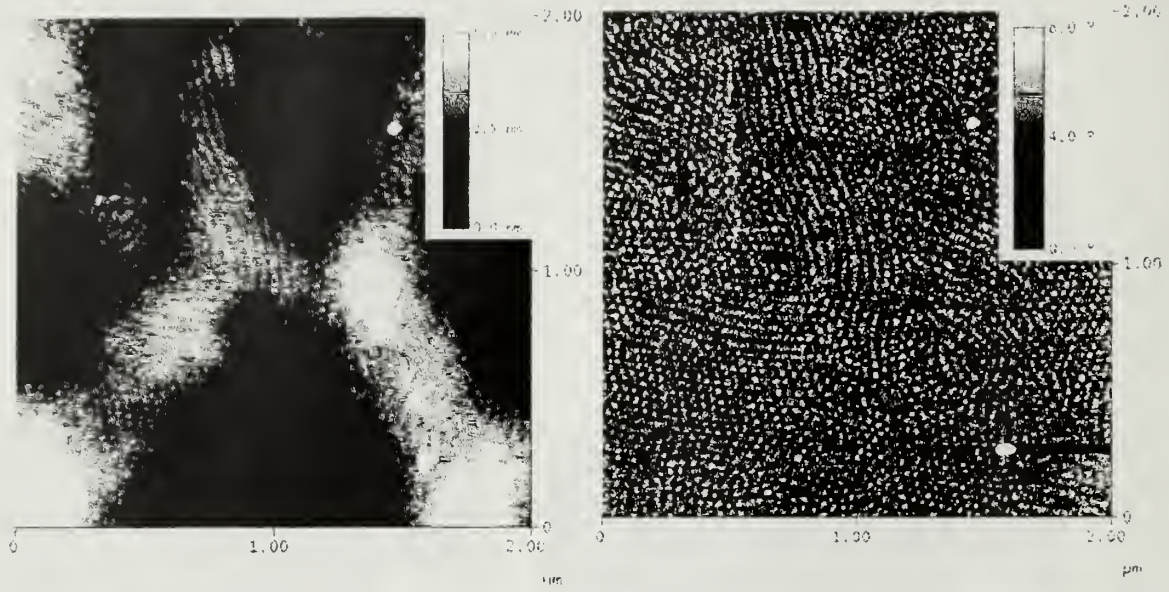

**Figure 5.10: SPM of PS-b-P2VP (55k-b-25k) Solvent Annealing with Toluene for 16 hours**

Figure 5.10 shows the height and phase images collected by SPM on the sample annealed in toluene for 16 hours. The light colored P2VP domains are visible in the PS matrix. Overall, the film appears relatively smooth and exhibits several grains of hexagonally packed P2VP domains perpendicular to the surface.

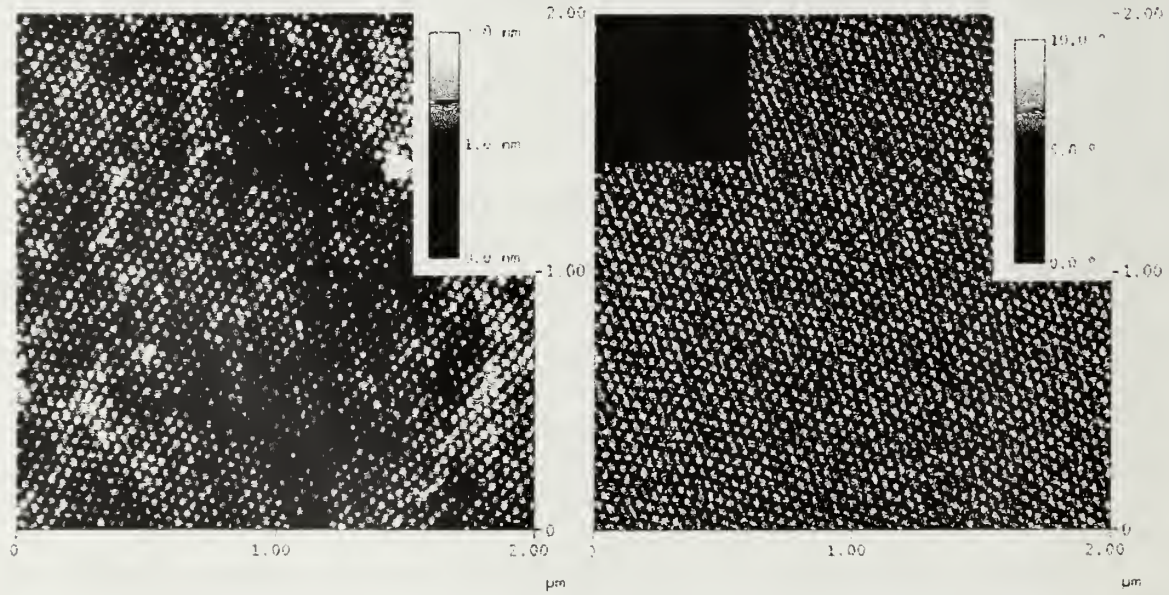

**Figure 5.11: SPM of PS-b-P2VP (55k-b-25k) Solvent Annealing with a Toluene:Hexane mixture for 16 hours**

Figure 5.11 shows the height and phase images collected by SFM on the sample annealed in a 50:50 toluene-hexane mixture for 16 hours. In this case, the sample appeared smooth and exhibited nearly defect-free hexagonal packing of the P2VP cylinders. These results are interesting considering toluene is a poor solvent for P2VP and the 50:50 mixture of toluene and a saturated hydrocarbon is a theta solvent for styrene just above room temperature.[17]

Finally, the sample was treated for two minutes with an aqueous solution of iron (II) chloride (5 mg/mL) followed by an oxygen plasma etch to remove the polymer matrix. The reaming pattern of iron oxide particles is visible in Figure 5.12. While the particles retained most of the hexagonal packing of the original film, several empty spots and many smaller grains were scattered throughout the sample.

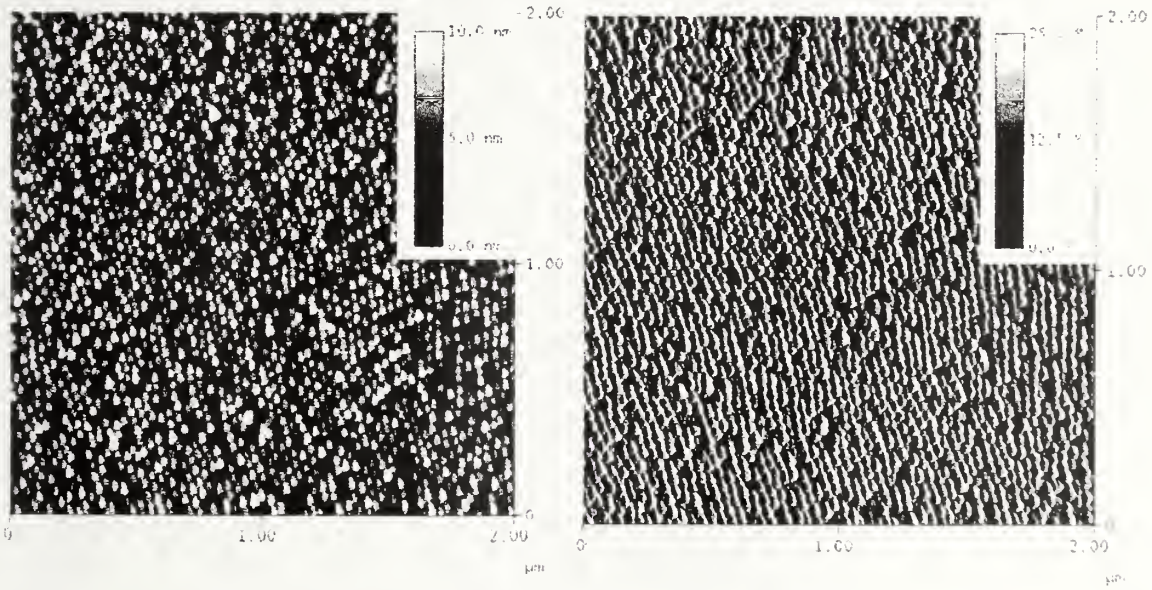

**Figure 5.12: SPM of PS-b-P2VP (55k-b-25k) After Iron (II) Chloride and Oxygen Plasma Treatment**

### 5.3 Conclusion

The domain orientation and order of PS-b-P2VP copolymers in this study were controlled by shearing and solvent annealing. Shearing produced highly ordered samples with calculated orientations of greater than 80% using melt pressing and parallel plate rheometry; while solvent annealing proved to be a simple method for controlling the orientation of the copolymer thin films. Moreover, solvent annealing the copolymer in a mixture of toluene and hexane resulted in nearly defect-free hexagonally packed cylinders oriented normal to the surface which was then successfully replicated through metallization with iron.

**5.4 References**


1. Kim, S. H.; Misner, M. J.; Xu, T.; Kimura, M.; Russell, T. P., Highly Oriented and Ordered Arrays From Block Copolymers via Solvent Annealing. *Adv. Mater.* 2004, **16**, (3), 226-231.

2. Mansky, P.; Russell, T. P.; Hawker, C. J.; Pitsikalis, M.; Mays, J., Ordered Diblock Copolymer Films on Random Copolymer Brushes. *Macromolecules* 1997, **30**, 6810-6813.

3. Xu, T.; Zhu, Y.; Gido, S. P.; Russell, T. P., Electric Field Alignment of Symmetric Diblock Copolymer Thin Films. *Macromolecules* 2004, **37**, 2625-2629.

4. Seagalman, R. A.; Yokoyama, H.; Kramer, E. J., Graphoepitaxy of Spherical Domain Block Copolymer Films. *Adv. Mater.* 2001, **13**, (15), 1152-1155.

5. Edwards, E. W.; Stoykovich, M. P.; Solak, H. H.; Nealey, P. F., Long-Range Order and Orientation of Cylinder-Forming Block Copolymers on Chemically Nanopatterned Striped Surfaces. *Macromolecules* 2006, **39**, 3598-3607.

6. Edwards, E. W.; Montague, M. F.; Solak, H. H.; Hawker, C. J.; Nealey, P. F., Precise Control Over Molecular Dimensions of Block-Copolymer Domains Using the Interfacial Energy of Chemically Patterned Surfaces. *Adv. Mater.* 2004, **16**, (15), 1315-1319.

7. Gupta, V. K.; Krishnamoorti, R.; Chen, Z. R.; Kornfield, J. A.; Smith, S. D.; Satkowski, M. M.; Grothaus, J. T., Dynamics of Shear Alignment in a Lamellar Diblock Copolymer: Interplay of Frequency, Strain Amplitude and Temperature. *Macromolecules* 1996, **29**, 875-884.

8. Angelescu, D. E.; Waller, J. H.; Adamson, D. H.; Deshpande, P.; Register, R. A.; Chaikin, P. M., Macroscopic Orientation of Block Copolymer Cylinders in Single-Layer Films by Shearing. *Adv. Mater.* 2004, **16**, (19), 1736-1740.

9. Gupta, V. K.; Krishnamoorti, R.; Kornfield, J. A.; Smith, S. D., Evolution of Microstructure during Shear Alignment in a Polystyrene-Polyisoprene Lamellar Diblock Copolymer. *Macromolecules* 1995, **28**, (4464-4474).

10. Gupta, V. K.; Krishnamoorti, R.; Kornfield, J. A.; Smith, S. D., Role of Strain in Controlling Lamellar Orientation during Flow Alignment of Diblock Copolymers. *Macromolecules* 1996, **29**, 1359-1362.

11. Kitade, S.; Ochiai, N.; Takahasi, Y.; Noda, I., Lamellar Orientation of Diblock Copolymer Solutions Under Steady Shear Flow. *Macromolecules* 1998, **31**, 8083-8090.

12. Laurer, J. H.; Pinheiro, B. S.; Polis, D. L.; Winey, K. L., Persistence of Surface-Induced Alignment in Block Copolymers upon Large-Amplitude Oscillatory Shear Processing. *Macromolecules* 1999, (32), 4999-5003.

13. Patel, S. S.; Larson, R. G.; Winey, K. L.; Wantanbe, H., Shear Orientation and Rheology of a Lamellar Polystyrene-Polyisoprene Block Copolymer. *Macromolecules* 1995, **28**, 4313-4318.

14. Riise, B. L.; Fredrickson, G. H.; Larson, R. G.; Pearson, D. S., Rheology and Shear-Induced Alignment of Lamellar Diblock and Triblock Copolymers. *Macromolecules* 1995, **28**, 7653-7659.

15. Kim, S. H.; Misner, M. J.; Russell, T. P., Solvent-Induced Ordering in Thin Film Diblock Copolymer/Homopolymer Mixtures. *Adv. Mater.* 2004, **16**, (23-24), 2119-2123.

16. Strobl, G. R., *The Physics of Polymers: Concepts for Understanding Their Structures and Behavior*. Springer: New York, 1997.

17. Brandrup, J.; Immergut, E. H., *Polymer Handbook*. 3rd ed.; 1989.

# CHAPTER 6

# PREPARATION OF POLY(STYRENE)-*BLOCK*-POLY(2-VINYLPYRIDINE) NANOCOMPOSITES IN CONFINED GEOMETRIES

## 6.1 Introduction

Diblock copolymers confined between parallel walls.[1] or more recently in nanoporous membranes.[2-5] are of interest due to the wide range of new morphologies that are experimentally observable. These structures may differ from a polymers bulk behavior in their long period or uniquely confined morphology.

Changes in a polymers morphology or long period can be attributed to interfacial interactions. structural frustrations. and a loss of symmetry in the confined geometry.[2-4, 6] A recent example was documented in work by Stucky et al. where mesoporous silica in aluminum oxide templates were prepared by varying pore diameters. Their work found that these variations in pore diameter caused the formation of many different helical structures which are not available in bulk systems.

In this chapter. the preparation of block copolymer in confined geometries is detailed. PS-*b*-P2VP polymers confined in aluminum oxide or carbon coated membranes were subsequently metallized with silver and gold.

## 6.2 Experimental

In this project. polystyrene-*block*-poly(2-vinylpyridine) copolymers were confined in both aluminum oxide and amorphous carbon coated membranes. These confined samples were then metallized with either silver or gold and characterized using transmission electron microscopy (TEM).

### 6.2.1 Materials

All materials in this project were used as received unless otherwise stated. Homopolymers and block copolymers were prepared by living anionic polymerization, as described in Chapter 2 or purchased from Polymer Source, Inc. More details about these samples are listed in Table 6.1 below. Iodine, sodium borohydride and metal precursors including (1,5-Cyclooctadiene) (hexafluoroacetylacetanato)silver(I) and hydrogen tetrachloroaurate ($HAuCl_4$) were purchased from Aldrich Chemical Company and Strem Inc., respectively. Coleman grade carbon dioxide and ultra-high purity hydrogen were purchased from Merriam-Graves Company. Aluminum oxide membranes with an average pore size of 200 nm manufactured by Millipore Inc., and silicon wafers were purchased from Fisher Scientific and International Wafer Services, respectively. All wafers were cleansed using a NoChromix™ – sulfuric acid bath and thoroughly rinsed with deionized water prior to use.

**Table 6.1: Homopolymer and block copolymer samples used in this work**

| **Homopolymer** | **$M_n$ kg/mol** | | | |
|---|---|---|---|---|
| Polyacrylonitrile | 14.4 | | | |
| **Polymer** | **PS kg/mol** | **P2VP kg/mol** | **Morphology** | **Period nm** |
| PS-*b*-P2VP | 25 | 23 | Lamellar | 34.3 |
| PS-*b*-P2VP | 54 | 50 | Lamellar | 53.7 |
| PS-*b*-P2VP | 44 | 18 | Cylindrical | 31.3 |
| PS-*b*-P2VP | 64 | 35 | Cylindrical | 36.8 |
| PS-*b*-P2VP | 14 | 47 | Cylindrical | 33.7 |
| PS-*b*-P2VP | 81 | 21 | Spherical | 43.7 |

### 6.2.2 Preparation and Characterization of Polystyrene-*b*-Poly(2-vinylpyridine) Confined in Nanoporous Aluminum Oxide Templates

Thick films (50-100 μm) of PS-*b*-P2VP were drop cast from solutions of the polymer in toluene or chloroform (5-10 wt%) and allowed the samples to dry overnight. Samples were then annealed in a vacuum oven at 170 °C for 24 hours to remove any residual solvent from the polymer. Next, an aluminum oxide membrane was placed on the polymer's surface and the stack was clamped between two glass slides to ensure contact of the membrane to the polymer was maintained. Stacks were then annealed at 170 °C for two days to allow the formation of microphase separated nanorods within the membrane. Finally, the aluminum oxide was dissolved by placing the sample in a 5% aqueous solution of sodium hydroxide. Remaining polymer rods were dried under

vacuum at 60°C and embedded in epoxy resin for microtoming. A diagram of this procedure is shown in Figure 6.1 below.

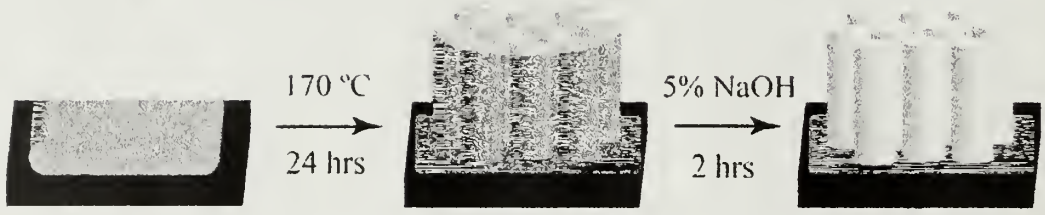


**Figure 6.1: Preparation and Confinement of PS-b-P2VP in Aluminum Oxide Membranes**

Figure 6.2 below contains two TEM images of symmetric PS-*b*-P2VP copolymers that were confined in aluminum oxide membranes. The first image is of a (25k-b-23k) sample that was microtomed perpendicular to its rods to expose the concentric ring morphology, where the P2VP domain was stained by iodine. The outermost layer is P2VP, since it preferentially wets the aluminum oxide. The second image is a cross-sectional view of a (54k-b-50k) sample cut parallel to its rods, exposing lamellar morphology.


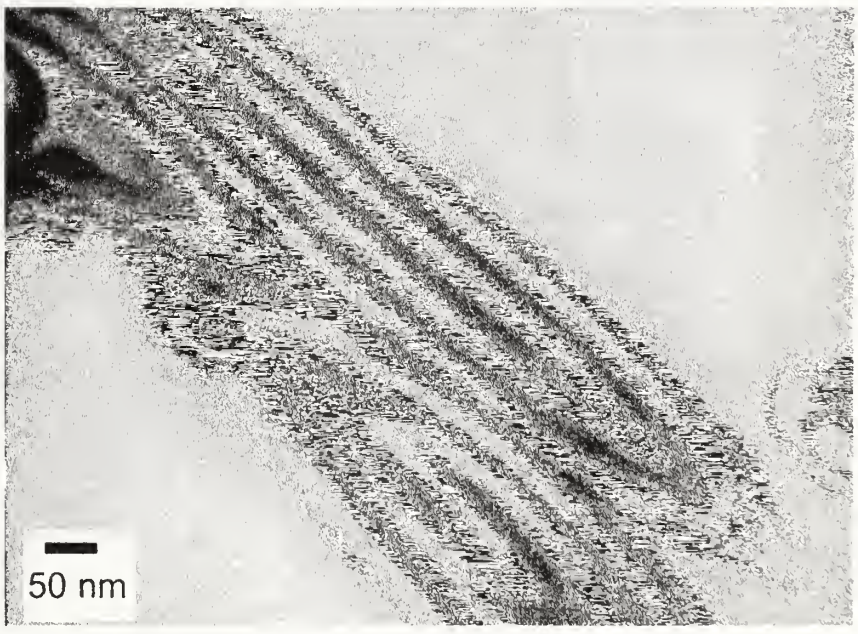


**Figure 6.2: Confined PS-*b*-P2VP in Aluminum Oxide Membranes (a) 25k-*b*-23k and (b) 54k-*b*-50k**

Next, asymmetric polymers with cylindrical morphologies and molecular weights of (44k-b-18k) and (14k-b-47k) were confined. Microtomed images of these samples are shown below in Figures 6.3 (a) and (b).

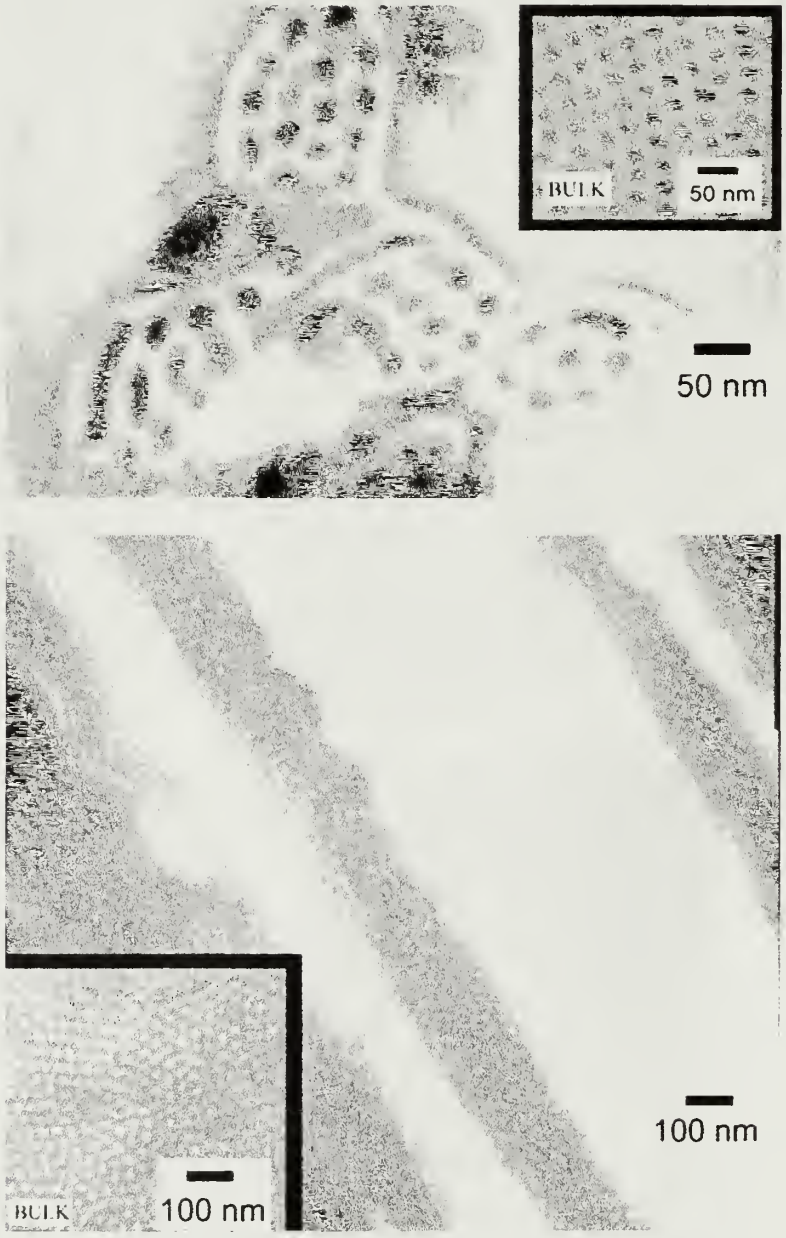


**Figure 6.3: Confined PS-*b*-P2VP in Aluminum Oxide Membranes (a) 44k-*b*-18k and (b) 14k-*b*-47k**

The inset image at upper right in Figure 6.2 (a) shows the bulk morphology of the copolymer with its cylindrical morphology visible with iodine stained P2VP cylinders (25nm) in a styrene matrix. The larger image in Figure 6.2 (a) depicts the copolymer confined in an aluminum oxide membrane. Again, the P2VP wets the membrane surface and forms cylinders ~20 nm in diameter within the styrene matrix. The P2VP domains are approximately twenty percent smaller than their bulk counterparts. This decrease is most likely due to the confinement and additional wetting layer of P2VP on the exterior of the rod. Similar results were previously reported by Xiang et al. [2] on styrene-butadiene copolymers. Figure 6.2 (b) shows both the bulk morphology (inset) and confined geometry of a (14k-b-47k) sample. In both images, cylinders of PS are visible in a matrix of P2VP; however, in the confined sample the domains appear poorly aligned.

### 6.2.3 Preparation and Characterization of Polystyrene-*b*-Poly(2-vinylpyridine) Confined in Amorphous Carbon Nanotubes

Amorphous carbon nanotubes were prepared by drop casting polyacrylonitrile (PAN) solutions (~10%) onto silicon substrates, followed by the placement of an aluminum oxide membrane onto the solution. Capillary forces then drew the solution into the membrane and the solvent was removed under vacuum at 150 °C. Next, the tubes were stabilized at 250 °C in air for 30 minutes followed by pyrolosis at 600 °C for the amorphous carbon. Finally, the structures of these tubes were studied using transmission electron microscopy upon the removal of the aluminum oxide by aqueous sodium hydroxide. Fellow researcher, Juin-Tai Chen, at University of Massachusetts Amherst developed this procedure[7] and collaborated in this component of the project.

Figure 6.4 contains two TEM images of the amorphous carbon tubes. Tube diameters vary from ~200 to 500 nm, as shown in the images below.

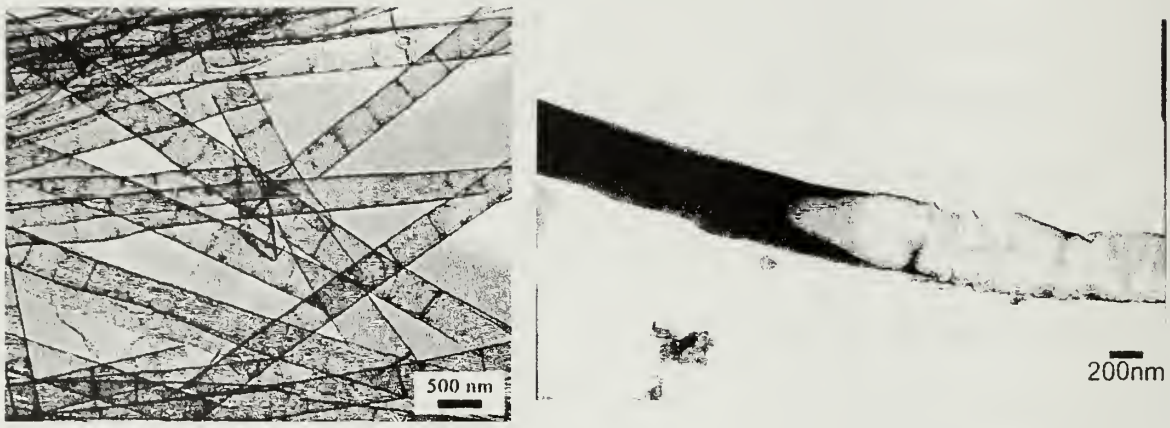


**Figure 6.4 TEM of Amorphous Carbon Nanotubes Prepared From PAN**

The formed carbon nanotubes were then studied to determine whether they could change the surface interactions of the polymers when confined in an aluminum oxide membrane. This was accomplished by following the procedure outlined in Figure 6.5.

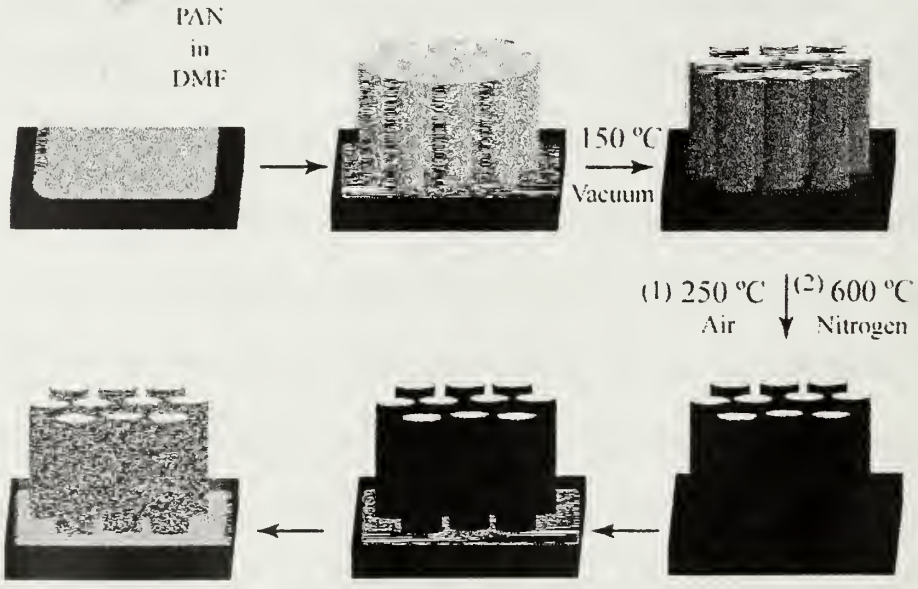


**Figure 6.5: Preparation and Confinement of PS-b-P2VP in Amorphous Carbon Coated Aluminum Oxide Membranes**

Figure 6.5 above outlines the procedure for the confinement of PS-*b*-P2VP in amorphous carbon nanotubes. First, the carbon tubes were prepared as described in the previous section. Next, the aluminum oxide supported tubes were placed on the copolymer film and annealed at 170 °C. The block copolymer was then drawn into the carbon tubes by capillary forces and the membrane removed by aqueous sodium hydroxide. The remaining rods were then embedded in epoxy and microtomed.

Figure 6.6 below shows two samples confined in carbon nanotubes. Figure 6.6 (a) is an image of asymmetric PS-*b*-P2VP with a molecular weight of 64k-b-35k. This image shows a large percentage of empty carbon nanotubes and a few which are filled with polymer. The filled tubes show cylinders of P2VP stained with iodine and the PS wets the carbon layer. Figure 6.6 (b) is an image of symmetric PS-b-P2VP with a molecular weight of 25k-b-23k. This sample again shows the PS wets the carbon layer and the dark P2VP domains stained with iodine. Therefore, this carbon layer may be used to change the sequence of the layers within pores.

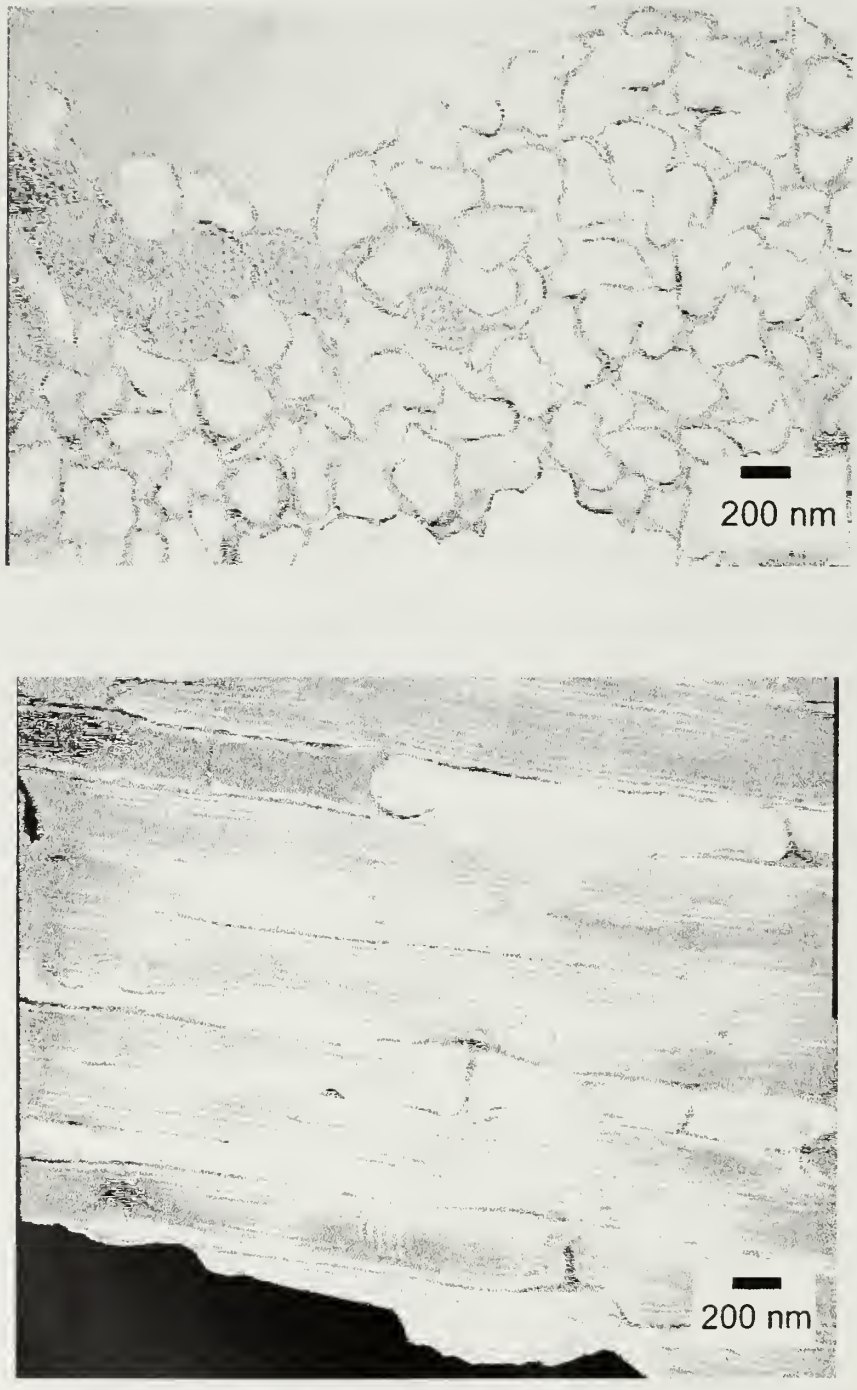


**Figure 6.6: Confined PS-*b*-P2VP in Amorphous Carbon Nanotubes (a) 64k-*b*-35k and (b) 25k-*b*-23k**

### 6.2.4 Preparation, Metallization, and Characterization of Polystyrene-*b*-Poly(2-vinylpyridine) Confined in Aluminum Oxide Membranes

Thick films (50-100 μm) of PS-*b*-P2VP were prepared by the drop cast method from solutions of the polymer in toluene or chloroform (5-10 wt%) and by allowing the sample to dry overnight. The samples were then annealed in a vacuum oven at 170 °C for 24 hours to remove any residual solvent from the polymer. Next, an aluminum oxide membrane was placed on the polymers surface and the stack was clamped between two glass slides to ensure contact of the membrane to the polymer was maintained. This stack was then annealed at 170 °C for two days to allow for the formation of microphase separated nanorods within the membrane. After the formation of the nanorods, the aluminum oxide was dissolved by placing the sample in a 5% aqueous solution of sodium hydroxide. Finally, the P2VP domain was metallized with silver or gold using the procedure described in Chapter 3. For metallizations with gold, the nanorods were exposed to a 9:1 water/ethanol solution of $HAuCl_4$ (5 mg/mL) for two minutes.[8-10] The samples were then rinsed thoroughly with dionized water and reduced with a 9:1 water/ethanol solution of sodium borohydride (5 mg/mL). All the samples were then embedded in epoxy and microtomed for TEM analysis.

Figure 6.7 shows a PS-*b*-P2VP (54k-*b*-50k) sample that was confined and metallized with silver. The two images, microtomed perpendicular and parallel to the rod axis, respectively, show the high selectivity of the metallization to the P2VP domain and silver particles with diameters less than 10 nm in diameter.

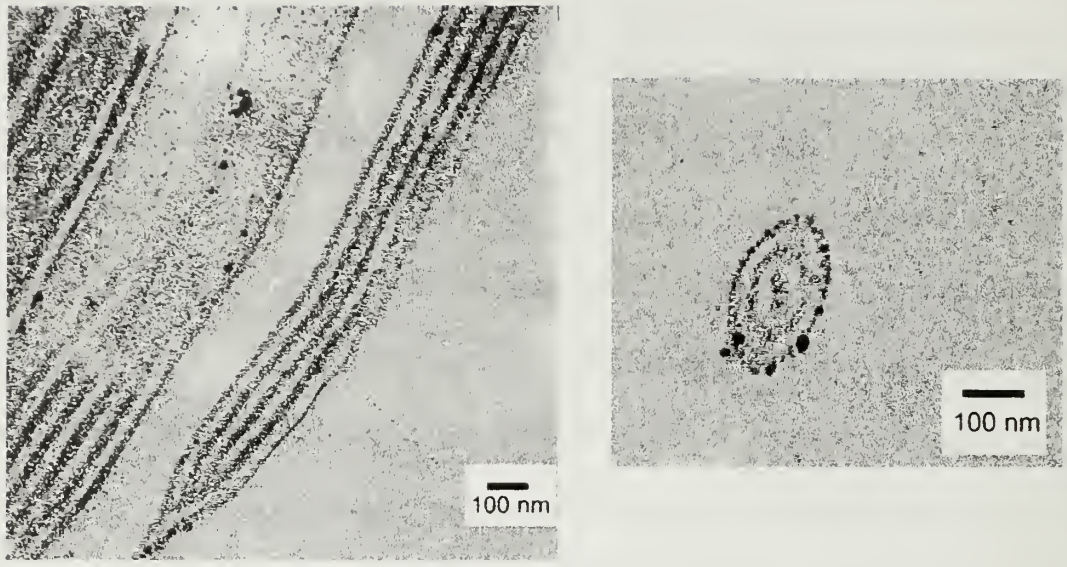


**Figure 6.7: Confined PS-*b*-P2VP (54k-*b*-50k) Confined and Metallized with Silver**

Figure 6.8 shows a similar PS-*b*-P2VP (54k-*b*-50k) sample that was confined and metallized with gold. The two images below, cut perpendicular and parallel to the rods, demonstrate the high selectivity of the metallization to the P2VP domain and gold particles less than 10 nm in diameter. The larger particles around the perimeter of the rod are caused from the reduction excess of $HAuCl_4$ which was not completely rinsed from the sample.

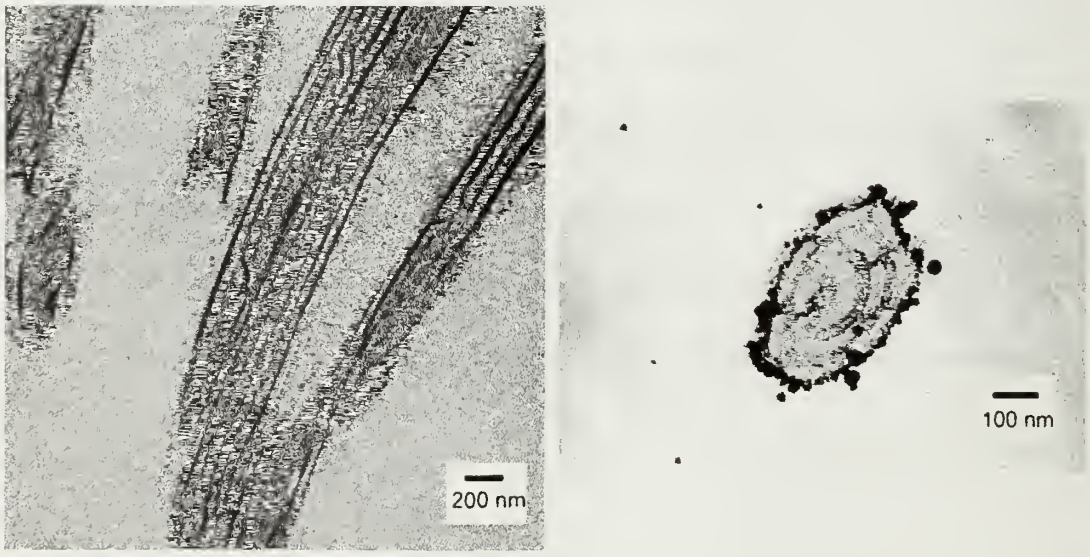


**Figure 6.8: Confined PS-*b*-P2VP (54k-*b*-50k) Confined and Metallized with Gold**

### 6.3 Conclusions

A thorough study of the confinement and metallization of PS-*b*-P2VP in aluminum oxide membranes and amorphous carbon nanotubes was conducted. It was observed that the P2VP preferentially wets the aluminum oxide and styrene wets the amorphous carbon. For symmetric and asymmetric polymers, concentric ring and hexagonally packed cylindrical morphologies were observed, respectively. Selective metallization of the P2VP domain with silver and gold was also achieved within the nanorods.

## 6.4 References


1. Walton, D. G.; Kellogg, G. J.; Mayes, A. M.; Lambooy, P.; Russell, T. P., A Free Energy Model for Confined Diblock Copolymers. *Macromolecules* 1994, **27**, 6225-6228.

2. Xiang, H.; Shin, K.; Kim, T.; Moon, S. I.; McCarthy, T. J.; Russell, T. P., Block Copolymers under Cylindrical Confinement. *Macromolecules* 2004, **37**, 5660-5664.

3. Xiang, H.; Shin, K.; Kim, T.; Moon, S.; McCarthy, T. J.; Russell, T. P., The influence of confinement and curvature on the morphology of block copolymers. *Journal of Polymer Science, Part B: Polymer Physics* 2005, **43**, (23), 3377-3383.

4. Xiang, H.; Shin, K.; Kim, T.; Moon, S.; McCarthy, T. J.; Russell, T. P., From Cylinders to Helices upon Confinement. *Macromolecules* 2005, **38**, (4), 1055-1056.

5. Shin, K.; Xiang, H.; Moon, S.; Kim, T.; McCarthy, T. J.; Russell, T. P., Curving and Frustrating Flatland. *Science* 2004, **306**, (5693), 76.

6. Stucky, G. D.; Wu, Y.; Cheng, G.; Kastov, K.; Sides, S., Composite mesostructures by nano-confinment. *Nature Materials* 2004, **3**, 816-822.

7. Chen, J.-T.; Shin; Leiston-Belanger, J.; Zhang, M.; Russell, T. P., Amorphous Carbon Nanotubes with Tunable Properties via Template Wetting. *Advanced Functional Materials* 2006, (Early View).

8. Youk, J. H.; Park, M. K.; Locklin, J.; Advincula, R.; Yang, J.; Mays, J., Preparation of Aggregation Stable Gold Nanoparticles Using Star-Block Copolymers. *Langmuir* 2002, **18**, (1), 2455-2458.

9. Sohn, B. H.; Seo, B. H., Fabrication of the Multilayer Nanostructure of Alternating Polymers and Gold Nanoparticles with Thin Films of Self-Assembling Diblock Copolymers. *Chem. Mater.* 2001, **13**, 1752-1757.

10. Chan, Y. N. C.; Schock, R. R.; Cohen, R. E., Synthesis of Silver and Gold Nanoclusters within Microphase-Separated Diblock Copolymers. *Chem. Mater.* 1992, **4**, (1), 24-27.

# CHAPTER 7

# CONCLUSIONS AND FUTURE WORK

## 7.1 Conclusions

In this research, homopolymer and block copolymers of poly(2-vinylpyridine) and poly(styrene)-b-poly(2-vinylpyridine) were metallized using supercritical carbon dioxide soluble metal precursors. First, the interactions of poly(2-vinylpyridine) with silver, platinum and zinc metal precursors and metal nanoparticles subsequent to reduction were investigated in Chapter 3. It was determined that the metal precursors underwent a ligand exchange reaction with the vinylpyridine and that, after reduction, the metal nanoparticles no longer interacted with the polymer.

Chapters 4-6 described the selective metallization of the copolymers in thin films, confined geometries, and sheared samples. The selectivity of the metallilization arises from the ability of the P2VP to undergo ligand exchange reactions and quaterization. In Chapter 4 it was determined that a serial process could be used to metallize the films while maintaining the microphase separated structure. It was also shown that upon annealing the formed silver nanoparticles aggregated at the air-polymer interface.

Chapter 5 explored the use of shearing and solvent annealing to enhance the order and orientation of the copolymer domains. Two types of shearing and solvent annealing techniques were studied. It was established that simple melt pressing and parallel plate rheomety produced similar results with calculated domain orientations of greater than 80%. Solvent annealing, using different solvents in both closed and controlled flow systems, resulted in orientations both parallel and perpendicular to the substrate. For the

controlled flow system, a 50:50 mixture of toluene and hexane resulted in the best order and orientation of the copolymer domains.

Finally, Chapter 6 discussed the confinement and metallization of the copolymers in aluminum oxide membranes and amorphous carbon tubes. Transmission electron microscopy of the samples showed that the wetting of the P2VP on the aluminum oxide resulted in unique morphologies such as concentric rings that are not available in thin film or bulk samples. The amorphous carbon changed the surface interaction of the copolymer within the pores, resulting in a PS wetting layer.

### 7.2 Suggestions for Future Work

Though this research answered many questions about the metallization, stability and confinement or ordered block copolymers, there is more work that can be investigated. Future work in this area should include metallization with more than one metal using seeding and electroless plating in a polymer films. Both of these topics will be discussed below.

The metallization of block copolymers using supercritical carbon dioxide has proved to be an easy way to produce nanocomposites without destroying the block copolymers morphology or orientation. Successive or co-infusion metal precursor infusion could produce core-shell or alloy nanoparticles within one domain of the polymer. It may also be possible to add a catalyst such as platinum to aid in the reduction of hard to reduce precursors. Preliminary work has been done in this area and UV-VIS spectroscopy was used to monitor the reaction.

Figure 7.1 (a) and (b) below are the UV-VIS spectra of a P2VP thin film on quartz the was infused with 5:1 and 1:1 mixtures of Ag(COD)hfac and Pt(COD)$Me_2$ and reduced with hydrogen at 60 °C. There are three peaks at 263, 315, and 430 nm which correspond to the P2VP, the hfac ligand of the precursor, and the silver nanoparticles after reduction, respectively. Data from Chapter 3 showed that the silver precursor did not completely reduce in the presence of hydrogen after 24 hours, however, with the co-infusion, complete reduction was achieved after a 12 hour reduction in hydrogen. In (b) the presence of a peak at 351 nm suggests the formation of silver-platinum nanoparticles. Henglein et al. studied the formation of similar silver-platinum nanoparticles and found similar UV-VIS absorbencies.[1] Future work with co-infusions should include the determination of the particles crystal structure and morphology.

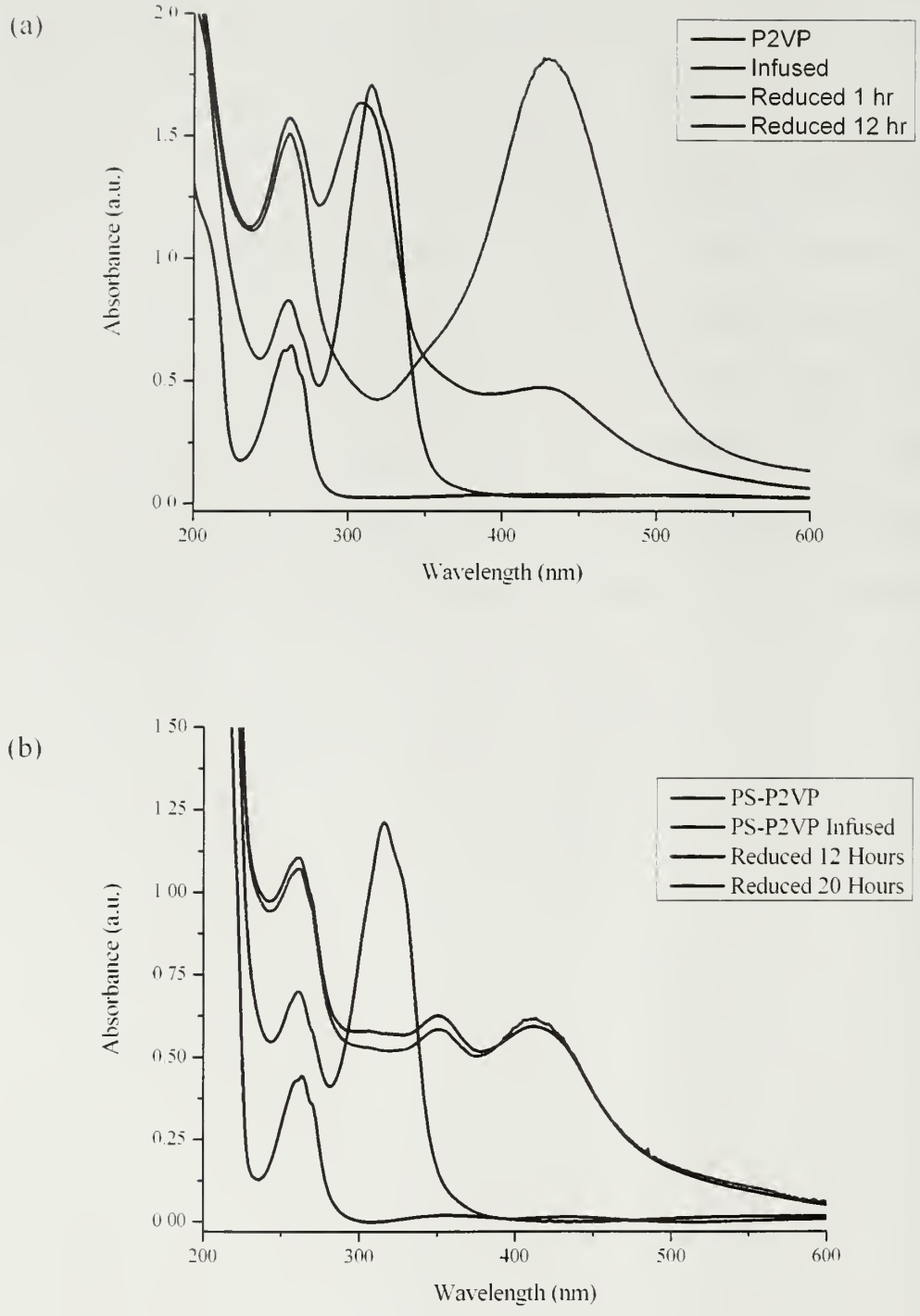


**Figure 7.1 UV-VIS Spectroscopy of Co-Infused P2VP with Ag(COD)hfac and Pt(COD)Me2 with Ratios of (a) 5:1 and (b) 1:1**

Electroless Plating involves the chemical reduction and deposition of metal ions onto a catalytic surface such as palladium. Metals including copper have been deposited by this method to produce both micro- and nanoscale metal structures. This method has been studied by Rubner et al.[2] to deposit copper in thick copolymer films seeded with palladium. They were able to deposit copper in the films to depths to 8 μm. This method should be investigated in the confined PS-*b*-P2VP systems to produce structures such as copper nano-wires or capacitors.

## 7.3 References


1. Henglein, A., Reduction of $Ag(CN)_2^-$ on Silver and Platinum Colloidal Nanoparticles. *Langmuir* 2001, **17**, 2329-2333.

2. Boontongkong, Y.; Cohen, R. E.; Rubner, M. F., Selective Electroless Copper Deposition within Block Copolymer Microdomains. *Chem. Mater.* 2000, **12**, 1628-1633.

## BIBLIOGRAPHY


*The Aldrich Library of Infrared Spectra* III ed.: Aldrich Chemical Company: 1981.

Agnew, N. H., Transition metal complexes of poly(vinylpyridines). *Journal of Polymer Science: Polymer Chemistry Edition* 1976, **14**, (11), 2819-2830.

Aizawa, M.; Buriak, J. M., Nanoscale Patterning of Two Metals on Silicon Surfaces Using an ABC Triblock Copolymer Template. *J. Am. Chem. Soc.* 2006, **128**, (17), 5877-5886.

Angelescu, D. E.; Waller, J. H.; Adamson, D. H.; Deshpande, P.; Register, R. A.; Chaikin, P. M., Macroscopic Orientation of Block Copolymer Cylinders in Single-Layer Films by Shearing. *Adv. Mater.* 2004, **16**, (19), 1736-1740.

Bal, M.; Ursache, A.; Tuominen, M. T.; Goldbach, J. T.; Russell, T. P., Nanofabrication of integrated magnetoelectronic devices using patterned self-assembled copolymer templates. *Appl. Phys. Lett.* 2002, **81**, (18), 3479-3481.

Balsara, N. P.; Hammouda, B.; Kensani, P. K.; Jonnalagadda, S. V.; Straty, G. C., In-Situ Small-Angle Neutron Scattering from a Block Copolymer Solution under Shear. *Macromolecules* 1994, **27**, 2566-2573.

Bates, F. S., Block Copolymers near the Microphase Separation Transition 2. Linear Dynamic Mechanical Properties. *Macromolecules* 1984, **17**, 2607-2613.

Bates, F. S.; Fredrickson, G. H., Block Copolymers - Designer Soft Materials. *Physics Today* 1999, **52**, (2), 32-38.

Bennett, R. D.; Xiong, G. Y.; Ren, Z. F.; Cohen, R. E., Using Block Copolymer Micellar Thin Films as Templates for the Production of Catalysts for Carbon Nanotube Growth. *Chem. Mater.* 2004, **16**, (26), 5589-5595.

Boontongkong, Y.; Cohen, R. E.; Rubner, M. F., Selective Electroless Copper Deposition within Block Copolymer Microdomains. *Chem. Mater.* 2000, **12**, 1628-1633.

Brandrup, J.; Immergut, E. H., *Polymer Handbook*, 3rd ed.: 1989.

Brown, G. D.; Watkins, J. J., Carbon Dioxide - Dilated Block Copolymer Templates for Nanostructured Materials. *Mat. Res. Soc. Symp. Proc.* 2000, **585**, 169-174.

Brown, G. M.; Rausch, M. D., Oxidation-state and electron-transfer properties of mixed-valence 1,1'-polyferrocene ions *Inorg. Chem.* 1975, **14**, (3), 506-511.

Chan, Y. N. C.; Schock, R. R.; Cohen, R. E., Synthesis of Silver and Gold Nanoclusters within Microphase-Seperated Diblock Copolymers. *Chem. Mater.* 1992, **4**, (1), 24-27.

Chen, J.-T.; Shin; Leiston-Belanger, J.; Zhang, M.; Russell, T. P., Amorphous Carbon Nanotubes with Tunable Properties via Template Wetting. *Advanced Functional Materials* 2006, (Early View).

Chiu, Y., Fabrication and Nonlinear Optical Properties of Nanoparticle Silver Oxide Films. *Journal of Applied Physics* 2003, **94**, (3), 1996-2001.

Ciardelli, F.; Tsuchida, E.; Wöhrle, D., *Macromolecule-Metal Complexes*. Springer: Berlin, 1996.

Creighton, J. A.; Eadon, D. G., Ultraviolet-Visible Absorption Spectra of the Colloidal Metallic Elements. *J. Chem. Soc. Faraday Trans.* 1991, **87**, (24), 3881-3891.

Cummings, C. C.; Schrock, R. R.; Cohen, R. E., Synthesis of ZnS and CdS within ROMP Block Copolymer Microdomains. *Chem. Mater.* 1992, **4**, (1), 27-30.

DeSimone, J. M.; Guan, Z.; Elsbernd, C. S., Synthesis of fluoropolymers in supercritical carbon dioxide. *Science* 1992, **257**, (5072), 945-947.

Edwards, E. W.; Montague, M. F.; Solak, H. H.; Hawker, C. J.; Nealey, P. F., Precise Control Over Molecular Dimensions of Block-Copolymer Domains Using the Interfacial Energy of Chemically Patterned Surfaces. *Adv. Mater.* 2004, **16**, (15), 1315-1319.

Edwards, E. W.; Stoykovich, M. P.; Solak, H. H.; Nealey, P. F., Long-Range Order and Orientation of Cylinder-Forming Block Copolymers on Chemically Nanopatterned Striped Surfaces. *Macromolecules* 2006, **39**, 3598-3607.

Fink, Y.; Urbas, A. M.; Bawendi, M. G.; Jaonnopoulos, J. D.; Thomas, E. L., *J. Lightwave Technol.* 1999, **34**, 2256-2262.

Gao, J.; Fu, J.; Lin, C.; Lin, J.; Han, Y.; Yu, X.; Pan, C., Formation and Photoluminescence of Silver Nanoparticles Stabilized by Two-Armed Polymer with a Crown Ether Core. *Langmuir* 2004, **20**, 9775-9779.

Gauglitz, G.; Vo-Dinh, *Handbook of Spectroscopy*. Wiley-VCH: 2003: Vol. 1.

Glatter, O.; Kratky, O., *Small Angle X-ray Scattering*. Academic Press: New York, 1982.

Guan, Z.; Combes, J. R.; Menceloglu, Y. Z.; DeSimone, J. M., Homogeneous free radical polymerizations in supercritical carbon dioxide: 2. Thermal decomposition of 2,2'-azobis(isobutyronitrile). *Macromolecules* 1993, **26**, (11), 2663-2669.

Gupta, R. R.; RamachandraRao, V. S.; Watkins, J. J., Measurement of Probe Diffusion in CO2-Swollen Polystyrene Using in Situ Fluorescence Nonradiative Energy Transfer. *Macromolecules* 2003, **36**, (4), 1295-1303.

Gupta, V. K.; Krishnamoorti, R.; Chen, Z. R.; Kornfield, J. A.; Smith, S. D.; Satkowski, M. M.; Grothaus, J. T., Dynamics of Shear Alignment in a Lamellar Diblock Copolymer: Interplay of Frequency, Strain Amplitude and Temperature. *Macromolecules* 1996, **29**, 875-884.

Gupta, V. K.; Krishnamoorti, R.; Kornfield, J. A.; Smith, S. D., Evolution of Microstructure during Shear Alignment in a Polystyrene-Polyisoprene Lamellar Diblock Copolymer. *Macromolecules* 1995, **28**, (4464-4474).

Gupta, V. K.; Krishnamoorti, R.; Kornfield, J. A.; Smith, S. D., Role of Strain in Controlling Lamellar Orientation during Flow Alignment of Diblock Copolymers. *Macromolecules* 1996, **29**, 1359-1362.

Hadjichistidis, N.; Iatrou, H.; Pispas, S.; Pitsikalis, M., Anionic Polymerization: High Vacuum Techniques. *J. Polym. Sci. Part A Polym. Chem.* 2000, **38**, 3211-3234.

Hadjichristidis, N.; Pispas, S.; Floudas, G. A., ***Block Copolymers Synthetic Strategies, Physical Properties, and Applications***. John Wiley and Sons: Hoboken, New Jersey, 2003.

Hadziioannou, G.; Picot, C.; Skoulios, A.; Ionescu, M.-L.; Mathis, A.; Duplessix, R.; Gallot, Y.; Lingelser, J.-P., Low-Angle Neutron Scattering Study of the Lateral Extension of Chains in Lamellar Styrene/Isoprene Block Copolymers. *Macromolecules* 1982, **15**, 263-267.

Hameley, I. W., *The Physics of Block Copolymers*. Oxford University Press: New York, 1998.

Hashimoto, T.; Harada, M.; Sakamoto, N., Incorporation of Metal Nanoparticles into Block Copolymer Nanodomains via in-Situ Reduction of Metal Ions in Microdomain Space. *Macromolecules* 1999, **32**, 6867-6870.

He, S.; Yao, J.; Jiang, P.; Shi, D.; Zhang, H.; Xie, S.; Pang, S.; Gao, H., Formation of Silver Nanoparticles and Self Assembled Two-Dimensional Ordered Superlattice. *Langmuir* 2001, **17**, 1571-1575.

He, X.; Song, M.; Liang, H.; Pan, C., Self-Assembly of Symmetric Diblcok Copolymers in a Confined State: Monte Carlo Simulation. *J. Chem. Phys.* 2001, **114**, (23), 10510-10513.

Henglein, A., Reduction of $Ag(CN)_2^-$ on Silver and Platinum Colloidal Nanoparticles. *Langmuir* 2001, **17**, 2329-2333.

Ishizu, K.; Yamada, Y.; Saito, R.; Kanbara, T.; Yamamoto, T., Anisotropic conductivity on diblock copolymers with lamellar microdomains. *Polymer* 1993, **34**, 2256-2258.

Johnson, C. E.; Harris, D. C., Preparation, Purification, and Densification of Zinc Sulfide Powder from Organometallics. *Chem. Mater.* 1990, **2**, 141-149.

Kim, S. H.; Misner, M. J.; Russell, T. P., Solvent-Induced Ordering in Thin Film Diblock Copolymer/Homopolymer Mixtures. *Adv. Mater.* 2004, **16**, 2119.

Kim, S. H.; Misner, M. J.; Russell, T. P., Solvent-Induced Ordering in Thin Film Diblock Copolymer/Homopolymer Mixtures. *Adv. Mater.* 2004, **16**, (23-24), 2119-2123.

Kim, S. H.; Misner, M. J.; Xu, T.; Kimura, M.; Russell, T. P., Highly Oriented and Ordered Arrays From Block Copolymers via Solvent Annealing. *Adv. Mater.* 2004, **16**, (3), 226-231.

Kitade, S.; Ochiai, N.; Takahasi, Y.; Noda, I., Lamellar Orientation of Diblock Copolymer Solutions Under Steady Shear Flow. *Macromolecules* 1998, **31**, 8083-8090.

Kodaira, T.; Wantabe, A.; Ito, O.; Mochida, K., Third-order nonlinear optical properties of thin films of organogermane homopolymers and organogermane-organosilane copolymers. *Adv. MAter.* 1995, **7**, (11), 917-919.

Koji Ishizu, Y. Y. a. R. S.; Yamamoto, T. K. a. T., Anisotropic conductivity on diblock copolymers with lamellar microdomains *Polymer* 1993, **34**, 2256-2262.

Kuo, S. W.; Wu, C. H.; Chang, F. C., Thermal Properties, Interaction, Morphologies, and Conductivity Behavior in Blends of Poly(vinylpyridine)s and Zinc Perchlorate. *Macromolecules* 2004, **37**, (1), 192-200.

Laurer, J. H.; Pinheiro, B. S.; Polis, D. L.; Winey, K. L., Persistence of Surface-Induced Alignment in Block Copolymers upon Large-Amplitude Oscillatory Shear Processing. *Macromolecules* 1999, (32), 4999-5003.

Lin, Y.; Boeker, A.; He, J.; Sill, K.; Xiang, H.; Abetz, C.; Li, X.; Wang, J.; Emrick, T.; Long, S.; Wang, Q.; Balazs, A.; Russell, T. P., Self-directed self-assembly of nanoparticle/copolymer mixtures. *Nature* 2005, **434**, (7029), 55-59.

Lin, Y.; Zhang, Q.; Gupta, S.; Wang, Q.; Balazs, A.; Emrick, T.; Russell, T. P. In *Nanoparticles at interfaces: From membranes to crack healing*, Abstracts of Papers, 230th ACS National Meeting, Washington, DC, 2005: Washington, DC, 2005.

Liu, Y.; Zhao, W.; Zheng, X.; King, A.; Singh, A.; Rafailovich, M. H.; Sokolov, J.; Dai, K. H.; Kramer, E. J.; Schwarz, S. A.; Gebilioglu, O.; Sinha, S. K., Surface-Induced Ordering in Asymmetric Block Copolymers. *Macromolecules* 1994, **1994**, 4000-4010.

Mafune, F.; Kohno, J.; Takeda, Y.; Kondow, T.; Swabe, H., Structure and Stability if Silver Nanoparticles in Aqueous Solution Produced by Laser Ablation. *J. Phys. Chem. B* 2000, **104**, (35), 8333-8337.

Maier, S. A.; Brongersma, M. L.; Kik, P. G.; Meltzer, S.; Requicha, A. A. G.; Atwater, H. A., Plasmonics - A Route to Nanoscale Optical Devices. *Advanced Materials* 2001, **13**, (19), 1501-1505.

Malynych, S.; Chumanov, G., Light-Induced Coherent Interactions between Silver Nanoparticles in Two-Dimentional Array. *JACS* 2003, **125**, 2896-2898.

Manners, I., Ring-opening polymerization of metallocenophanes. *Adv. MAter.* 1994, **6**, (1), 68-71.

Mansky, P.; Russell, T. P.; Hawker, C. J.; Pitsikalis, M.; Mays, J., Ordered Diblock Copolymer Films on Random Copolymer Brushes. *Macromolecules* 1997, **30**, 6810-6813.

Marambio, O. G., Poly(N-phenylmaleimide-co >-acrylic acid)-copper(II) and poly(N-phenylmaleimide-co-acrylic acid)-cobalt(II) complexes: Synthesis, characterization, and thermal behavior. *Journal of Polymer Science Part A: Polymer Chemistry* 2005, **43**, (20), 4933-4941.

Möller, M., Inorganic Nanoclusters in Organic Glasses - Novel Materials for Electro-Optical Applications. *Synthetic Metals* 1991, 1159-1162.

Pai, R. A.; Humayun, R.; Schulberg, M. T.; Sengupta, A.; Sun, J.; Watkins, J. J., Mesoporous Silica Prepared Using Preorganized Templates in Supercritical Fluids. *Science* 2004, **303**, 507-510.

Partenheimer, W.; Johnson, E. H., Heats of Reaction of Triphenylphosphine with Compounds of the type Heaxafluoroacetylacetonato(olifin)Silver. *Inorganic Chemistry* 1973, **12**, (6), 1274-1278.

Patel, S. S.; Larson, R. G.; Winey, K. L.; Wantanbe, H., Shear Orientation and Rheology of a Lamellar Polystyrene-Polyisoprene Block Copolymer. *Macromolecules* 1995, **28**, 4313-4318.

Perlmutter-Hayman, B., Cooperatvie Binding to Macromolecules. A Formal Approach. *Acc. Chem. Res.* 1986, **19**, 90-96.

Petit, C.; Lixon, P.; Pileni, M., In Situ Synthesis of Silver Nanoclusters in AOT Reverse Micelles. *J. Phys. Chem.* 1993, **97**, 12974-12983.

Riise, B. L.; Fredrickson, G. H.; Larson, R. G.; Pearson, D. S., Rheology and Shear-Induced Alignment of Lamellar Diblock and Triblock Copolymers. *Macromolecules* 1995, **28**, 7653-7659.

Rossetti, R.; Ellison, J. L.; Gibson, J. M.; Brus, L. E., Size Effects in the Excited Electronic States of Small Collodial CdS Crystallites. *J. Chem. Phys.* 1984, **80**, (9), 4464-4469.

Russell, T. P., X-ray and Neutron Reflectivity for the investigation of polymers. *Materials Science Reports* 1990, 173-271.

Saito, R.; Okamura, S.; Ishizu, K., Introduction of Colloidal Silver into Poly(2-vinylpyridine) Microdomain of Microphase Separated Poly(Styrene-b-2-vinylpyridine) Film. *Polymer* 1992, **33**, (5), 1099-1101.

Schultz, M. F.; Khandpur, A. K.; Bates, F. S., Phase Behavior of Polystyrene-Poly(2-vinylpyridine) Diblock Copolymers. *Macromolecules* 1996, **29**, 2857-2867.

Seagalman, R. A.; Yokoyama, H.; Kramer, E. J., Graphoepitaxy of Spherical Domain Block Copolymer Films. *Adv. Mater.* 2001, **13**, (15), 1152-1155.

Seregina, M. V.; Bronstein, L. M.; Platonova, O. A.; Chernyshov, D. M.; Valetsky, P. M., Preparation of Noble metal Colloids in Block Copolymer Micelles and Their Catalytic Properties in Hydrogenation. *Chem. Mater.* 1997, **9**, 923-931.

Sevink, G. J. A.; Zvenlindovsky, A. V.; Fraaije, J. G. E. M., Morphology of symmetric block copolymer in a cylindrical pore. *J. Chem. Phys.* 2001, **115**, (17), 8226-8230.

Shin, K.; Xiang, H.; Moon, S.; Kim, T.; McCarthy, T. J.; Russell, T. P., Curving and Frustrating Flatland. *Science* 2004, **306**, (5693), 76.

Silverstein, R. M.; Bassler, G. C.; Morrill, T. C., *Spectrometric Identification of Organic Compounds*. Fifth ed.; John Wiley and Sons: New York, 1991.

Sohn, B. H.; Seo, B. H., Fabrication of the Multilayer Nanostructure of Alternating Polymers and Gold Nanoparticles with Thin Films of Self-Assembling Diblock Copolymers. *Chem. Mater.* 2001, **13**, 1752-1757.

Spall, W. D.; Laintz, K. E., A Survey on the use of Supercritical Carbon Dioxide as a Cleaning Solvent. *Supercritical Fluid Cleaning* 1998, **162**, (194), 162-194.

Spatz, J. P.; Moller, M.; Noeske, M.; Behm, R. J.; Pietralla, M., Nanomosaic Surfaces by Lateral Phase Seperation of a Diblock Copolymer. *Macromolecules* 1997, **30**, 3874-3880.

Strobl, G. R., *The Physics of Polymers: Concepts for Understanding Their Structures and Behavior*. Springer: New York, 1997.

Stucky, G. D.; Wu, Y.; Cheng, G.; Kastov, K.; Sides, S., Composite mesostructures by nano-confinment. *Nature Materials* 2004, **3**, 816-822.

Suh, K. Y.; Kim, Y. S.; Lee, H. H., Capillary Force Lithography. *Adv. Mater.* 2001, **13**, (18), 1386.

82. Tsutsumi, K.; Funaki, Y.; Hirokawa, Y.; Hashimoto, T., Selective Incorporation of Palladium Nanoparticles into Microphase Separated Domains of Poly(2-vinylpyridine)-block-polyisoprene. *Langmuir* 1999, **15**, 5200-5203.

Udayasankar, K.; Manohar, B.; Chokkalingam, A., A Note on Supercritical Carbon Dioxide Decaffeination of Coffee. *Journal of Food Science and Technology* 1986, **23**, (6), 326.

Vitosa, L.; Rubana, A. V.; Skrivera, H. L.; Kollárb, J., The surface energy of metals *Surface Science* 1998, **411**, (1-2), 186-202.

Vogt, B. D.; Brown, G. D.; RamachandraRao, V. S.; Watkins, J. J., Phase Behavior of Nearly Symmetric Polystyrene-block-polyisoprene

Copolymers in the Presence of CO2 and Ethane. *Macromolecules* 1999, **32**. (23). 7907-7912.

Vogt. B. D.: RamachandraRao. V. S.: Gupta. R. R.: Lavery. K. A.: Francis. T. J.: Russell. T. P.: Watkins. J. J.. Phase Behavior of Polystyrene-block-poly(n-alkyl methacrylate)s Dilatedwith Carbon Dioxide. *Macromolecules* 2003, **36**. (22). 4029-4036.

Walton. D. G.: Kellogg. G. J.: Mayes. A. M.: Lambooy. P.: Russell. T. P.. A Free Energy Model for Confined Diblock Copolymers. *Macromolecules* 1994, **27**. 6225-6228.

Wang. Y.: Suna. A.: Mahier. W.: Kasowski. R.. PbS in Polymers. From Molecules to Bulk Solids. *J. Chem. Phys.* 1987, **87**. (12). 7315-7322.

Watkins. J. J.: McCarthy. T. J.. Polymerization in Supercritical Fluid-Swollen Polymers: A New Route to Polymer Blends. *Macromolecules* 1994, **27**. (17). 4845-4847.

Watkins. J. J.: McCarthy. T. J.. Polymer/Metal Nanocomposite Synthesis in Supercritical CO2 *Chem. Mater.* 1995, **7**. (11). 1991-1994.

Wexler. R. M.: Tsai. M. C.: Friend. C. M.: Muetterties. E. L.. Pyridine Coordination Chemistry of Nickel and Platinum. *J. Am. Chem. Soc.* 1982, **104**. (7). 2034-2036.

Winey. K. L.: Patel. S. S.: Larson. R. G.: Wantanbe. H.. Morphology of a Lamellar Diblock Copolymer Allighned Perpendicular to the Sample Plane: Transmission Electron Microscopy and Samll-Angle X-ray Scattering. *Macromolecules* 1993, **26**. (4373-4375).

Winey. K. L.: Patel. S. S.: Larson. R. G.: Wantanbe. H.. Interdependence of Shear Deformations and Block Copolymer Morphology. *Macromolecules* 1993, **26**. 2542-2549.

Wissinger. R. G.: Paulaitis. M. E.. Swelling and Sorption in Polymer-$CO_2$ Mixtures at Elevated Pressures. *Journal of Polymer Science Part B* 1987, **25**. (12). 2497-2510.

Wöhrle. D.. Polymer square planar metal chelates for science and industry. Synthesis. properties and applications. *Adv. Polym. Sci.* 1983, **50**. 45-134.

Wöhrle. D.: Ciardelli. F.. *Macromolecule-metal complexes*. Springer: New Yrk. 1996.

Wöhrle. D.: Pomogailo. A. D.. *Metal Complexes and Metals in Macromolecules: Synthesis. Structure and Properties*. Wiley-VCH: 2003.

Wu, D. Y.; Hayashi, M.; Chang, C. H.; Liang, K. K.; Lin, S. H., Bonding Interaction, Low-lying States and Excited Charge-Transfer States of Pyridine-Metal Clusters: Pyridine-Mn (Cu, Ag, Au; n=2-4). *Journal of Chemical Physics* 2003, **118**, (9), 4073-4085.

Xiang, H.; Shin, K.; Kim, T.; Moon, S.; McCarthy, T. J.; Russell, T. P., The influence of confinement and curvature on the morphology of block copolymers. *Journal of Polymer Science, Part B: Polymer Physics* 2005, **43**, (23), 3377-3383.

Xiang, H.; Shin, K.; Kim, T.; Moon, S.; McCarthy, T. J.; Russell, T. P., From Cylinders to Helices upon Confinement. *Macromolecules* 2005, **38**, (4), 1055-1056.

Xiang, H.; Shin, K.; Kim, T.; Moon, S. I.; McCarthy, T. J.; Russell, T. P., Block Copolymers under Cylindrical Confinement. *Macromolecules* 2004, **37**, 5660-5664.

Xu, T.; Zhu, Y.; Gido, S. P.; Russell, T. P., Electric Field Alignment of Symmetric Diblock Copolymer Thin Films. *Macromolecules* 2004, **37**, 2625-2629.

Yoda, S.; Hasegawa, A.; Suda, H.; Uchimaru, Y.; Haraya, K.; Tsuji, T.; Otake, K., Preparation of a Platinum and Palladium/Polyimide Nanocomposite Film as a Precursor of Metal-Doped Carbon Molecular Sieve Membrane via Supercritical Impregnation. *Chem. Mater.* 2004, **16**, 2363-2368.

Youk, J. H.; Park, M. K.; Locklin, J.; Advincula, R.; Yang, J.; Mays, J., Preparation of Aggregation Stable Gold Nanoparticles Using Star-Block Copolymers. *Langmuir* 2002, **18**, (1), 2455-2458.